Regional modeling of polycyclic aromatic hydrocarbons and other persistent organic pollutants: model development and applications

Qing Mu

geb. am 06.08.1989 in Wuhan, China

Dissertation

zur Erlangung des Grades

‘Doktor rerum naturalium (Dr. rer. nat.)’

im Promotionsfach Chemie

am Fachbereich Chemie, Pharmazie und Geowissenschaften

der Johannes Gutenberg-Universität in Mainz

Max Planck Graduate Center

Mainz, April 2018

I hereby declare that I wrote the dissertation submitted without any unauthorized external assistance and used only sources acknowledged in the work. All textual passages which are appropriated verbatim or paraphrased from published and unpublished texts as well as all information obtained from oral sources are duly indicated and listed in accordance with bibliographical rules. In carrying out this research, I complied with the rules of standard scientific practice as formulated in the statutes of Johannes Gutenberg-University Mainz to insure standard scientific practice.

Abstract

Polycyclic aromatic hydrocarbons (PAHs) and other persistent organic pollutants (POPs) are hazardous pollutants in the environment. Due to the relatively long environmental lifetime, they can often be distributed globally. POPs can accumulate along food chains and reach toxic levels for biota. Moreover, their physical and chemical processes in the Earth system are complex. In particular, (1) many substances are semi-volatile such that they partition between particulate and gas phase; (2) upon deposition to the soil, many substances which resist biodegradation in the soil, can re-volatilize into the atmosphere; (3) the degradation of the particulate phase in the air is not well accounted for in the ambient conditions, which is over-simplified or completely neglected. As these processes are not well described or missing in the current atmospheric models, the characterization of atmospheric cycling, fate, environmental exposure to and long-range transport potential of these pollutants is hindered. In this study, a regional atmospheric chemical transport model is updated by improving and including up-to-date terrestrial cycling processes of PAH/POP.

In this PhD work, the regional chemical transport model WRF-Chem is extended to include all the up-to-date physical and chemical processes of PAH/POP, such as emission, transport, gas-particle partitioning, air-soil gas exchange, heterogeneous degradation, gas-phase reaction, cloud scavenging, dry deposition and wet deposition. The extended model is named WRF-Chem-PAH/POP. Predicted atmospheric concentrations and particulate mass fractions are evaluated against near-source and remote-outflow observation data in high resolutions. The predictions have been largely improved compared with previous modeling studies. Besides, sensitivity tests verify the necessity to include homogeneous reaction with NO_3 and multiphase reaction with O_3 in the model.

The WRF-Chem-PAH/POP model is applied to study the multiphase degradation of benzo[a]pyrene (BaP), one of the most toxic PAHs. A new kinetic framework depending on environmental temperature and humidity is implemented. Temperature and humidity can change the phase state of BaP-absorbed organic particles, influence the chemical reactivity and thus long-range transport potential of BaP. Model results show that the new kinetic scheme can significantly improve model predictions at various kinds of sites systematically, implying a need to re-evaluate the underestimated long-range transport potential of BaP.

Re-volatilization of soil accumulated POPs under the South Asian summer monsoon is also explored by the WRF-Chem-PAH/POP model. The onset of summer monsoon brings clean air masses from the southern hemisphere and corresponds with the observed reduction of atmospheric pollution levels over the southern parts of India. The enhanced difference between air and soil concentrations triggers the re-volatilization of POPs from soils, which are accumulated in soils as a result of multidecadal agricultural (e.g. pesticides) and industrial (e.g. polychlorinated biphenyls) activities. These pollutants are banned since decades but continue to cycle in the environment. The modeled results agree well with the observations and confirm this explanation of the phenomenon.

In conclusion, WRF-Chem-PAH/POP is one of the most up-to-date large-scale PAH/POP models, which is unique with regard to temporal and spatial resolutions. It provides a powerful tool to study the fate of and environmental exposure to PAH/POP.

Zusammenfassung

Polyzyklische aromatische Kohlenwasserstoffe (PAHs) und persistente organische Schadstoffe (POPs) sind gefährliche Schadstoffe. Aufgrund ihrer relativ langen Lebensdauer in der Umwelt können diese Stoffe häufig global verteilt sein. POPs können sich in der Nahrungskette anreichern und für die Biota, Flora und Fauna, giftige Konzentrationen erreichen. Außerdem sind ihre physikalischen und chemischen Prozesse ihres Zyklierens im Erdsystem sehr komplex. Insbesondere dadurch, dass (1) viele Stoffe mittelflüchtig sind und sich deshalb zwischen Gas- und Partikelphase verteilen; (2) viele Substanzen, die im Boden nicht biologisch abbaubar sind, nach ihrer Ablagerung wieder in die Atmosphäre re-emittiert werden (revolatisieren); (3) der Abbau der Partikelphase in der Luft für Umgebungsbedingungen nicht gut erfasst ist und zu stark vereinfacht oder komplett vernachlässigt wird. Da diese Prozesse in aktuellen Atmosphärenchemiemodellen nicht ausreichend gut beschrieben sind, ist die Beschreibung von Zyklieren, Verbleib und Ferntransport, sowie der Umweltexposition gegenüber diesen Schadstoffen unvollständig. In dieser Studie wird ein regionales Atmosphärenchemiemodell durch Verbesserung und Miteinbeziehung von aktuellen physikalischen und chemischen Prozessen von PAHs und POPs aktualisiert.

In dieser Doktorarbeit wurde das regionale Atmosphärenchemiemodell WRF-Chem um aktuelle physikalische und chemische Prozesse der PAHs und POPs erweitert, wie Emission, Transport, Gas-Partikel-Partitionierung, Luft-Boden-Gasaustausch, heterogener Abbau, Gasphasenreaktion, Wolkenspülung, Trockenabscheidung und Nassabscheidung. Das erweiterte Modell wird WRF-Chem-PAH/POP genannt. Vorhergesagte Konzentrationen in der Atmosphäre und Massenanteile in der Partikelphase atmosphärischer Aerosole werden mittels Vergleich mit Beobachtungsdaten von nahe an Emissionsquellen liegenden Messpunkten und fernab gelegenen Orten in hoher zeitlicher Auflösung bewertet. Die Vorhersagen konnten im Vergleich zu vorherigen Modellen erheblich verbessert werden. Darüber hinaus bestätigen Sensitivitätstests die Notwendigkeit, homogene Reaktionen von NO_3 und O_3 in das Modell einzubeziehen.

Das WRF-Chem-PAH/POP Modell wurde angewendet um den mehrphasigen Abbau von Benzo[a]pyren (BaP), einem der toxischsten polyzyklischen aromatischen Kohlenwasserstoffe, zu untersuchen. Es wurde eine neuartige, von der Umgebungstemperatur und der Luftfeuchtigkeit abhängige Beschreibung der chemischen Kinetik eingeführt. Temperatur und Feuchtigkeit können den Phasenzustand von BaP absorbierenden organischen Partikeln verändern, die chemische

Reaktivität beeinflussen und somit auch das Ferntransportpotenzial von BaP verändern. Modellergebnisse zeigen, dass die neuartige Beschreibung der Kinetik Modellvorhersagen für verschiedene Typen von Messorten signifikant verbessern kann. Das hat zur Folge, dass das Ferntransportpotenzial, bislang zu gering eingeschätzten, neu zu bewerten ist.

Auch die Re-emission von im Boden angereicherten POPs während des südasiatischen Sommermonsuns wurde mit WRF-Chem-PAH/POP untersucht. Der Beginn des Sommermonsuns bringt extrem reine Luftmassen von der Südhalbkugel, was eine Verringerung der Schadstoffkonzentrationen in der Atmosphäre über den südlichen Teilen Indiens bewirkt. Die verstärkte Differenz zwischen Luft- und Bodenkonzentrationen löst die Re-emission der POPs aus dem Boden aus, welche sich im Boden als Folge von landwirtschaftlicher (z. B. Pestizide) bzw. industrieller (z. B. polychlorierte Biphenyle) Aktivitäten aus mehreren Jahrzehnten angereichert haben. Trotzdem diese Schadstoffe seit Jahrzehnten verboten sind, setzen sie ihren Kreislauf in der Umwelt fort. Die modellierten Ergebnisse stimmen gut mit den Beobachtungen überein und bestätigen die Beschreibung des Phänomens.

Zusammenfassend lässt sich sagen, dass WRF-Chem-PAH/POP eines der aktuellsten und umfassenden PAH/POP-Modelle ist, welches einzigartig in Bezug auf die zeitliche und örtliche Auflösung ist. Es stellt ein leistungsfähiges Werkzeug zur Untersuchung von Transport und Verbleib von der PAHs und POPs, sowie der Umweltexposition gegenüber diesen Substanzen dar.

Contents

1. Introduction

1.1 Motivation

Due to high toxicity and carcinogenicity, polycyclic aromatic hydrocarbons (PAHs) and other persistent organic pollutants (POPs) pose great hazard to ecosystems (Hylland, 2006) and human health (World Health Organization, 2003; Lv et al., 2016). POPs are even bioaccumulated through the food chain. Thus, they are regulated in international chemicals legislation. It is important to develop a both spatially and temporally highly resolved model to study the life cycle and fate of PAHs/POPs. The model output can be further used to evaluate their environmental exposure.

Figure 1.1 shows the cycling processes of PAH/POP in the terrestrial ecosystem. They are released into the atmosphere from sources such as industry, transport, agriculture and open fire (Shen et al., 2013). Homogeneous gas-phase reactions with OH, O_3 and NO_3 are the main degradation paths for the gas-phase PAH/POP (Atkinson et al., 1989; Kwok et al, 1994; Klöpffer and Wagner, 2007), while multiphase reaction with O_3 is significant for the particulate-phase PAH/POP (at least verified for some PAHs) (Keyte et al., 2013). Partitioning between particulate and gas phase occurs simultaneously. Both gases and particles can be scavenged through cloud processes, dry deposition and wet deposition. Soil burden from atmospheric depositions can re-volatilize into the atmosphere once chemical equilibrium between soil and air is reached (Cousins et al., 1999).

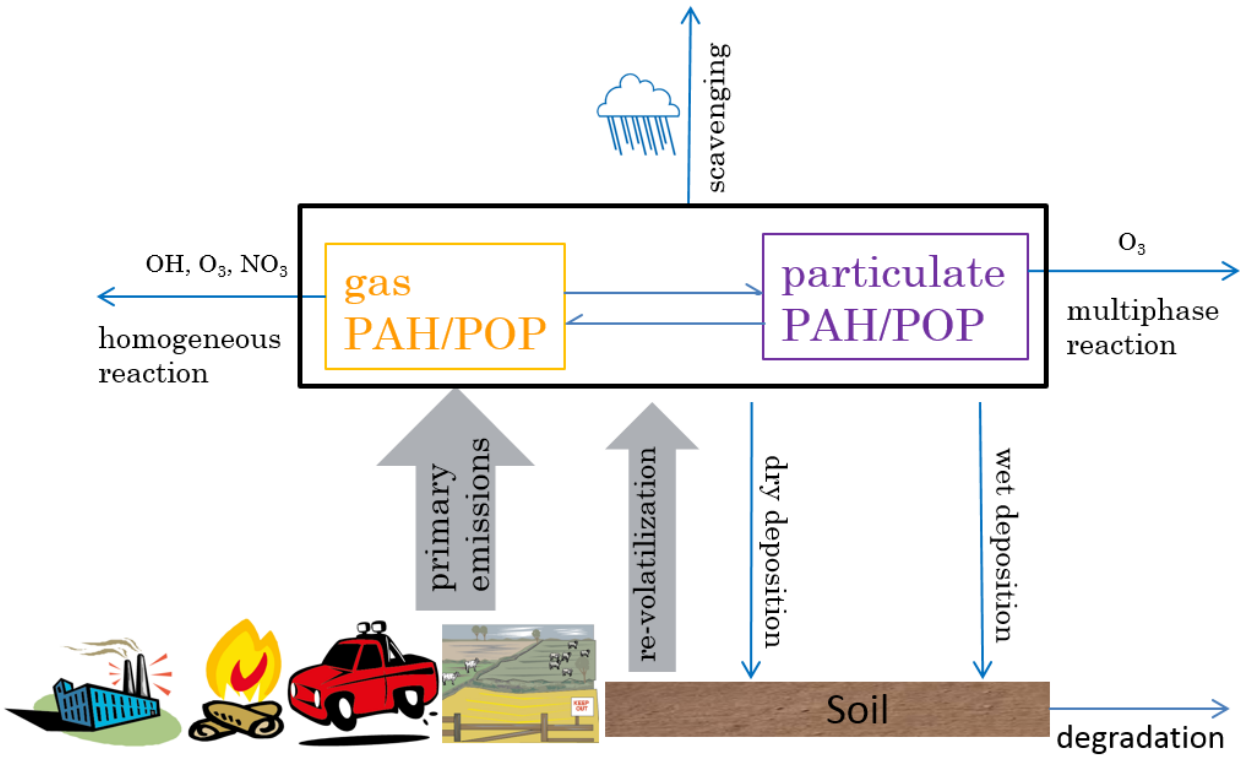

Figure 1.1. Cycling processes of PAH/POP in the terrestrial ecosystem.

In the following sub-sections, key processes will be introduced in detail. Multiphase chemistry is very important for the degradation and fate of those PAHs/POPs which mostly maintain in the particulate phase, such as benzo[a]pyrene (BaP), but most rate coefficients determined in laboratory measurements cannot represent ambient conditions which span over wide ranges of temperature and humidity. It is necessary to implement dependencies of rate coefficients on temperature and humidity. Besides, the depositions to the soil can re-volatilize into the atmosphere under certain conditions so that this important process should also not be neglected.

The WRF-Chem-PAH/POP model is to resolve detailed transport and transformation processes of PAH/POP, particularly in better temporal and spatial resolutions. Previous global and regional models have demonstrated their ability to reproduce monthly or annual variations of PAHs (Aulinger et al., 2007; Matthias et al., 2009; Bieser et al., 2012; San José et al., 2013; Efstathiou et al., 2016; Galarneau et al., 2014; Zhang et al., 2009; Zhang et al., 2011a, b; Inomata et al., 2012, 2013; Sehili and Lammel, 2007; Lammel et al., 2009; Friedman and Selin, 2012; Friedman et al., 2014a, b; Shen et al., 2014; Shrivastava et al., 2017) and halogenated POPs (Koziol and

Pudykiewicz, 2001; Strand and Hov, 1996; Hansen et al., 2004; Semeena et al., 2006; Gong et al., 2007; Meng et al., 2007; Octaviani et al., 2015) in the atmosphere, but to my knowledge, none of them resolve diurnal variation, let alone in the gas and particulate phases.

Besides, relevant processes (e.g. multiphase chemistry, gas-particle partitioning, and re-volatilization) are not well constrained in the previous modelling studies. Therefore, the newly developed WRF-Chem-PAH/POP model reflects the most up-to-date understanding of PAH/POP in the terrestrial ecosystem with the following original or updated features: (1) the gas-phase reactions include not only reactions with OH but also those with O_3 and NO_3 radical. During nights with high NO_3, the reaction with NO_3 causes a considerable nighttime decrease of gaseous PAH concentrations near Beijing (see single study 2.1.1); (2) the multiphase degradation of particulate BaP is treated with a new elaborated kinetic scheme, which considers particle phase change and chemical reactivity as a function of temperature and relative humidity. Compared with previous BaP degradation schemes, the new scheme greatly improves model performance in both near-source summer time (Xianghe site) and remote winter time (Gosan site) cases; (3) the gas-particle partitioning accounts for absorption into organic matter and adsorption onto soot (Dachs and Eisenreich, 2000; Lohmann and Lammel, 2004), which is an improvement from adsorption to only unspecific aerosol surfaces i.e., Junge-Pankow scheme (Pankow, 1987; Junge, 1977); (4) the air-soil gas exchange process embedded in the WRF-Chem-PAH/POP model is important for persistent semi-volatile PAHs/POPs.

1.2 Important processes of PAH/POP

1.2.1 Gas-particle partitioning

As for the gas-particle partitioning of PAH, one of the earliest and most widely used gas-particle partitioning schemes was parameterized by Pankow (1987) based on the work of Junge (1977), assuming that semivolatile organic compounds are sorbed to the surface of all atmospheric particles determined only by vapor pressure (adsorption). The mass fraction associated with the particulate phase is calculated according to the aerosol surface concentration and the substance's vapor pressure over the sub-cooled liquid. This parameterization often underestimates particulate mass fraction, because the chemically specific adsorption and absorption processes are neglected

(Bidleman et al., 1988). This PhD work considers one absorption process and one chemically specific adsorption process, both of which pose important impacts on the gas-particle partitioning of PAH (Dachs and Eisenreich, 2000; Lohmann and Lammel, 2004). Detailed equations and parameters of gas-particle partitioning of PAH are found in Section 2.2.3 of Appendix B.1.

Gas-particle partitioning of halogenated POPs is described as a single-parameter linear free-energy relationship, assuming absorption in organic matter to determine the overall process. The octanol-air partitioning coefficient, *K*oa, is chosen as the single parameter in the gas-particle partitioning relationship. This *K*oa model has been found to predict satisfactorily (Finizio et al., 1997).

1.2.2 Air-soil exchange

Persistent semivolatile substances are subject to re-volatilization. Air-soil gas diffusive exchange is calculated based on an air-soil model (Strand and Hov, 1996; Jury et al., 1983).

The simulated soil in the model is assumed as a thin surface layer consisting of certain ratios of air, water and organic matter (Jury et al., 1983). The change of gas concentrations in soil/air with time is determined by the soil/air layer depths, air-soil diffusive gas exchange flux, wet deposition flux as well as the degradation rate in soil. The air-soil diffusive gas exchange flux is the most important variable which is parameterized by the exchange velocity (given by the air and liquid diffusion coefficients, water-air partitioning coefficient, and water/air fractions in soil, respectively), air concentration, and partitioning coefficient between soil and air. PAH/POP are also subject to biodegradation in soil. Detailed equations and parameters of air-soil exchange are found in Section 2.2.4 of Appendix B.1.

1.2.3 Multiphase degradation of BaP

BaP, one of the most toxic PAHs, is a criteria pollutant in the European Union, the USA and Japan. Atmospheric BaP stays almost entirely in the particulate phase and undergoes multiphase degradation with ozone (Keyte et al., 2013). However, this reaction is not well characterized yet

especially for complex particle compositions in the ambient environment. According to previous laboratory experiments, the multiphase reaction is faster on the solid substrate than on liquid substrate, and slower when organic coating shields BaP from the oxidant (Pöschl et al., 2001; Kwamena et al., 2004; Kahan et al., 2006; Shiraiwa et al., 2009; Zhou et al., 2012; Zhou et al., 2013). Up to now, however, laboratory experiments have limitations that they were only performed at room temperature, and most of them were conducted at the ozone level of up to three orders of magnitude higher than that in the troposphere. Field observations show considerable degradation rate of BaP in the atmosphere (Schauer et al. 2003), and recent studies indicate that aerosol phase state, depending on temperature and humidity, has substantial impacts on the rates of gas uptake, chemical aging and oxidation of organic aerosol particles (e.g., Shiraiwa et al. 2011, Berkemeier et al. 2016). A largely simplified scheme was used by Shrivastava et al. (2017) to examine the impact of temperature and humidity on the multiphase reaction and transport of BaP, based on the experimental results of Zhou et al. (2012) and Zhou et al. (2013). In this PhD project, an elaborate kinetic scheme of the multiphase reaction, first time as a function of temperature and relative humidity covering ambient ranges, is developed and applied in model applications.

1.3 WRF-Chem model

The WRF-Chem-PAH/POP model is developed based on the open source community model WRF-Chem (Weather Research Forecast model with Chemistry module, using version 3.6.1 in this study). The physics and transport processes are based on the Advanced Research WRF core (ARW). Subroutines in the chemistry module include emission, photolysis reaction, chemical reaction in both gas and particulate phases, cloud chemistry, convective transport, and depositions. They are integrated as dynamic transport processes over the same time step, realizing the fully "online" coupling between chemistry and meteorology (Grell et al., 2005). WRF-Chem is one of the most commonly applied chemical transport models in the regional scale. Since its first release in 2002, WRF-Chem has been widely used and well evaluated for regional air quality (Kuik et al., 2016; Li et al., 2016; Zhong et al., 2016) and climate (Yahya et al., 2017; Liao et al., 2014; Zhang et al., 2014) study.

Depending on the specific chemical mechanism, WRF-Chem includes dozens of reactions and chemical compounds. It is quite time consuming and easy to make errors when manually making

changes to the reaction system, etc. adding new reaction equations. However, to rebuild the reaction systems by major revisions are sometimes unavoidable. Therefore, the Kinetic PreProcessor (KPP) automatic code generation has become a good tool to assist the work (Sandu et al., 2003; Sandu and Sander, 2006; Damian et al., 2002) and it has been successfully implemented into the WRF-Chem model. Moreover, a WRF-Chem-KPP coupler can automatically create the interface between the KPP modules and the WRF-Chem model. The coupler is compiled automatically with WRF-Chem compilation and significantly minimizes the effort to modify compounds and/or reactions to the chemical mechanisms.

The following model configurations are made. Gas-phase reactions follow the Regional Atmospheric Chemistry Mechanism (RACM) (Stockwell et al., 1997). The aerosol parameterization takes the Modal Aerosol Dynamics Model for Europe (MADE) (Ackermann et al., 1998) for the inorganic aerosols, and the Secondary Organic Aerosol Model (SORGAM) (Schell et al., 2001) for the secondary organic aerosols. The MADE/SORGAM aerosol module in WRF-Chem uses the mode approach. To include PAH/POP in air-soil gas exchange processes, the Noah soil scheme (Chen and Dudhia, 2001) is chosen. The short chemistry time step of 150 seconds also made the model suitable for simulating short-lived compounds. All other chemical compounds simulated in the standard WRF-Chem model are also simulated normally in WRF-Chem-PAH/POP.

Figure 1.2 shows the framework of modifications in the standard WRF-Chem model in order to include new PAH/POP species.

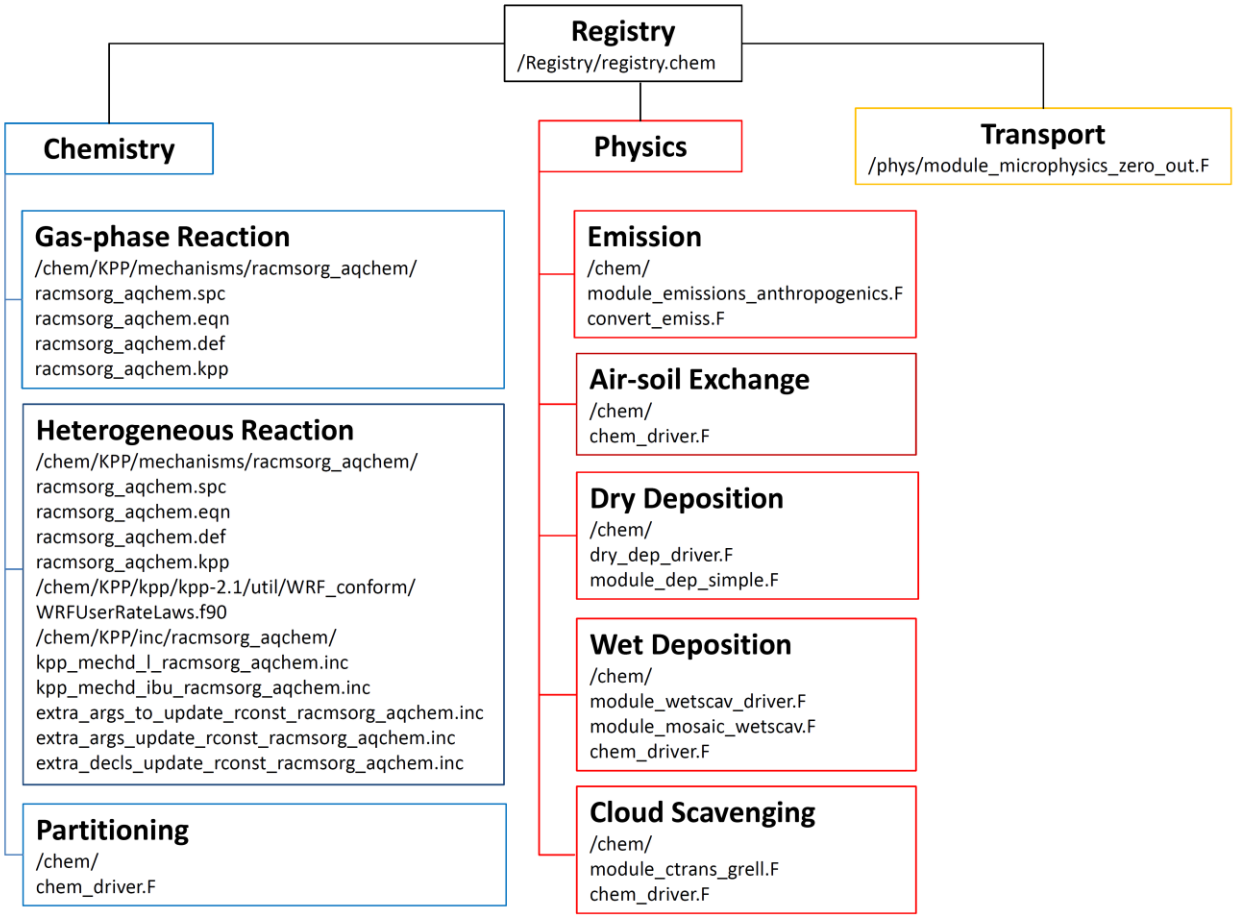

Figure 1.2. Framework of PAH/POP extensions in the WRF-Chem routines. All of the above routines have been modified. Air-soil exchange has been added as a new module. The most important modules for the application studies are emission, transport, heterogeneous reaction and air-soil exchange (see Fig. 1.3).

1.4 Design of the PhD study

This PhD thesis aims at developing a regional PAH/POP model which includes all the significant processes of atmospheric cycling in the terrestrial environment, to evaluate the model against various kinds of observations in high temporal resolution, to apply the model for better understanding of physicochemical processes of PAH/POP. An overview of the related publications is shown in Fig. 1.3.

Model development and evaluation is the base of the PhD work. Thus, the first study is to develop the WRF-Chem-PAH/POP model and evaluate it against observations in high temporal resolution (Mu et al., ready for submission). Based on the WRF-Chem-PAH/POP model, two major applications are performed: (1) to study the long-range transport potential of BaP influenced by a newly developed kinetic multiphase scheme (Mu et al., *Sci. Adv.*, 2018); (2) to explore the air-soil exchange of POPs before and during the South Asia summer monsoon (Lammel et al., *ACP*, submitted). Results of model development and these two application studies are summarized in Chapter 2.1.

The major goals and work of the PhD study are summarised as follows:

(1) Develop the WRF-Chem-PAH/POP model. Extend the regional scale WRF-Chem chemical transport model to include all the important processes of PAH/POP. These processes include emissions, transport, gas-phase reaction, multiphase reaction, gas-particle partitioning, cloud scavenging, dry deposition, wet deposition and air-soil diffusive gas exchange. The most up-to-date schemes till 2016 are implemented. Evaluate model performance against observations at near-source and major outflow sites in East Asia, under high temporal and spatial resolutions. Sensitivity tests show that including some previously neglected processes in the model development is indispensable.

(2) Implement a kinetic multiphase degradation framework for particulate BaP, depending on temperature and humidity, into the WRF-Chem-PAH/POP model. Compare the new kinetic scheme with existing laboratory schemes at various measurement sites from near-source to the remote Arctic sites. Imply the long-range transport potential of particulate PAH in different seasons, altitudes and latitudes.

(3) Adapt the WRF-Chem-PAH/POP model for POPs in a South Asia domain. Simulate the pre-monsoon and monsoon scenarios in India. Compare the simulated near-ground air concentrations and direction of air-soil exchange fluxes of POPs with observations. The simulation supports the hypothesis that the summer monsoon triggers the re-volatilization (or suppresses the dry gaseous deposition) of POPs which have accumulated in soil.

During the PhD study, I have also participated in the following studies: new chemical pathway of sulfate formation (Cheng et al., *Sci. Adv.*, 2016), emission and long-range transport of elemental

carbon (EC) (Chen et al., *ACP*, 2016a), and particle size of sea salt and nitrate (Chen et al., *ACP*, 2016b).

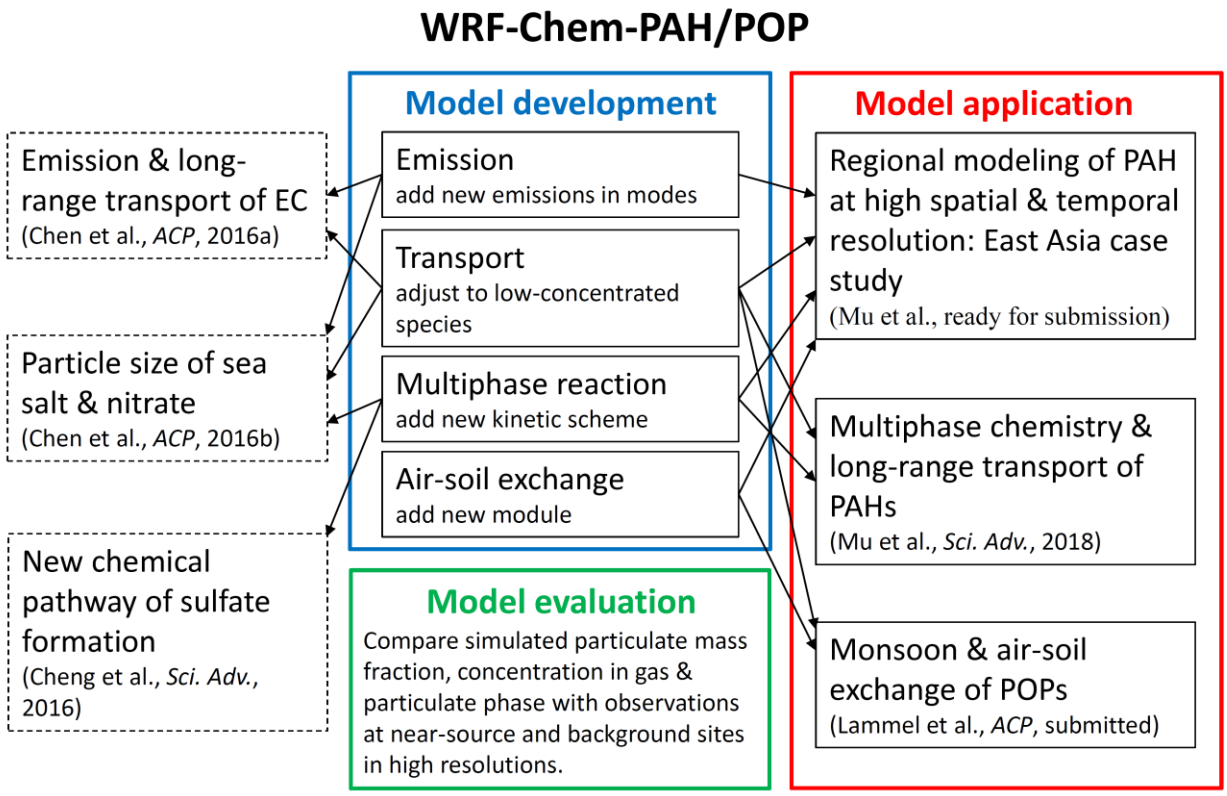

Figure 1.3. Design of the PhD study. The PhD study is about WRF-Chem-PAH/POP model development (blue box), evaluation (green box) and application (red box). The dashed boxes represent model applications that are not the main focus of this PhD work but with my contributions. All the new features developed in the model are applied in all the application studies. The arrows indicate the study with an emphasis of the corresponding newly implemented process.

2. Results and conclusions

2.1 Single studies

2.1.1 Model development and evaluation

The online coupled meteorology-chemistry model WRF-Chem is extended to thoroughly study the fate and atmospheric distribution of semivolatile PAH/POP compounds. The WRF-Chem-PAH/POP model demonstrates the latest scientific understanding (until 2016) of current PAH/POP studies, but with some updated or new features. The selected PAHs/POPs are representative of different volatility and hydrophobicity. The simulated concentrations and particulate mass fractions of PAHs were compared with observations in high temporal resolution (Section 4 of Appendix B.1). Concentration levels and particulate mass fractions of PAHs can be generally well reproduced by the WRF-Chem-PAH/POP model at near-source and major outflow regions in East Asia, in high temporal and spatial resolutions. Further simulation tests indicate that the gas-phase reaction with NO_3 and the multiphase reaction with O_3 are unneglectable (Section 5 of Appendix B.1). The technique of adding extra new species and solution of the transport problem in WRF-Chem are not limited to PAH/POP.

More details can be found in Appendix B.1, Mu et al., ready for submission.

2.1.2 Multiphase reaction scheme of BaP

Temperature and humidity have a substantial impact on the phase state, diffusivity and reactivity of BaP-containing particles. This study develops a new kinetic scheme that realistically describes the multiphase reaction of BaP with O_3 depending on temperature and humidity ("BaP degradation kinetic scheme" of Appendix B.2). The new multiphase reaction scheme can well improve the simulations of multi-scale models, agreeing better with the observed BaP concentrations than the previous schemes in various kinds of sites ("Model versus observation" of Appendix B.2). Modeling results show that low temperature and humidity can greatly increase the lifetime of BaP

and enhance its atmospheric dispersion through both the planetary boundary layer and the free troposphere ("East Asia outflow" and "Transport to the Arctic" of Appendix B.2). It is implied that temperature and humidity effects should also be carefully considered for other multiphase reactions in aerosols, clouds and fogs.

More details can be found in Appendix B.2, Mu et al., *Sci. Adv.*, 2018.

2.1.3 Air-soil exchange with onset of the South Asian summer monsoon

The study simulates the air concentration and air-soil exchange of POPs before and during the South Asian summer monsoon (Section 2.3 of Appendix B.3). The simulated results agree generally well with observations. This confirms the hypothesis that the clean air masses from the Indian Ocean are brought to the coast by the onset of South Asian summer monsoon. The clean air masses can enhance the re-volatilization of nowadays banned chemicals hexachlorocyclohexane (HCH) and polychlorinated biphenyls (PCBs) from background soil to the atmosphere, and restrain the dry deposition of dichlorodiphenyltrichloroethane (DDT) in India (Section 3.2 of Appendix B.3).

More details can be found in Appendix B.3, Lammel et al., *Atmos. Chem. Phys.*, submitted.

2.1.4 Summary and conclusion

(1) Successfully develop and evaluate the WRF-Chem-PAH/POP model.

The PhD work first extended the processes of PAH/POP into the regional chemical transport model WRF-Chem to study the atmospheric fate of PAH/POP, including volatile (e.g. PHE), semivolatile (e.g. CHR) and non-volatile (e.g. BaP) compounds. The included processes for PAH/POP are: emission, air-soil gas exchange, gas-to-particle partitioning, gas-phase reaction, multiphase reaction, cloud process, dry deposition and wet deposition. Also, the transport module is updated to be applied for any low-concentrated species. High temporal and spatial resolutions are unique for this model. It is evaluated against daily to diurnal continuous observations in both gas and particulate phases. The model simulates atmospheric

concentrations and particulate mass fractions of PAHs at near-source and major outflow sites reasonably well. The multiphase reaction with O_3 and the gas-phase reaction with NO_3 are indispensable for the understanding of the atmospheric cycling of at least some PAHs.

(2) Implement the kinetic multiphase degradation scheme of BaP and proof its significance on the long-range transport potential of BaP.

The new kinetic scheme considers the strong temperature/RH effects on organic aerosol phase state and the corresponding long-range transport potential of BaP. Aerosol particles are more liquid in warm/humid environments, while more solid in cold environment. The phase state and degradation rate of BaP may vary largely depending on temperature/RH and hence the season (summer vs winter), altitude (surface vs high altitude) and latitude (tropical vs polar). For example, under low temperatures, particulate organic matter and reactive compounds sorbed to it will degrade slower and may transported much further. The large impact of temperature/RH on the diffusivity/reactivity is not limited to BaP and the oxidant ozone, but has implications for other inorganic and organic particulate-phase compounds subject to oxidant attack. Those reactions can also be described as functions of temperature and humidity when more kinetic data is available. Hence, the atmospheric fate and long-range transport potential of more pollutants can be characterized.

(3) Simulate and reveal that South Asian summer monsoon can trigger the re-volatilization of pre-contaminated soil POPs.

The PhD work provides the modeling proof for this so far overlooked process of pollutant cycling over the Indian subcontinent. The results show that re-volatilizations of a number of persistent pollutants are triggered by the low concentrations in relatively pristine air, most pronounced in areas that receive marine background air, i.e. in southwestern India during monsoon onset. This re-volatilization weakens as a function of distance from the coast, as the monsoon advection propagates across the subcontinent. Also, the monsoon rains enhance air-to-soil transfer of pollutants. The southwesterly monsoon in 2014 was relatively weak according to the South Asian summer monsoon index compared to the long-term mean. Even stronger re-volatilization is expected for strong monsoon events. A similar mechanism can be expected for other semivolatile organic substances such as PAH, fluorinated and brominated chemicals.

3. References

Atkinson, R., Baulch, D. L., Cox, R. A., Hampson, R. F., Kerr, J. A., and Troe, J.: Evaluated kinetic and photochemical data for atmospheric chemistry - Supplement-III, Int. J. Chem. Kinet., 21, 115-150, 10.1002/kin.550210205, 1989.

Aulinger, A., Matthias, V., and Quante, M.: Introducing a partitioning mechanism for PAHs into the Community Multiscale Air Quality modeling system and its application to simulating the transport of benzo(a) pyrene over Europe, J. Appl. Meteorol. Clim., 46, 1718-1730, 10.1175/2007jamc1395.1, 2007.

Berkemeier, T., Steimer, S. S., Krieger, U. K., Peter, T., Pöschl, U., Ammann, M., and Shiraiwa, M.: Ozone uptake on glassy, semi-solid and liquid organic matter and the role of reactive oxygen intermediates in atmospheric aerosol chemistry, Phys. Chem. Chem. Phys., 18, 12662-12674, 10.1039/c6cp00634e, 2016.

Bieser, J., Aulinger, A., Matthias, V., and Quante, M.: Impact of emission reductions between 1980 and 2020 on atmospheric benzo[a]pyrene concentrations over Europe, Water Air Soil Poll., 223, 1393-1414, 10.1007/s11270-011-0953-z, 2012.

Bidleman, T. F.: Atmospheric processes, Environ. Sci. Technol., 22, 361-367, 10.1021/es00169a002, 1988.

Binkowski, F. S., and Roselle, S. J.: Models-3 community multiscale air quality (CMAQ) model aerosol component - 1. Model description, J. Geophys. Res., 108, 4183, 10.1029/2001jd001409, 2003.

Chen, Y., Cheng, Y. F., Nordmann, S., Birmili, W., Denier van der Gon, H. A. C., Ma, N., Wolke, R., Wehner, B., Sun, J., Spindler, G., Mu, Q., Pöschl, U., Su, H., and Wiedensohler, A.: Evaluation of the size segregation of elemental carbon (EC) emission in Europe: influence on the simulation of EC long-range transportation, Atmos. Chem. Phys., 16, 1823-1835, 10.5194/acp-16-1823-2016, 2016a.

Chen, Y., Cheng, Y. F., Ma, N., Wolke, R., Nordmann, S., Schüttauf, S., Ran, L., Wehner, B., Birmili, W., Denier van der Gon, H. A. C., Mu, Q., Barthel, S., Spindler, G., Stieger, B., Muller, K., Zheng, G. J., Pöschl, U., Su, H., and Wiedensohler, A.: Sea salt emission, transport and influence on size-segregated nitrate simulation: a case study in northwestern Europe by WRF-Chem, Atmos. Chem. Phys., 16, 12081-12097, 10.5194/acp-16-12081-2016, 2016b.

Cheng, Y., Zheng, G., Wei, C., Mu, Q., Zheng, B., Wang, Z., Gao, M., Zhang, Q., He, K., Carmichael, G., Pöschl, U., and Su, H.: Reactive nitrogen chemistry in aerosol water as a source of sulfate during haze events in China, Sci. Adv., 2, 10.1126/sciadv.1601530, 2016.

Cousins, I. T., Beck, A. J., Jones, K. C.: A review of the processes involved in the exchange of semivolatile organic compounds (SVOC) across the air-soil interface, Sci. Total Environ., 228, 5-24, 1999.

Dachs, J., and Eisenreich, S. J.: Adsorption onto aerosol soot carbon dominates gas-particle partitioning of polycyclic aromatic hydrocarbons, Environ. Sci. Technol., 34, 3690-3697, 10.1021/Es991201+, 2000.

Efstathiou, C. I., Matejovicová, J., Bieser, J., and Lammel, G.: Evaluation of gas-particle partitioning in a regional air quality model for organic pollutants, Atmos. Chem. Phys., 16, 15327-15345, 10.5194/acp-16-15327-2016, 2016.

Finizio, A., Mackay, D., Bidleman, T., and Harner, T.: Octanol-air partition coefficient as a predictor of partitioning of semi-volatile organic chemicals to aerosols, Atmos. Environ., 31, 2289-2296, 10.1016/S1352-2310(97)00013-7, 1997.

Friedman, C. L., and Selin, N. E.: Long-Range atmospheric transport of polycyclic aromatic hydrocarbons: a global 3-D model analysis including evaluation of arctic sources, Environ. Sci. Technol., 46, 9501-9510, 10.1021/Es301904d, 2012.

Friedman, C. L., Pierce, J. R., and Selin, N. E.: Assessing the influence of secondary organic versus primary carbonaceous aerosols on long-Range atmospheric polycyclic aromatic hydrocarbon transport, Environ. Sci. Technol., 48, 3293-3302, 10.1021/Es405219r, 2014a.

Friedman, C. L., Zhang, Y. X., and Selin, N. E.: Climate change and emissions impacts on atmospheric PAH transport to the Arctic, Environ. Sci. Technol., 48, 429-437, 10.1021/Es403098w, 2014b.

Galarneau, E., Makar, P. A., Zheng, Q., Narayan, J., Zhang, J., Moran, M. D., Bari, M. A., Pathela, S., Chen, A., and Chlumsky, R.: PAH concentrations simulated with the AURAMS-PAH chemical transport model over Canada and the USA, Atmos. Chem. Phys., 14, 4065-4077, 10.5194/acp-14-4065-2014, 2014.

Gong, S. L., Huang, P., Zhao, T. L., Sahsuvar, L., Barrie, L. A., Kaminski, J. W., Li, Y. F., and Niu, T.: GEM/POPs: a global 3-D dynamic model for semi-volatile persistent organic pollutants - Part 1: Model description and evaluations of air concentrations, Atmos. Chem. Phys., 7, 4001-4013, 2007.

Hansen, K. M., Christensen, J. H., Brandt, J., Frohn, L. M., and Geels, C.: Modelling atmospheric transport of alpha-hexachlorocyclohexane in the Northern Hemisphere with a 3-D dynamical model: DEHM-POP, Atmos. Chem. Phys., 4, 1125-1137, 2004.

Huang, P., Gong, S. L., Zhao, T. L., Neary, L., and Barrie, L. A.: GEM/POPs: a global 3-D dynamic model for semi-volatile persistent organic pollutants - Part 2: Global transports and budgets of PCBs, Atmos. Chem. Phys., 7, 4015-4025, 2007.

Hylland, K.: Polycyclic aromatic hydrocarbon (PAH) ecotoxicology in marine ecosystems, J. Toxicol. Env. Heal. A., 69, 109-123, 10.1080/15287390500259327, 2006.

Inomata, Y., Kajino, M., Sato, K., Ohara, T., Kurokawa, J. I., Ueda, H., Tang, N., Hayakawa, K., Ohizumi, T., and Akimoto, H.: Emission and atmospheric transport of particulate PAHs in Northeast Asia, Environ. Sci. Technol., 46, 4941-4949, 10.1021/Es300391w, 2012.

Inomata, Y., Kajino, M., Sato, K., Ohara, T., Kurokawa, J., Ueda, H., Tang, N., Hayakawa, K., Ohizumi, T., and Akimoto, H.: Source contribution analysis of surface particulate polycyclic aromatic hydrocarbon concentrations in northeastern Asia by source-receptor relationships, Environ. Pollut., 182, 324-334, 10.1016/j.envpol.2013.07.020, 2013.

Jury, W. A., Spencer, W. F., and Farmer, W. J.: Behavior assessment model for trace organics in soil. 1. Model description, J. Environ. Qual., 12, 558-564, 1983.

Kahan, T. F., Kwamena, N. O. A., and Donaldson, D. J.: Heterogeneous ozonation kinetics of polycyclic aromatic hydrocarbons on organic films, Atmos. Environ., 40, 3448-3459, 10.1016/j.atmosenv.2006.02.004, 2006.

Keyte, I. J., Harrison, R. M., and Lammel, G.: Chemical reactivity and long-range transport potential of polycyclic aromatic hydrocarbons - a review, Chem. Soc. Rev., 42, 9333-9391, 10.1039/C3cs60147a, 2013.

Klöpffer W., Wagner B. O.: Atmospheric degradation of organic substances: persistence, transport potential, spatial range. Wiley, 2008.

Koziol, A. S., and Pudykiewicz, J. A.: Global-scale environmental transport of persistent organic pollutants, Chemosphere, 45, 1181-1200, 10.1016/S0045-6535(01)00004-2, 2001.

Kwamena, N. O. A., Thornton, J. A., and Abbatt, J. P. D.: Kinetics of surface-bound benzo[a]pyrene and ozone on solid organic and salt aerosols, J. Phys. Chem. A, 108, 11626-11634, 10.1021/Jp046161x, 2004.

Kwok, E. S. C., Harger, W. P., Arey, J., and Atkinson, R.: Reactions of gas-phase phenanthrene under simulated atmospheric conditions, Environ. Sci. Technol., 28, 521-527, 10.1021/es00052a027, 1994.

Lammel, G., Sehili, A. M., Bond, T. C., Feichter, J., and Grassl, H.: Gas/particle partitioning and global distribution of polycyclic aromatic hydrocarbons - A modelling approach, Chemosphere, 76, 98-106, 10.1016/j.chemosphere.2009.02.017, 2009.

Lohmann, R., and Lammel, G.: Adsorptive and absorptive contributions to the gas-particle partitioning of polycyclic aromatic hydrocarbons: state of knowledge and recommended parametrization for modeling, Environ. Sci. Technol., 38, 3793-3803, 10.1021/Es035337q, 2004.

Lv, Y., Li, X., Xu, T. T., Cheng, T. T., Yang, X., Chen, J. M., Iinuma, Y., and Herrmann, H.: Size distributions of polycyclic aromatic hydrocarbons in urban atmosphere: sorption mechanism and source contributions to respiratory deposition, Atmos. Chem. Phys., 16, 2971-2983, 10.5194/acp-16-2971-2016, 2016.

Matthias, V., Aulinger, A., and Quante, M.: CMAQ simulations of the benzo(a)pyrene distribution over Europe for 2000 and 2001, Atmos. Environ., 43, 4078-4086, 10.1016/j.atmosenv.2009.04.058, 2009.

Meng, F., Zhang, B. N., Gbor, P., Wen, D. Y., Yang, F. Q., Shi, C. N., Aronson, J., and Sloan, J.: Models for gas/particle partitioning, transformation and air/water surface exchange of PCBs and PCDD/Fs in CMAQ, Atmos. Environ., 41, 9111-9127, 10.1016/j.atmosenv.2007.08.009, 2007.

Octaviani, M., Stemmler, I., Lammel, G., and Graf, H. F.: Atmospheric transport of persistent organic pollutants to and from the Arctic under present-day and future climate, Environ. Sci. Technol., 49, 3593-3602, 10.1021/e55056369, 2015.

Pankow, J. F.: Review and comparative-analysis of the theories on partitioning between the gas and aerosol particulate phases in the atmosphere, Atmos. Environ., 21, 2275-2283, 10.1016/0004-6981(87)90363-5, 1987.

Pöschl, U., Letzel, T., Schauer, C., and Niessner, R.: Interaction of ozone and water vapor with spark discharge soot aerosol particles coated with benzo[a]pyrene: O_3 and H_2O adsorption, benzo[a]pyrene degradation, and atmospheric implications, J. Phys. Chem. A, 105, 4029-4041, 10.1021/Jp004137n, 2001.

San José, R., Perez, J. L., Callen, M. S., Lopez, J. M., and Mastral, A.: BaP (PAH) air quality modelling exercise over Zaragoza (Spain) using an adapted version of WRF-CMAQ model, Environ. Pollut., 183, 151-158, 10.1016/j.envpol.2013.02.025, 2013.

Schauer, C., Niessner, R., and Pöschl, U.: Polycyclic aromatic hydrocarbons in urban air particulate matter: Decadal and seasonal trends, chemical degradation, and sampling artifacts, Environ. Sci. Technol., 37, 2861-2868, 10.1021/es034059s, 2003.

Sehili, A. M., and Lammel, G.: Global fate and distribution of polycyclic aromatic hydrocarbons emitted from Europe and Russia, Atmos. Environ., 41, 8301-8315, 10.1016/j.almosenv.2007.06.050, 2007.

Semeena, V. S., Feichter, J., and Lammel, G.: Impact of the regional climate and substance properties on the fate and atmospheric long-range transport of persistent organic pollutants - examples of DDT and gamma-HCH, Atmos. Chem. Phys., 6, 1231-1248, 2006.

Shen, H. Z., Huang, Y., Wang, R., Zhu, D., Li, W., Shen, G. F., Wang, B., Zhang, Y. Y., Chen, Y. C., Lu, Y., Chen, H., Li, T. C., Sun, K., Li, B. G., Liu, W. X., Liu, J. F., and Tao, S.: Global

atmospheric emissions of polycyclic aromatic hydrocarbons from 1960 to 2008 and future predictions, Environ. Sci. Technol., 47, 6415-6424, 10.1021/Es400857z, 2013.

Shen, H. Z., Tao, S., Liu, J. F., Huang, Y., Chen, H., Li, W., Zhang, Y. Y., Chen, Y. C., Su, S., Lin, N., Xu, Y. Y., Li, B. G., Wang, X. L., and Liu, W. X.: Global lung cancer risk from PAH exposure highly depends on emission sources and individual susceptibility, Sci. Rep., 4, 10.1038/Srep06561, 2014.

Shiraiwa, M., Garland, R. M., and Pöschl, U.: Kinetic double-layer model of aerosol surface chemistry and gas-particle interactions (K2-SURF): Degradation of polycyclic aromatic hydrocarbons exposed to O_3, NO_2, H_2O, OH and NO_3, Atmos. Chem. Phys., 9, 9571-9586, 10.5194/acp-9-9571-2009, 2009.

Shiraiwa, M., Ammann, M., Koop, T., and Pöschl, U.: Gas uptake and chemical aging of semisolid organic aerosol particles, Proc. Natl. Acad. Sci. USA, 108, 11003-11008, 10.1073/pnas.1103045108, 2011.

Shrivastava, M., Lou, S., Zelenyuk, A., Easter, R. C., Corley, R. A., Thrall, B. D., Rasch, P. J., Fast, J. D., Massey Simonich, S. L., Shen, H., and Tao, S.: Global long-range transport and lung cancer risk from polycyclic aromatic hydrocarbons shielded by coatings of organic aerosol, Proc. Natl. Acad. Sci. USA, 114, 1246-1251, 10.1073/pnas.1618475114, 2017.

Strand, A., and Hov, Ø.: A model strategy for the simulation of chlorinated hydrocarbon distributions in the global environment, Water Air Soil Poll., 86, 283-316, 10.1007/Bf00279163, 1996.

WHO: Polynuclear aromatic hydrocarbons in drinking-water, background document for development of WHO guidelines for drinking-water quality, 2003.

Zhang, Y., Tao, S., Ma, J., and Simonich, S.: Transpacific transport of benzo[a]pyrene emitted from Asia, Atmos. Chem. Phys., 11, 11993-12006, 10.5194/acp-11-11993-2011, 2011a.

Zhang, Y. X., Tao, S., Shen, H. Z., and Ma, J. M.: Inhalation exposure to ambient polycyclic aromatic hydrocarbons and lung cancer risk of Chinese population, Proc. Natl. Acad. Sci. USA, 106, 21063-21067, 10.1073/pnas.0905756106, 2009.

Zhang, Y. X., Shen, H. Z., Tao, S., and Ma, J. M.: Modeling the atmospheric transport and outflow of polycyclic aromatic hydrocarbons emitted from China, Atmos. Environ., 45, 2820-2827, 10.1016/j.atmosenv.2011.03.006, 2011b.

Zhou, S., Lee, A. K. Y., McWhinney, R. D., and Abbatt, J. P. D.: Burial effects of organic coatings on the heterogeneous reactivity of particle-borne benzo[a]pyrene (BaP) toward ozone, J. Phys. Chem. A, 116, 7050-7056, 10.1021/Jp3030705, 2012.

Zhou, S. M., Shiraiwa, M., McWhinney, R. D., Pöschl, U., and Abbatt, J. P. D.: Kinetic limitations in gas-particle reactions arising from slow diffusion in secondary organic aerosol, Faraday Discuss., 165, 391-406, 10.1039/C3fd00030c, 2013.

A. Personal list of publications

Journal Articles

1 Mu, Q., Lammel, G., Gencarelli, C. N., Hedgecock, I. M., Chen, Y., Přibylová, P., Zhang, Y., Zheng, G., Zhang, Q., Shiraiwa, M., Spichtinger, P., Su, H., Pöschl, U., and Cheng, Y.: Regional modelling of polycyclic aromatic hydrocarbons: WRF-Chem-PAH model development and East Asia case studies. Ready for submission.

2 Mu, Q., Shiraiwa, M., Octaviani, M., Ma, N., Ding, A., Su, H., Lammel, G., Pöschl, U., Cheng, Y.: Temperature effect on phase state and reactivity controls atmospheric multiphase chemistry and transport of PAHs. Sci. Adv., 4, 10.1126/sciadv.aap7314, 2018.

3 Lammel, G., Degrendele, C., Gunthe, S., Mu, Q., Muthalagu, A., Audy, O., Biju, C., Petr, K., Mulder, M., Octaviani, M., Příbylová, P., Shahpoury, P., Stemmler, I., Valsan, A.: Re-volatilisation of soil accumulated pollutants triggered by the summer monsoon in India. Atmos. Chem. Phys., submitted.

4 Cheng, Y., Zheng, G., Wei, C., Mu, Q., Zheng, B., Wang, Z., Gao, M., Zhang, Q., He, K., Carmichael, G., Pöschl, U., and Su, H.: Reactive nitrogen chemistry in aerosol water as a source of sulfate during haze events in China, Sci. Adv., 2, 10.1126/sciadv.1601530, 2016.

5 Chen, Y., Cheng, Y.-F., Nordmann, S., Birmili, W., Denier van der Gon, H. A. C., Ma, N., Wolke, R., Wehner, B., Sun, J., Spindler, G., Mu, Q., Pöschl, U., Su, H., and Wiedensohler, A.: Evaluation of the size segregation of elemental carbon (EC) emission in Europe: influence on the simulation of EC long-range transportation, Atmos. Chem. Phys., 16, 1823-1835, 10.5194/acp-16-1823-2016, 2016a.

6 Chen, Y., Cheng, Y., Ma, N., Wolke, R., Nordmann, S., Schüttauf, S., Ran, L., Wehner, B., Birmili, W., Denier van der Gon, H. A. C., Mu, Q., Barthel, S., Spindler, G., Stieger, B., Müller, K., Zheng, G.-J., Pöschl, U., Su, H., and Wiedensohler, A.: Sea salt emission, transport and influence on size-segregated nitrate simulation: a case study in northwestern Europe by WRF-Chem, Atmos. Chem. Phys., 16, 12081-12097, 10.5194/acp-16-12081-2016, 2016b.

7 Lou, S., Liao, H., Yang, Y., and Mu, Q.: Simulation of the interannual variations of tropospheric ozone over China: Roles of variations in meteorological parameters and anthropogenic emissions, Atmos. Environ., 122, 839–851, 10.1016/j.atmosenv.2015.08.081, 2015.

8 Mu, Q. and Liao, H.: Simulation of the interannual variations of aerosols in China: role of variations in meteorological parameters, Atmos. Chem. Phys., 14, 9597-9612, 10.5194/acp-14-9597-2014, 2014.

9 Zhu, J., Wang, T., Xing, L., Mu, Q., and Zhou, D.: Analysis on the characteristics and mechanism of a heavy haze episode in Jiangsu Province, China Environmental Science, 31(12), 1943-1950, 2011.

Oral presentations

1 Mu Q., et al.: WRF-Chem-POP model development and applications. Oral presentation. WRF-Chem DE meeting, Potsdam, Germany, June 2017.

2 Mu Q., et al.: WRF-Chem-PAH model development and validation with observations in East Asia. Oral presentation. Max Planck Graduate Center Lecture Cycle, Mainz, Germany, May 2016.

Poster presentations

1 Mu Q., et al.: Regional modeling of polycyclic aromatic hydrocarbon-model development and evaluation. Poster presentation. General Assembly of the European Geoscience Union, Vienna, Austria, April 2015.

2 Mu Q., et al.: Simulation of the interannual variations of aerosols in China: role of variations in meteorological parameters. Poster presentation. Conference on Earth System Science, Mainz, Germany, March 2015.

3 Mu Q. and Liao H.: Simulation of the interannual variations of aerosols in China: role of meteorology. Poster presentation. The 6th International GEOS-Chem meeting, Boston, USA, May 2013.

B. Selected publications

Mu, Q., Lammel, G., Gencarelli, C. N., Hedgecock, I. M., Chen, Y., Přibylová, P., Zhang, Y., Zheng, G., Zhang, Q., Shiraiwa, M., Spichtinger, P., Su, H., Pöschl, U., and Cheng, Y.: Regional modelling of polycyclic aromatic hydrocarbons: WRF-Chem-PAH model development and East Asia case studies. Ready for submission.[1]

Mu, Q., Shiraiwa, M., Octaviani, M., Ma, N., Ding, A., Su, H., Lammel, G., Pöschl, U., Cheng, Y.: Temperature effect on phase state and reactivity controls atmospheric multiphase chemistry and transport of PAHs. Sci. Adv., 4, 10.1126/sciadv.aap7314, 2018.

Lammel, G., Degrendele, C., Gunthe, S., Mu, Q., Muthalagu, A., Audy, O., Biju, C., Petr, K., Mulder, M., Octaviani, M., Příbylová, P., Shahpoury, P., Stemmler, I., Valsan, A.: Re-volatilisation of soil accumulated pollutants triggered by the summer monsoon in India. Atmos. Chem. Phys., submitted.

[1] An earlier version of this article was retracted because of mistakes that have been corrected in the present version (Mu et al., Atmos. Chem. Phys., 17, 12253-12267, 2017; https://doi.org/10.5194/acp-17-12253-2017-editorial-note).

B.1 Mu et al., ready for submission

Regional modelling of polycyclic aromatic hydrocarbons: WRF-Chem-PAH model development and East Asia case studies

Qing Mu[1], Gerhard Lammel[1,2], Christian N. Gencarelli[3], Ian M. Hedgecock[3], Ying Chen[1,4*], Petra Přibylová[2], Yuxuan Zhang[1], Guangjie Zheng[5], Qiang Zhang[6], Manabu Shiraiwa[1,7], Peter Spichtinger[8], Hang Su[9,1], Ulrich Pöschl[1], and Yafang Cheng[1,9]

[1]Multiphase Chemistry Department, Max Planck Institute for Chemistry, Mainz, Germany
[2]Research Centre for Toxic Compounds in the Environment, Masaryk University, Brno, Czech Republic
[3]CNR-Institute of Atmospheric Pollution Research, Division of Rende, Rende, Italy
[4]Leibniz Institute for Tropospheric Research, Leipzig, Germany
[5]Brookhaven National Laboratory, Brookhaven, USA
[6]Ministry of Education Key Laboratory for Earth System Modeling, Department of Earth System Science, Tsinghua University, Beijing, China
[7]Department of Chemistry, University of California, Irvine, USA
[8]Institute for Atmospheric Physics, Johannes Gutenberg University, Mainz, Germany
[9]Institute for Environmental and Climate Research, Jinan University, Guangzhou, China

*now at Lancaster Environment Centre, Lancaster University, United Kingdom

Author contributions:

Y. F. C., G. L., U. P., and H. S. conceived the study. Q. M. accomplished model development, case simulation, data processing and visualization. M. S., Y. F. C., H. S. and U. P. developed the kinetic heterogeneous degradation scheme of BaP for model implementation. C. N. G. and I. M. H. provided the code of WRF-Chem-Hg (Gencarelli et al., 2014) and helped with model development. Y. C. contributed to data processing. P. P., Y. Z., G. Z. and Q. Z. produced and quality-controlled the field data at the Xianghe site. Y. F. C., Q. M., G. L., H. S., U. P. and P. S. discussed the results. Q. M., Y. F. C. and G. L. wrote the manuscript.

Regional modelling of polycyclic aromatic hydrocarbons: WRF-Chem-PAH model development and East Asia case studies

Qing Mu[1], Gerhard Lammel[1,2], Christian N. Gencarelli[3], Ian M. Hedgecock[3], Ying Chen[1,4*], Petra Přibylová[2], Yuxuan Zhang[1], Guangjie Zheng[5], Qiang Zhang[6], Manabu Shiraiwa[1,7], Peter Spichtinger[8], Hang Su[9,1], Ulrich Pöschl[1], Yafang Cheng[1,9]

[1]Multiphase Chemistry Department, Max Planck Institute for Chemistry, Mainz, Germany
[2]Research Centre for Toxic Compounds in the Environment, Masaryk University, Brno, Czech Republic
[3]CNR-Institute of Atmospheric Pollution Research, Division of Rende, Rende, Italy
[4]Leibniz Institute for Tropospheric Research, Leipzig, Germany
[5]Brookhaven National Laboratory, Brookhaven, USA
[6]Ministry of Education Key Laboratory for Earth System Modeling, Department of Earth System Science, Tsinghua University, Beijing, China
[7]Department of Chemistry, University of California, Irvine, USA
[8]Institute for Atmospheric Physics, Johannes Gutenberg University, Mainz, Germany
[9]Institute for Environmental and Climate Research, Jinan University, Guangzhou, China
*now at Lancaster Environment Centre, Lancaster University, United Kingdom

Correspondence to: Y. Cheng (yafang.cheng@mpic.de) or G. Lammel (g.lammel@mpic.de)

Abstract. Polycyclic aromatic hydrocarbons (PAHs) are hazardous pollutants, with increasing emissions in pace with economic development in East Asia, but their fate and distributions in the atmosphere have not yet been well understood. We extend the regional atmospheric chemistry model WRF-Chem (Weather Research Forecast model with Chemistry module) to comprehensively study the atmospheric fate and distributions of the low concentrated, slowly degrading semivolatile compounds. The WRF-Chem-PAH model reflects the state-of-the-art understanding of the current PAH studies with several new or updated features. It is applied for PAHs covering a wide range of volatility and hydrophobicity i.e., phenanthrene, chrysene and benzo[a]pyrene, in East Asia. Simulated concentrations and particulate mass fractions of PAHs are evaluated against observations with high temporal resolution. The WRF-Chem-PAH model can reasonably well simulate the concentration levels and particulate mass fractions of PAHs near the sources and in the major outflow region of East Asia, at high spatial and temporal resolutions. A sensitivity study shows that the heterogeneous reaction with ozone and the homogeneous reaction with the nitrate radical significantly influence the fate and distributions of PAHs.

1 Introduction

Polycyclic aromatic hydrocarbons (PAHs), released into the atmosphere as by-products of all kinds of combustion processes, are harmful for human health via inhalation as well as ingestion pathways (World Health Organization, 2003; Lv et al., 2016) and for ecosystems (Hylland, 2006). In the atmospheric environment PAHs are partly readily degradable, partly undergo long-range transport and reach remote areas (Keyte et al., 2013). PAHs have been included in the United Nations Economic Commission for Europe Convention on Long-range Transboundary Air Pollution and Protocol on Persistent Organic Pollutants. Some hazardous substances, mostly benzo[a]pyrene (BaP), are criteria pollutants in many countries, including the European Union, the USA and Japan. The United States Environmental Protection Agency (USEPA) prioritized 16 PAHs in the 1970s, which have been mostly targeted in the environment since then, but this selection is questionable considering toxicity and occurrence of PAHs (Andersson and Achten, 2015).

As PAHs are mainly emitted from incomplete combustion of various kinds of organic matters, their emissions increase dramatically in Asia due to rapid economic development and energy consumption. According to Zhang and Tao (2009), and Zhang et al. (2011a), the total emission of the 16 USEPA prioritized PAH was about 290 Gg yr^{-1} in Asia in the year 2004, which was more than 50% of global emissions. The high levels of PAHs in Asia pose a hazard to the ecosystems and human health on regional and global scales (Hung et al., 2005).

As recently outlined by Galarneau et al. (2014), a wide range of different modelling approaches have been used to investigate the atmospheric fate and large-scale distribution of PAHs (van Jaarsveld et al., 1997; Halsall et al., 2001; Yaffe et al., 2001; Prevedouros et al., 2004; Aulinger et al., 2007; Liu et al., 2007; Sehili and Lammel, 2007; Lang et al., 2007, 2008; Prevedouros et al., 2008; Lammel et al., 2009; Matthias et al., 2009; Zhang et al., 2009, 2011a, b; Bieser et al., 2012; Friedman and Selin, 2012; Inomata et al., 2012, 2013; San José et al., 2013; Friedman et al., 2014a, b; Shen et al., 2014; Galarneau et al., 2014; Efstathiou et al., 2016; Shrivastava et al., 2017). Since its initial release in 2002, the WRF-Chem model (Weather Research and Forecasting model with Chemistry module) has been widely applied and verified for regional air quality (Zhang et al., 2010; Zhang et al., 2013) and climate (Liao et al., 2014; Yahya et al., 2016) studies with high temporal and spatial resolutions. In comparison to the previous PAH modelling studies, this one is unique as it (1) includes all processes which determine PAH cycling in the atmospheric environment over land (i.e., new heterogeneous degradation scheme, several oxidants in homogeneous degradation processes, and re-volatilisation from soil, among others), (2) validates against observed concentrations of PAHs in gas and particulate phase separately, (3) validates atmospheric concentrations and particulate mass fractions of PAHs against diurnal observations, and (4) explores the significance of the heterogeneous reaction of PAH with ozone (O_3) and the gas-phase reaction with the nitrate radical (NO_3).

2 Model development

The WRF-Chem-PAH model is based on the regional open-source community model WRF-Chem (version 3.6.1) with fully coupled meteorological and chemical components (Grell et al., 2005). The WRF-Chem model is used with a short chemistry time step (150 s) suitable for studying short-lived species with high spatial heterogeneity (Lowe et al., 2015).

The Regional Atmospheric Chemistry Mechanism (RACM) (Stockwell et al., 1997) is used for homogeneous gas-phase reactions. The aerosol module includes the Modal Aerosol Dynamics Model for Europe (MADE) (Ackermann et al., 1998) for the inorganic fraction, and the Secondary Organic Aerosol Model (SORGAM) (Schell et al., 2001) for the secondary organic aerosols. MADE/SORGAM in the WRF-Chem model uses the modal approach with three log-normally distributed modes: Aitken, accumulation and coarse mode. All pollutant species normally simulated in the standard RACM/SORGAM mechanism are also simulated in the WRF-Chem-PAH model.

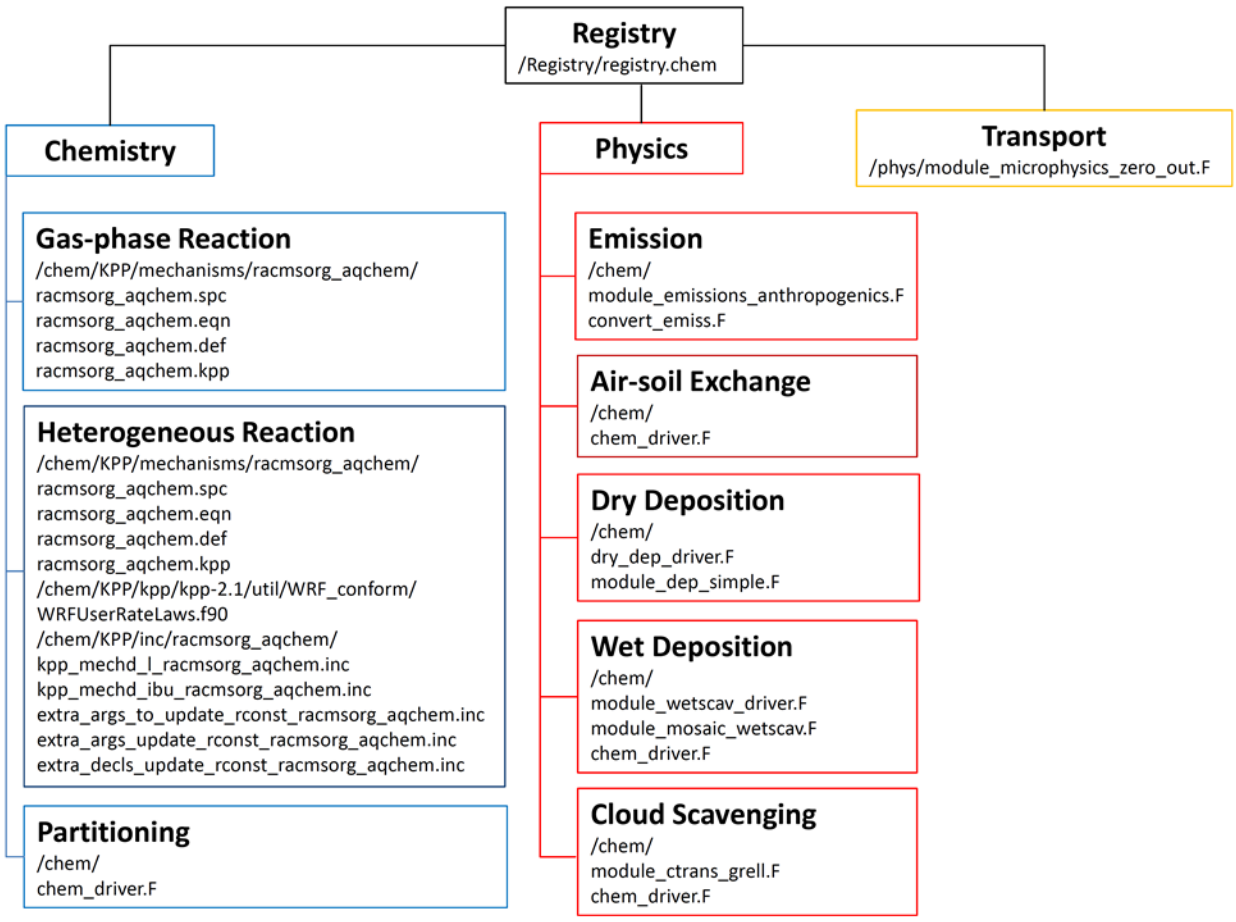

Figure 1. Framework of PAH extensions in WRF-Chem.

2.1 Framework

Figure 1 shows the framework of PAH extensions in the WRF-Chem model, where modules/subroutines that have been modified to implement PAH extensions are listed. All the new variables related to emissions and concentration fields of PAHs or used in relevant parameterisations i.e., air-soil gas exchange, gas-phase/heterogeneous reactions, cloud scavenging, dry/wet deposition, advective transport and cumulus convection, are first defined in registry.chem and then included in respective sub-modules/routines.

The subroutine chem_driver is the main driver for handling chemistry related tasks at a particular time step, including emissions, photolysis, gas- and particulate-phase reactions, convective transport, cloud chemistry, and dry/wet depositions. Based on the existing structure, all the chemical reactions involving gaseous and particulate PAHs mentioned in section 2.2.1 and 2.2.2 have been added to the RACMSORG_AQCHEM chemical mechanism by using the KPP and the WRF-Chem KPP Coupler (Salzmann and Lawrence, 2006). Fixed rate coefficients are used for gas-phase reactions, while for heterogeneous reactions oxidant/temperature/humidity -dependent functions are formulated. Gas-particle partitioning of semivolatile PAHs (and organic compounds in general) is implemented based on the substance-specific empiric equilibrium relationship in addition to the MADE/SORGAM module. Dry deposition, wet deposition and wet scavenging from cumulus convection are calculated in the respective subroutines, using the dry deposition velocity and the fraction of gaseous species dissolved in

cloud water calculated in module_dep_simple and module_mosaic_wetscav, respectively. The air-soil gas exchange for organic compounds (secondary emission, see Section 2.2.4) is implemented in addition to the primary emission module.

The simulated PAHs in our current WRF-Chem-PAH model include phenanthrene (PHE), chrysene (CHR) and BaP, representing volatile, semivolatile and non-volatile PAH compounds, respectively. The WRF-Chem-PAH model framework is not limited to three species, and all semivolatile compounds can be similarly implemented.

2.2 Atmospheric processes of PAHs

2.2.1 Gas-phase reactions

Reactions of gas-phase PAHs with hydroxyl radical (OH), NO_3 and O_3 are considered in this model. While NO_3 reaction appears to be less significant than OH reaction as the main PAH degradation process, observations of some nitro-PAH yields suggest that nighttime reactions of PAHs with NO_3 can be very significant (Atkinson and Arey, 1994; Keyte et al., 2013). The significance of NO_3 oxidation is further discussed in Section 6. Here, the PAH oxidative loss is calculated as a second-order process using the model-predicted OH and NO_3 concentrations (Table 1). At this stage, the products of PAH reactions are not explicitly considered in the model.

Table 1. Physical and chemical properties of PAHs and soil.

Parameter	Symbol	Unit	RP[a]	PHE	CHR	BaP	Reference
molecular weight	MW	g mol^{-1}		178.2	228.3	252.3	
gas-phase OH reaction rate constant	k_{OH}	cm^3 molec^{-1} s^{-1}		[a]3.1E-11	[b]5.0E-11	[b]1.5E-10	[a]Atkinson et al. (1989); [b]Klöpffer and Wagner (2008)
gas-phase NO_3 reaction rate constant	k_{NO3}	cm^3 molec^{-1} s^{-1}		[a]1.2E-13	4E-12	[b]5.4E-11	[a]Kwok et al. (1994); [b]Kloepffer and Wagner (2007)
gas-phase O_3 reaction rate constant	k_{O3}	cm^3 molec^{-1} s^{-1}		[a]4.0E-19	[b]4.0E-19	[b]2.6E-17	[a]Kwok et al. (1994); [b]Kloepffer and Wagner (2007)
soot-water partitioning coefficient	K_{SW}	L kg^{-1}		4.34E+05	2.82E+07	9.59E+07	Galarneau et al. (2014)
octanol-air partitioning coefficient	K_{OA}	dimensionless	m	3293	4754	5382	Odabasi et al. (2006)
			b	-3.37	-5.65	-6.50	
air-water partitioning coefficient	K_{AW}	dimensionless	m	-5689.20	-12136.16	-4437.10	Bamford et al. (1999)
			b	12.750	32.235	3.988	
soil degradation rate	k_{soil}	s^{-1}		1.00E-08	1.00E-08	1.00E-08	Mackay and Paterson (1991)
water content of soil	l	dimensionless		0.3	0.3	0.3	Jury et al. (1983)
air content of soil	α	dimensionless		0.2	0.2	0.2	Jury et al. (1983)
soil depth	z_s	m		0.15	0.15	0.15	Jury et al. (1983)
bulk density of soil	ρ_s	kg m^{-3}		1350	1350	1350	Jury et al. (1983)
organic carbon fraction of soil	f_{OC}	dimensionless		0.0125	0.0125	0.0125	Jury et al. (1983)
air diffusion coefficient of soil	D_{air}	m^2 s^{-1}		5.00E-06	5.00E-06	5.00E-06	Jury et al. (1983)
water diffusion coefficient of soil	D_{water}	m^2 s^{-1}		5.00E-10	5.00E-10	5.00E-10	Jury et al. (1983)

[a] RP = regression parameter for semi-logarithmic temperature-dependent form. m and b represent slope and intercept, respectively. log K_{OA} = m/T(K) + b. ln K_{AW} = m/T(K) + b.

2.2.2 Heterogeneous degradation of particulate BaP

In this study, we have applied a more elaborate parameterisation of the heterogeneous reaction kinetics of BaP degradation by ozone as a function of temperature and relative humidity based on the experimental data of Zhou et al. (2013) and the kinetic multi-layer model KM-SUB (Shiraiwa et al., 2010). The model approach and parameterisation build on a Langmuir-Hinshelwood reaction mechanism involving the decomposition of O_3 and the formation of long-lived reactive oxygen intermediates (Shiraiwa et al., 2011; Berkemeier et al., 2016). This scheme has first been developed by Mu et al. (2018). Table S2 lists the parameterisations of the reaction rates. Text S1 reviews the previous study of the heterogeneous degradation of BaP.

2.2.3 Gas/particle partitioning

The default configuration of the WRF-Chem model uses a thermodynamic equilibrium scheme (SORGAM) to simulate gas-to-particle mass distribution of condensable and water-soluble species (Binkowski and Roselle, 2003). This approach is inappropriate for semivolatile and hydrophobic substances. Instead, an empiric equilibrium partitioning expression for PAHs is applied. We consider both absorption into organic matter and adsorption to soot, which are found to be significant contributors to PAH gas-particle partitioning (Dachs and Eisenreich, 2000; Lohmann and Lammel, 2004).

Correspondingly, the equilibrium partitioning expression for PAHs accounts for two contributions, absorption into organic matter and adsorption onto elemental carbon (EC) following Dachs and Eisenreich (2000):

$$K_p = 10^{-12}\left(\frac{1.5 f_{OC}}{\rho_{oct}} K_{OA} + f_{EC} K_{SA}\right) = \frac{\sum c_p / c_{TSP}}{c_g} \quad (1)$$

$$\theta = \left(1 + \frac{1}{K_p c_{TSP}}\right)^{-1} \quad (2)$$

Here f_{OC} and f_{EC} are the mass fractions of organic carbon (OC) and EC in the particulate matter; ρ_{oct} is the density of octanol (0.82 kg L^{-1}) and K_{OA} is the octanol–air partitioning coefficient (Odabasi et al., 2006); K_{SA} is the soot–air partitioning coefficient (L kg^{-1}); $\sum c_p$ is the particulate PAH concentration integrated over the aerosol size distribution (ng m^{-3}); c_{TSP} is the total suspended particulate concentration (µg m^{-3}); c_g is the PAH gas-phase concentration (ng m^{-3}). The factor of 1.5 is assumed to convert the mass concentration of OC into that of organic matter following Dachs and Eisenreich (2000). For PAHs, K_{SA} values are not directly available from experiments, but can be calculated as the ratio of the soot–water partitioning coefficient K_{SW} to the air–water partitioning coefficient K_{AW} (Galarneau et al., 2014). For this purpose, we adopted K_{SW} values from Galarneau et al. (2014), who had derived these values from K_{SW} values reported for different combustion technologies (Jonker and Koelmans, 2002) in combination with the emission inventory of Galarneau et al. (2007), and K_{AW} values from Bamford et al. (1999) (Table 1).

2.2.4 Air-soil gas exchange

Semivolatile PAHs are subject to re-volatilization (Lammel et al., 2009; Galarneau et al., 2014). An air-soil gas exchange module is therefore included in the WRF-Chem-PAH model. Air-soil gas exchange is parameterised following Strand and Hov (1996), which is based on Jury et al. (1983) and has also been described by Hansen et al. (2004) as follows.

Model soil is a 0.15 m thick layer consisting of fixed volumes of soil organic matter, air and water, assuming the same properties as Jury et al. (1983) (Table 1). PAH concentrations in soil/air, c_s/c_a, changing with time is expressed by:

$$\frac{\partial c_s}{\partial t} = \frac{1}{z_s}\left(F_{exc,soil} + F_{wet}\right) - k_{soil} c_s \quad (3)$$

$$\frac{\partial c_a}{\partial t} = -\frac{1}{z_a} F_{exc,soil} \quad (4)$$

where z_s and z_a are the soil and atmospheric layer depths (m), respectively, $F_{exc,soil}$ is the air-soil gas exchange flux, F_{wet} is the wet deposition flux, and k_{soil} is the degradation rate in soil. The air-soil gas exchange flux is given by:

$$F_{exc,soil} = v_s\left(c_a - \frac{c_s}{K_{soil-air}}\right) \quad (5)$$

where v_s is the exchange velocity, c_a is the PAH concentration in air, and $k_{soil\text{-}air}$ is the partitioning coefficient between soil and air. The exchange velocity is given by:

$$v_s = \frac{D_{air} a^{10/3}(1-l-a)^{-2} + D_{water} l^{10/3} K_{WA}(1-l-a)^{-2}}{z_s/2} \quad (6)$$

where D_{air} and D_{water} are the air and liquid diffusion coefficients, K_{WA} is the water-air partitioning coefficient depending on the soil temperature and equals the inverse of K_{AW}, l and a are the water and air fractions in soil. Partitioning between soil and air is given by Karickhoff (1981):

$$K_{soil-air} = 4.11 \times 10^{-4} \times \rho_s f_{oc} K_{OA} \quad (7)$$

where ρ_s is the density of soil, f_{OC} is the OC fraction in soil and 4.11×10^{-4} is a constant with units of m^3 kg^{-1}. PAHs are subject to biodegradation in soil, processes which are actually not well quantified. The degradation rate in soil k_{soil} is assumed to be 10^{-8} s^{-1} based on a laboratory model ecosystems study (Lu et al., 1977), following a global PAH model (Friedman et al., 2014a; Friedman et al., 2014b).

Due to a lack of monitoring data, the PAH concentrations in soil are initialized by the global multicompartmental model output: a pseudo-steady state of anthracene (ANT), fluoranthene (FLT) and BaP concentrations in the soil compartment has been safely reached by a global simulation over 10 years with a horizontal resolution of 2.8° x 2.8° (Lammel et al., 2009). PHE/CHR concentrations in soil are scaled from ANT/FLT concentrations according to the ratio upon primary emission. Figure S1 shows the air-soil gas exchange flux at a receptor site based on the above air-soil exchange scheme.

2.2.5 Wet and dry depositions

In analogy to Gencarelli et al. (2014), the dry deposition of gas-phase species in the WRF-Chem model is based on the standard resistance approach described by Wesely (1989). The standard WRF-Chem routines have been extended to include the deposition of gas-phase PAH compounds, and the dry deposition flux is calculated as the product of the deposition velocity and the concentration of gaseous PAH in the lowermost model level. The dry deposition of particulate-phase PAH species is calculated using the standard WRF-Chem particulate deposition parameterisations.

The model accounts for wet deposition of PAH species through the schemes for gas and particulate convective transport, in-cloud and below-cloud scavenging of PAH species (sub-grid resolution, following the University of California Irvine chemistry transport model; Neu and Prather, 2012).

3 Modification of transport scheme for low concentrated species

The transport of BaP seems stopped (Fig. 2a) when we follow the WRF-Chem manual's suggestion by running with the monotonic advection (chem, moist, scalar_adv_opt = 2), while the transport of other chemical species behaves normally e.g., EC, as shown in Fig. 2d. This is because the atmospheric concentration of BaP is too low, down to 10^{-9} to 10^{-12} ppmv. Other species are dealt with similarly, when artificially brought to extremely low concentrations, as confirmed for EC: The species does not undergo transport when dividing the EC concentration by 10^{10} before and then multiply by 10^{10} after the advection subroutine. Figure 2c and 2d show clear differences between the transportation of EC in these two cases. Besides, the near source concentration of BaP is too low compared with the observation, because in the unmodified (conventional) transport non-zero BaP concentrations in air are limited to the immediate vicinities to strong sources and undergo fast degradation.

One of the important features of how the chemical transport model (Chem) couples with WRF in the WRF-Chem model is that the transport of chemical species is done by WRF. In WRF, monotonic advection is not a positive definite option, so that mp_zero_out = 2 is usually set to make sure that the

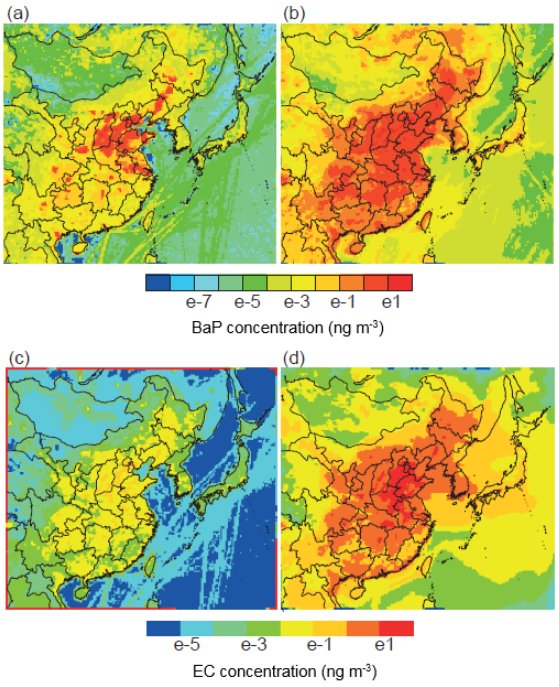

Figure 2. Simulated near-ground concentrations of BaP with (a) conventional transport scheme and (b) modified transport scheme for low concentrated species, and EC with (c) scaled low concentration and (d) normal concentration with conventional transport scheme averaged on 14 February 2003.

transport tendency of all the moisture variables will not grow below zero. To this end, the mp_zero_out_thresh is set as suggested to a small value of 10^{-8}, and the transport tendency of moisture variables will be mapped to 0 when concentrations are smaller than mp_zero_out_thresh. In the coupled WRF-Chem model, when dealing with chemical transport, the WRF advection module treats all the chemical species as if they are moisture variables following the same criterion of exceedance of mp_zero_out_thresh. This is usually not a problem, because the concentrations of species transported are in general higher than this threshold. However, it is not the case for BaP, and the threshold truncates the BaP concentration and its transport tendency is forced to 0 and thus no transport occurs. To cope with this, we set mp_zero_out_thresh = 10^{-22} for PAH species but leave it to 10^{-8} to moisture variables and all other chemical species. After this modification in advective transportation, BaP adequately undergoes transport in the model and the near source concentrations of BaP are elevated too (Fig. 2b). This solution can be applied to all newly implemented low concentrated species in the WRF-Chem model.

4 Case study in East Asia

4.1 Model configuration

To apply the WRF-Chem-PAH model, we configure a domain that covers East China and Japan (15–55º N, 95–155º E; Fig. 2) with a horizontal resolution of 27 km by 27 km and 39 vertical layers up to 0.01 hPa.

The physics options applied in this study are summarized as follows (also see Table S1). The Purdue–Lin scheme (Lin et al., 1983) is used for microphysics. The planetary boundary layer is parameterised by the Mellor–Yamada–Janjic scheme (Janjic, 1994). As outlined in earlier studies like Gencarelli et al. (2014), the scheme describes vertical sub-grid-scale fluxes due to eddy transport in the whole atmospheric column, and the horizontal eddy diffusivity is calculated with a Smagorinsky first-order closure. The surface layer parameterisation takes the Eta Similarity surface layer scheme (Janjic, 1994). The land surface model describing air-soil interactions is the Noah Land Surface Model (Chen and Dudhia, 2001). The Grell-3D Ensemble scheme (Grell and Devenyi, 2002) is used for cumulus parameterisation. The long- and shortwave radiation is calculated on-line with rapid radiative transfer model (Mlawer et al., 1997) and the Goddard schemes (Chou and Suarez, 1994), respectively. Photolysis rates are calculated using the Fast-J photolysis scheme (Wild et al., 2000) and updated every 60 minutes.

For simulation of the standard aerosol precursors and aerosol species in the WRF-Chem model, anthropogenic emissions for NOx, CO, non-methane volatile organic

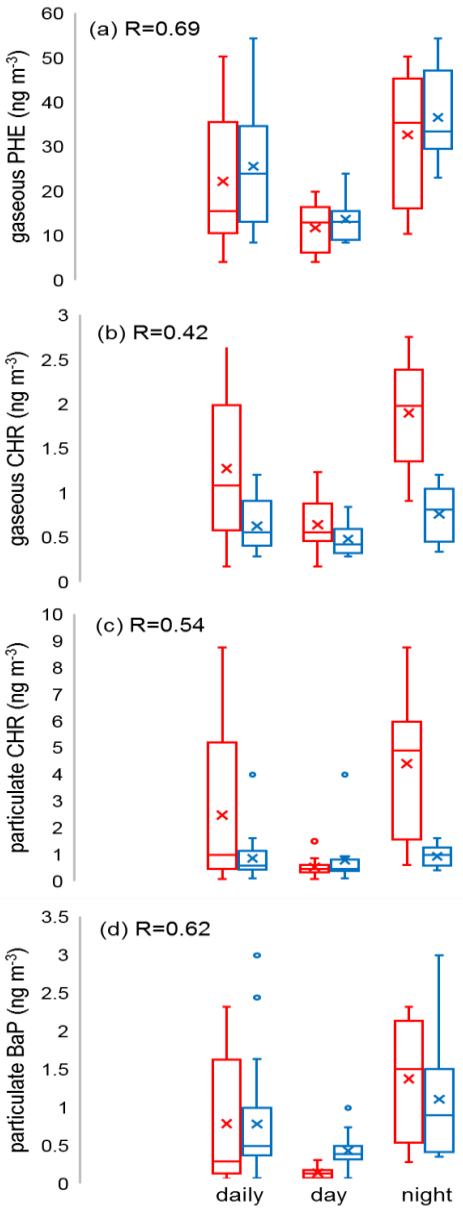

Figure 3. Simulated (red) and observed (blue) concentrations of (a) gaseous PHE, (b) gaseous CHR, (c) particulate CHR and (d) particulate BaP at the Xianghe site averaged over 11–22 July, 2013. The line and "X" in each box are the median and mean, while the boxes represent the 25th and 75th percentiles. Upper whisker is quartile 3 (Q3) + 1.5 × interquartile range (IQR) or maximum value, whichever is smaller; lower whisker is quartile 1 (Q1) - 1.5 × IQR or minimum value, whichever is larger. The Spearman's rank correlation coefficients R use combined daytime and nighttime data

compounds, SO_2, NH_3, EC, and OC are taken from the EDGAR-HTAP global monthly inventory (http://edgar.jrc.ec.europa.eu/national_reported_data/htap.php) in the year 2010. The emissions of EC and OC in 2010 are further extrapolated to the simulated year based on the interannual scaling factors taken from Lu et al. (2011), while no annual changes have been applied to emissions of other species. The EDGAR-HTAP inventory has a horizontal resolution of 0.1°. Hereby, biomass burning emissions are from the monthly Quick Fire Emissions Dataset (QFED) (Darmenov and Silva, 2013). Biogenic volatile organic compounds emissions are calculated from the Model of Emissions of Gases and Aerosols from Nature (MEGAN) (Guenther et al., 2006). Anthropogenic PAH emissions are re-gridded from a 0.1° × 0.1° global annual PAH emission inventory for the year 2008, with 69 detailed source types (Shen et al., 2013). For the specific simulated period, the interannual scaling factors in the simulated domain are taken from Shen et al. (2013), which are based on the historical fuel consumption data and IPCC SRES A1 scenario supposing a future world of rapid economic growth. Monthly scaling factors are taken from Zhang and Tao (2008). We apply a diurnal cycle of the PAH emissions with two maxima, 08:00 h and 19:00 h local time, following the cycle of EC. Biogenic contributions to PAH emission have been neglected. Figure S2 shows the average distributions of PHE, CHR and BaP emissions in July 2013. Figure S3 shows the interannual, monthly and hourly scaling factors for PAH emissions.

Meteorological initial and boundary conditions are based on the National Center for Environmental Prediction Final Analysis' (NCEP-FNL) reanalysis data. Meteorology (temperature, horizontal wind, and moisture) is nudged at all vertical levels. Chemical initial and boundary conditions of a standard set of tracers are from the global Model for Ozone and Related Chemical Tracers (MOZART-4) (Emmons et al., 2010), simulating with a horizontal resolution of 1.9º × 2.5º. The initial

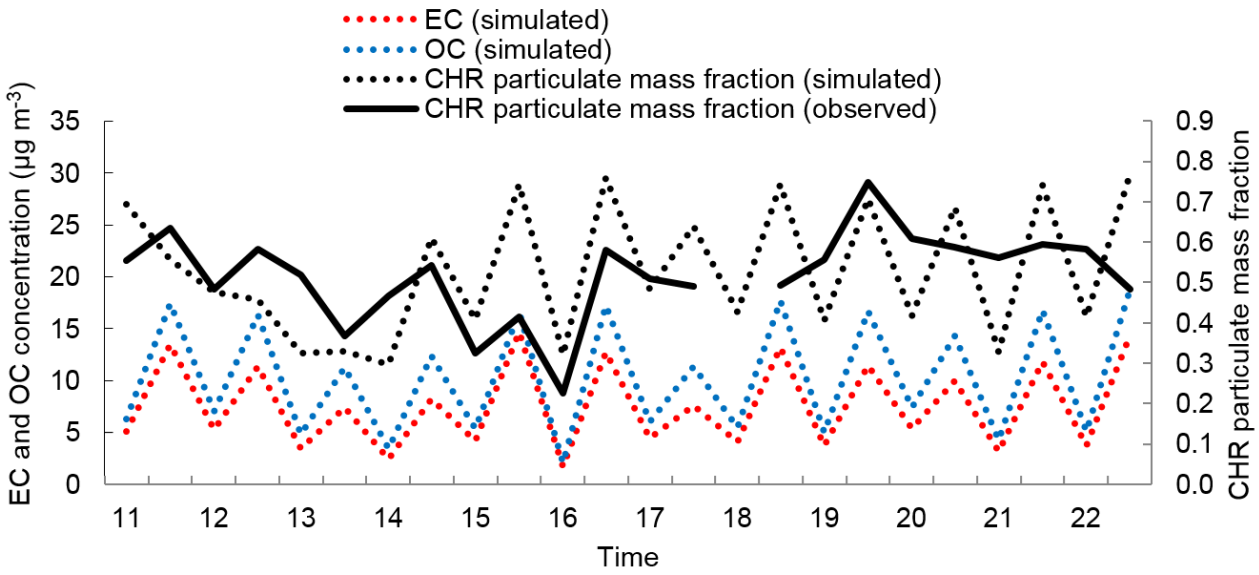

Figure 4. Simulated and observed particulate mass fraction of CHR, and simulated EC and OC concentrations at the Xianghe site during 11–22 July 2013 (10 h means).

PAH concentrations at all lateral boundaries are set to zero, because China is the dominant emission country in the region and the emission density is generally lower in the neighbouring countries. To reach a steady state equilibrium concentration of PAHs in air, a spin-up time of 48 hours is used.

4.2 Model evaluation

The WRF-Chem-PAH model is developed to capture the PAH transport episode with higher temporal and spatial resolutions, i.e. at diurnal to daily time scales and in both concentration level and particulate mass fraction. To this end, data sets of PAH field measurements with at least daily resolution and in both gaseous and particulate phase from two types of sites i.e., near-source and receptor, are studied.

The first dataset provides both daytime and nighttime samples. As part of the Program of Campaigns of Air Quality Research in Beijing and Surrounding Regions (CAREBeijing) 2013 campaign, measurements were made at the Xianghe Atmospheric Observatory (39.80° N, 116.96° E). Xianghe is a suburban and near-source site in the metropolitan area, 45 km southeast of Beijing and 70 km northwest of Tianjin (Fig. S2). The site is surrounded by the residential suburban areas and distanced about 5 km from the local town centre. Particulate- and gas-phase samples are collected twice a day (daytime samples 8:00 – 18:00 LT, nighttime samples 20:00 – 6:00 LT) during 11–22 July 2013. Details of the sampling methods and data quality control are described in Text S2.

Field datasets obtained at the Gosan station (33.28º N, 126.17º E, 72 m above sea level) are studied. Gosan is located on Jeju Island in the northern part of the East China Sea, about 100 km south of the Korean peninsula (Fig. S2). It is a representative background site and an ideal location for studying long-range transport of air pollutants in East Asia (Han et al., 2006; Kim et al., 2007; Kim et al., 2012). We focus on an intensive measurement period (14–25 February 2003) with continuous gas- and particulate phase PAHs (daily samples of 8:00–8:00 LT in the following morning) to represent a polluted continental outflow in East Asia in winter. Furthermore, a summer period, 6–17 June 2003, is simulated. Details of sampling and analysis methods are given in Kim et al., 2012.

4.2.1 Evaluation at the near source areas

PAH diurnal variabilities are well captured for both gas- and particulate-phase species at the Xianghe site, with correlation coefficients of 0.42–0.69 (Fig. 3, Table S3). Correlation coefficients of 0.30–0.58 between simulated and observed PAH concentrations in the area (Beijing; Inomata et al., 2012) are reported. This demonstrates the model's good capability in predicting the vertical and horizontal transport of PAH. The simulated gas-phase PHE has the best correlation rate of 0.69 and also the best predicted average concentrations among the other PAH species (Fig. 3). The model well catches the observed daily average concentration of particulate BaP (observed 0.78 ng m^{-3}, simulated 0.78 ng m^{-3}), while Inomata et al. (2012) underestimates daily concentration of BaP by about a factor of 2. The nighttime and daytime average concentrations of particulate BaP, 1.10 and 0.43 ng m^{-3}, are predicted as 1.37 and 0.14 ng m^{-3}, respectively. Both predicted gas- and particulate-phase CHR concentrations are overestimated (Fig. 3b–c). Further diurnal comparisons reveal that such overestimate of daily CHR concentrations mainly comes from nighttime rather than daytime discrepancies (Table S3). One reason may be that the same hourly, monthly and interannual scaling factors of CHR emissions (Fig. S3) are applied all over the domain, although these may have spatial and weekday-to-weekend variations. Furthermore, as partitioning strongly influences atmospheric lifetime, the bias in the predicted particulate mass fraction can cause a bias in the predicted concentrations of CHR.

The simulated values of particulate mass fractions are close to the measured values (black solid and dotted lines in Fig. 4): the observed (simulated) average particulate mass fraction is 0.52 (0.53) for 24 h, 0.49 (0.42) for daytime and 0.54 (0.65) for nighttime (Fig. S5). However, it is worth notifying that the good prediction of particulate mass fraction might also result from the combined effects of an overestimation of EC and an underestimation of OC concentrations. This is suggested by observation at the Xianghe site during a similar period in summer (9 to 14 July and 21 July to 1 August 2013; Teich et al., 2017): Compared with the observed average concentrations of EC and OC, 3.07 and 13.9 μg m^{-3}, respectively, our simulated concentrations of EC and OC, 7.6 and 10.4 μg m^{-3}, imply an overestimation of EC and an underestimation of OC concentrations. Besides, the correlation coefficient between simulated and observed particular mass fraction, 0.31, is not significant at the 95% confidence level (t-test), suggesting simulation uncertainties not only affecting the average but also the variation of EC and OC concentrations.

Overall, the model is found to predict the diurnal variations of PAH concentrations and particulate mass fractions reasonably well at the suburban site in the source region.

4.2.2 Evaluation of the Asian outflow

PAH predictions at remote sites are more challenging than near sources, as the uncertainties in chemistry and gas-particle partitioning propagate along transport. Model validations so far have been limited to seasonal features (Zhang et al., 2011a; Zhang et al., 2011b), while higher temporal feature has not been addressed yet. For example, discrepancies of a factor of 16–476 between predicted and observed average PAH (BaP, CHR, BbF, BkF, IcdP, DahA, BghiP) concentrations at the Waliguan site, a continental background site for ambient air monitoring in western China, are found much larger than at urban or suburban sites (Zhang et al., 2009). In our study, the predicted concentrations in the Gosan winter case agree well with the observations: the observed (simulated) average concentrations of

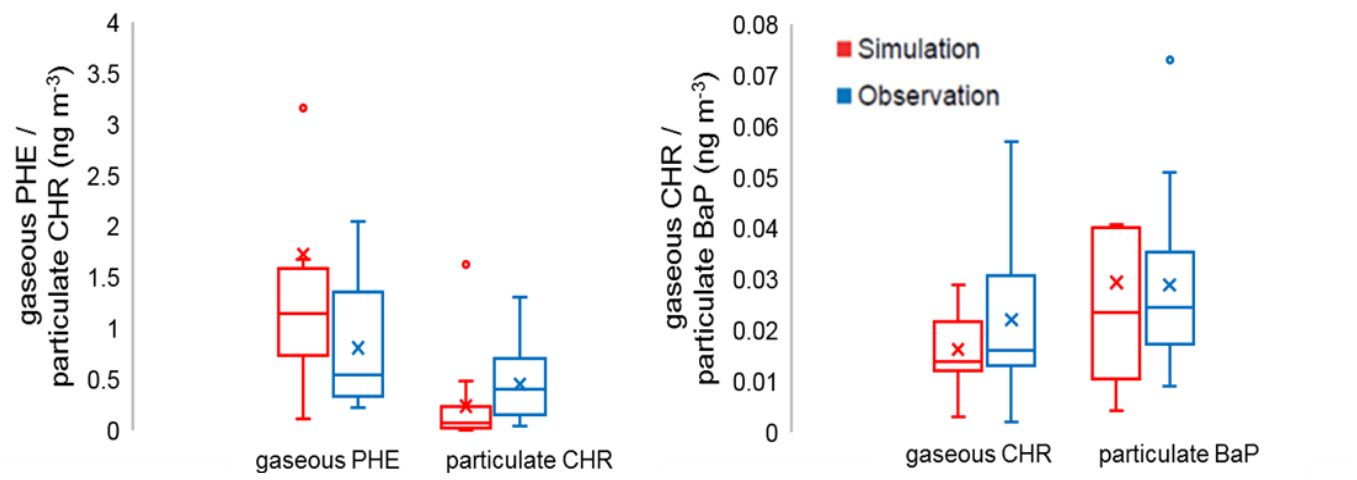

Figure 5. Simulated (red) and observed (blue) concentrations of gaseous PHE, particulate CHR, gaseous CHR and particulate BaP at the Gosan site averaged over 14–25 February 2003. The line and "X" in each box are the median and mean, while the boxes represent the 25th and 75th percentiles. Upper whisker is quartile 3 (Q3) + 1.5 × interquartile range (IQR) or maximum value, whichever is smaller; lower whisker is quartile 1 (Q1) - 1.5 × IQR or minimum value, whichever is larger.

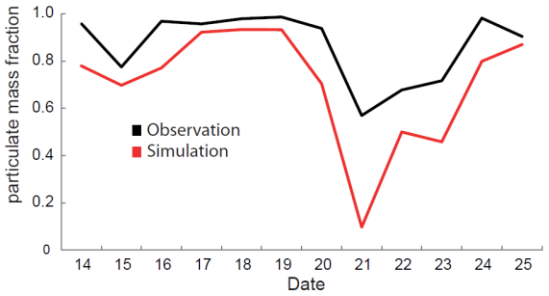

Figure 6. Simulated and observed daily averaged particulate mass fraction of CHR at the Gosan site during 14–25 February, 2003.

PAHs are 0.020 (0.022) ng m^{-3} for particulate BaP, 0.81 (1.73) ng m^{-3} for gaseous PHE, 0.029 (0.029) ng m^{-3} for gaseous CHR and 0.45 (0.24) ng m^{-3} for particulate CHR (Fig. 5, Table S4). Compared with previous studies, our simulated average concentrations of BaP agree well with the observation (deviation < 10%), while Zhang et al. (2011a) underestimates BaP by about 50%. For the Gosan summer case, our simulated average BaP concentration is 0.006 ng m^{-3} (Fig. S7), much closer to the observed value of 0.012 ng m^{-3} than the simulated BaP concentration of ≈0.001 ng m^{-3} by Zhang et al. (2011a). In general, the WRF-Chem-PAH model shows good/reasonable agreement with observations in both winter and summer seasons. However, although the daily average concentration levels of PAHs are reasonably well simulated, the day-to-day variation is not well captured at the remote back ground site Gosan (Fig. S6).

The correlation of observed and simulated daily average particulate mass fractions of CHR in the Gosan winter case is high (r = 0.73, see Fig. 6). The correlation is significantly lower at the Xianghe site (r = 0.37), which may be due to the proximity to sources. The phase equilibrium of CHR may not be established shortly after emission and the model may not resolve the spatial concentration gradients. An underestimation of simulated particulate mass fraction can be seen in both the winter and summer cases (Fig. 6 and Fig. S7). Such underestimation may be caused by the combined effects of uncertainties, such as the emission, degradation, dry/wet deposition and the long-range transport of OC/EC.

These results suggest that our newly developed WRF-Chem-PAH model is reasonably accurate in simulating the concentration levels and

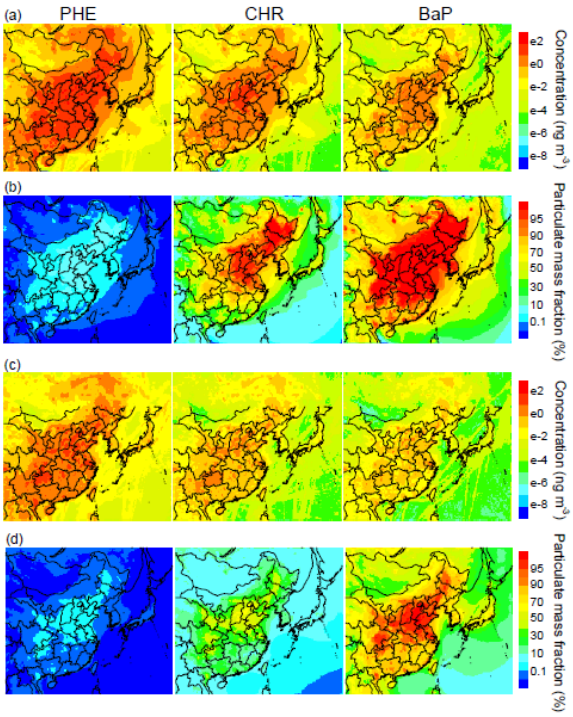

Figure 7. Simulated (a) surface concentrations and (b) particulate mass fractions of PHE, CHR and BaP averaged over 14–25 February, 2003. Simulated (c) surface concentrations and (d) particulate mass fractions of PHE, CHR and BaP averaged over 11–22 July, 2013.

particulate mass fractions of PAHs for the Asian outflow.

4.3 Distributions of PAHs in East Asia

To illustrate the distributions of PAHs in East Asia in both summer and winter, Fig. 7 shows the surface concentrations of three representative PAHs averaged over the summer period 11–22 July 2013 and winter period 14–25 February 2003. A distribution similar to 11–22 July 2013 is simulated for another summer period, 6–17 June 2003. The lifetimes of PAHs over Eastern China (20–42° N, 107–122° E mainland China; vertically averaged from surface to 2 km) are about 1.5–9 hours for PHE, 2–11 hours for CHR, 2 hours–3 days for BaP in summer and 9.5 hours–3.5 days for PHE, 11 hours–4.5 days for CHR, 1.5–6.5 days for BaP in winter, respectively. As a result of short lifetime, the atmospheric distribution of PAH is largely overlapped with emissions, because the concentration of PAH rapidly decreases away

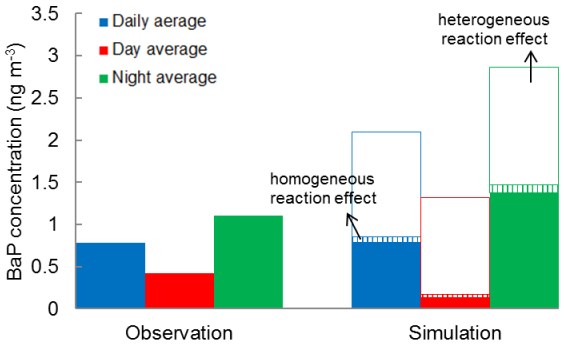

Figure 8. Simulated concentrations of BaP compared with observation at the Xianghe site during 11–22 July, 2013. The contributions of heterogeneous and homogeneous reaction are shown as blank areas and as small vertical bars, respectively, in the simulation bars.

from the source regions (Hafner et al., 2005). There is an obvious eastward outflow of PAH from the mainland to the East China Sea and further to the western Pacific Ocean (Zhang et al., 2011b). The simulated average concentration of 0.006 ng m-3 for particulate BaP during 14–25 February 2003 at a monitoring background site (26.19° N, 127.75° E) in Okinawa, Japan, which is located in the region of outflow pathways from China, is close to the observation 0.013 ng m^{-3} (monthly mean; http://tenbou.nies.go.jp/gis/monitor/). The concentrations of PAHs are higher in winter than summer, mainly due to higher emission fluxes and slower degradation rates.

The model calculated average particulate mass fractions are also shown in Fig. 7. The particulate mass fractions are higher in winter than in summer and in North China than in other regions. This is largely due to the distributions of OC/EC concentrations (high in North China), and seasonal and latitudinal variation of temperature. PHE has extremely small particulate mass fractions, while the particulate mass fractions of BaP are nearly 1 over most of China in winter but only 95% over North China in summer. On the other hand, CHR shows the largest spatial and seasonal variations among these three compounds. Our predicted distributions and particulate mass fractions of PAHs generally agree with the previous studies

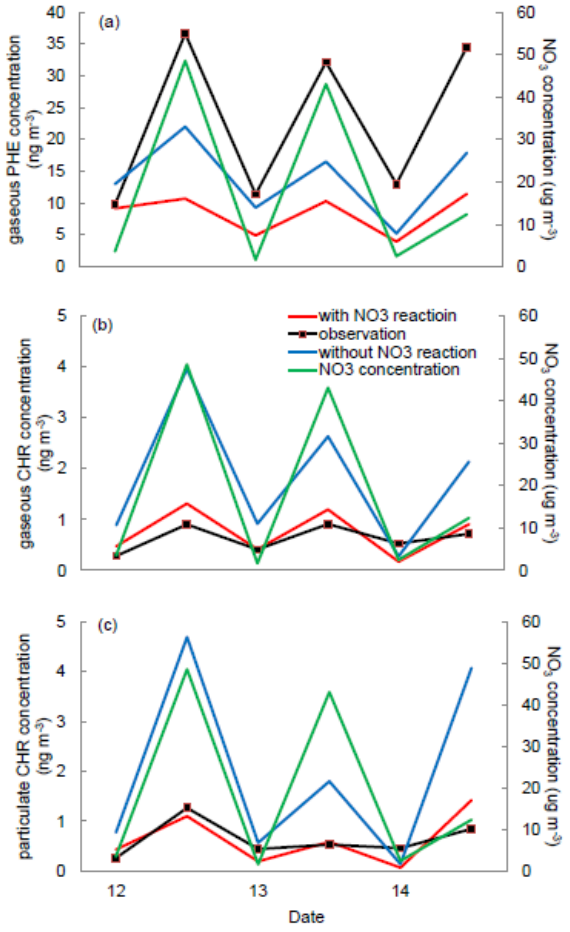

Figure 9. Simulated concentrations of (a) gaseous PHE, (b) gaseous CHR and (c) particulate CHR with and without reactions of NO_3 compared with observation and simulated concentrations of NO_3 during 12–14 July 2013.

in East Asia (Zhang et al., 2011b; Inomata et al., 2012).

5 Significance of PAH heterogeneous reaction with O_3 and gas-phase reaction with NO_3

We test the impact of heterogeneous and homogeneous reactions of BaP, as well as the homogeneous NO_3 reactions of CHR and PHE. In other PAH model studies, these processes are usually neglected (Zhang et al., 2011a; Zhang et al., 2011b).

As shown in Fig. 8, the simulation neglecting BaP reactivity significantly overestimates the near-ground concentration of the pollutant. Compared with the reaction scheme accounting for homogeneous and heterogeneous reactions, the model calculated BaP concentration increased from 0.14 to 1.32 ng m^{-3} for daytime, 1.37 to 2.86 ng m^{-3} for nighttime and 0.78 to 2.09 ng m^{-3} for 24 h mean. The observed daily average is, in fact, 0.78 ng m^{-3} (Fig. 8). The results indicate that the homogeneous gas-phase reaction of BaP is of little significance as compared to the heterogeneous reaction. This confirms that to account for BaP heterogeneous degradation in the model is indispensable.

Figure 9 shows the simulated concentrations of gas-phase PHE, gas- and particulate-phase CHR with and without NO_3 gas-phase reactions compared with observations at the Xianghe site. It is found that during nights with high NO_3 (48.5 and 43.0 ng m^{-3}, or ≈18 and ≈16 pptv as the 10 h mean, 12–14 July) the NO_3 reaction causes a significant night-time drop of PAH levels i.e., PHE and CHR by ≈-50% and -50 to -75%, respectively. This is surprisingly drastic for PHE regarding the rate coefficient, k_{NO3} = 1.2×10^{-13} cm^3 $molec^{-1}$ s^{-1} (Table 1), corresponding to a lifetime of τ_{NO3} ≈ 5 h, but τ_{NO3} ≈ 10 min for CHR (k_{NO3} = 4.0×10^{-12} cm^3 $molec^{-1}$ s^{-1}, Table 1). As an implication of rapid gas-particle partitioning in the model, the impact on the concentration of particulate-phase CHR is as significant as for gas-phase CHR.

6 Conclusions and discussion

We have developed the WRF-Chem-PAH model based on the standard WRF-Chem model to simulate the atmospheric fate of volatile, semivolatile and non-volatile PAH compounds. The implemented state-of-the-art processes for PAHs are: gas-particle partitioning, air-soil gas exchange, homogeneous gas-phase and heterogeneous reactions, cloud scavenging, dry and wet deposition, adjective transport and cumulus convection. The simulated PAHs in our current WRF-Chem-PAH model include PHE, CHR and BaP, representing volatile, semivolatile and non-volatile PAH compounds,

respectively. Also, the model can be applied for any similar semivolatile organic compound.

The model has been applied for East Asia. The model predicts observations (both atmospheric concentrations of PAHs and the particulate mass fraction of semivolatile CHR) at both a near-source and a major outflow site reasonably well considering big uncertainties in our current knowledge, most notably with regard to emission, gas-particle partitioning and atmospheric chemistry.

Both the sensitivity of simulated concentrations to the heterogeneous reaction with O_3 and the homogeneous reaction with NO_3 emphasise the importance of these reactions for the fate and distributions of the selected PAHs in the polluted atmospheric environment. However, chemical kinetic data and understanding of pathways are limited, in particular for semivolatile species and for heterogeneous chemistry in general (Keyte et al., 2013). Laboratory studies focusing on semivolatile PAHs, various aerosol matrices, and scenarios of particle mixing and aging are needed to improve PAH modelling.

The model accounts for secondary emissions of PAH i.e., re-volatilisation from soil (semivolatile PAHs only). However, as a consequence of prevailing westerly winds in combination with emissions being concentrated in Eastern China, unlike in South Asia (very little emissions in areas east of Northeast India and Bangla Desh) and other continents (Lammel et al., 2009; Galarneau et al., 2014), there is a large geographical overlap between secondary sources and primary sources over East Asia. Secondary emissions (re-volatilisation) from the sea surface of the Yellow Sea and the adjacent shelf areas (East and South China Seas) may also influence the regional distributions of PAH over the mainland. This is not addressed in this study (process not included), and should be investigated, in order to better assess trans-Pacific transport of PAHs and their even more toxic metabolites, nitro-PAHs (Zhang et al., 2011a).

Data availability: The observation data and code of this study are available from the corresponding author upon reasonable request.

Competing interests: The authors declare that they have no conflict of interest.

Acknowledgements: This work is supported by the Max Planck Society. The work of Y. Cheng and H. Su is also supported by the National Natural Science Foundation of China (41330635). We thank Young-Sung Ghim for providing the Gosan measurement data. We thank Georg Grell and Bill Skamarock for the explanation of WRF-Chem transport scheme. The coding work is supported by Yvlu Qiu, Feng Wang, Mega Octaviani, Tabish Ansari, Chao Wei and Stephan Nordmann. We also thank Pourya Shahpoury, Huizhong Shen, Rong Wang, Ye Huang, Fumo Yang and Pasquale Sellitto for valuable comments. An earlier version of this article was retracted because of mistakes that have been corrected in the present version (Mu et al., Atmos. Chem. Phys., 17, 12253-12267, 2017; https://doi.org/10.5194/acp-17-12253-2017-editorial-note).

References

Ackermann, I. J., Hass, H., Memmesheimer, M., Ebel, A., Binkowski, F. S., and Shankar, U.: Modal aerosol dynamics model for Europe: Development and first applications, Atmos. Environ., 32, 2981-2999, 10.1016/S1352-2310(98)00006-5, 1998.

Andersson, J. T., and Achten, C.: Time to Say Goodbye to the 16 EPA PAHs? Toward an Up-to-Date Use of PACs for Environmental Purposes, Polycycl. Aromat. Comp., 35, 330-354, 10.1080/10406638.2014.991042, 2015.

Atkinson, R., Baulch, D. L., Cox, R. A., Hampson, R. F., Kerr, J. A., and Troe, J.: Evaluated Kinetic and Photochemical Data for Atmospheric Chemistry - Supplement-Iii, Int. J. Chem. Kinet., 21, 115-150, 10.1002/kin.550210205, 1989.

Atkinson, R., and Arey, R.: Atmospheric chemistry of polycyclic aromatic hydrocarbons: Formation of mutagens, Environ. Health Persp. 102, 117-126, 1994.

Aulinger, A., Matthias, V., and Quante, M.: Introducing a partitioning mechanism for PAHs into the Community Multiscale Air Quality modeling system and its application to simulating the transport of benzo(a) pyrene over Europe, J. Appl. Meteorol. Clim., 46, 1718-1730, 10.1175/2007jamc1395.1, 2007.

Bamford, H. A., Poster, D. L., and Baker, J. E.: Temperature dependence of Henry's law constants of thirteen polycyclic aromatic hydrocarbons between 4 degrees C and 31 degrees C, Environ. Toxicol. Chem., 18, 1905-1912, 10.1002/etc.5620180906, 1999.

Berkemeier, T., Steimer, S. S., Krieger, U. K., Peter, T., Pöschl, U., Ammann, M., and Shiraiwa, M.: Ozone uptake on glassy, semi-solid and liquid organic matter and the role of reactive oxygen intermediates in atmospheric aerosol chemistry, Phys. Chem. Chem. Phys., 18, 12662-12674, 10.1039/c6cp00634e, 2016.

Bieser, J., Aulinger, A., Matthias, V., and Quante, M.: Impact of Emission Reductions between 1980 and 2020 on Atmospheric Benzo[a]pyrene Concentrations over Europe, Water Air Soil Poll., 223, 1393-1414, 10.1007/s11270-011-0953-z, 2012.

Binkowski, F. S., and Roselle, S. J.: Models-3 community multiscale air quality (CMAQ) model aerosol component - 1. Model description, J. Geophys. Res., 108, 10.1029/2001jd001409, 2003.

Chen, F., and Dudhia, J.: Coupling an advanced land surface-hydrology model with the Penn State-NCAR MM5 modeling system. Part I: Model implementation and sensitivity, Mon. Weather. Rev., 129, 569-585, 10.1175/1520-0493(2001)129<0569:Caalsh>2.0.Co;2, 2001.

Chou, M., and Suarez, M.: An efficient thermal infrared radiation parameterization for use in general circulation models, NASA Tech. Memo, 104606, 85pp, 1994.

Dachs, J., and Eisenreich, S. J.: Adsorption onto aerosol soot carbon dominates gas-particle partitioning of polycyclic aromatic hydrocarbons, Environ. Sci. Technol., 34, 3690-3697, 10.1021/Es991201+, 2000.

Darmenov, A. S., and Silva, A. d.: The Quick Fire Emissions Dataset (QFED) - Documentation of versions 2.1, 2.2 and 2.4, NASA Technical Report Series on Global Modeling and Data Assimilation, 32, 1–183, 2013.

Efstathiou, C. I., Matejovicova, J., Bieser, J., and Lammel, G.: Evaluation of gas-particle partitioning in a regional air quality model for organic pollutants, Atmos. Chem. Phys., 16, 15327-15345, 10.5194/acp-16-15327-2016, 2016.

Emmons, L. K., Walters, S., Hess, P. G., Lamarque, J. F., Pfister, G. G., Fillmore, D., Granier, C., Guenther, A., Kinnison, D., Laepple, T., Orlando, J., Tie, X., Tyndall, G., Wiedinmyer, C., Baughcum, S. L., and Kloster, S.: Description and evaluation of the Model for Ozone and Related chemical Tracers, version 4 (MOZART-4), Geosci. Model Dev., 3, 43-67, 2010.

Friedman, C. L., and Selin, N. E.: Long-Range Atmospheric Transport of Polycyclic Aromatic Hydrocarbons: A Global 3-D Model Analysis Including Evaluation of Arctic Sources, Environ. Sci. Technol., 46, 9501-9510, 10.1021/Es301904d, 2012.

Friedman, C. L., Pierce, J. R., and Selin, N. E.: Assessing the Influence of Secondary Organic versus Primary Carbonaceous Aerosols on Long-Range Atmospheric Polycyclic Aromatic Hydrocarbon Transport, Environ. Sci. Technol., 48, 3293-3302, 10.1021/Es405219r, 2014a.

Friedman, C. L., Zhang, Y. X., and Selin, N. E.: Climate Change and Emissions Impacts on Atmospheric PAH Transport to the Arctic, Environ. Sci. Technol., 48, 429-437, 10.1021/Es403098w, 2014b.

Galarneau, E., Makar, P. A., Sassi, M., and Diamond, M. L.: Estimation of atmospheric emissions of six semivolatile polycyclic aromatic hydrocarbons in southern Canada and the United States by use of an emissions processing system, Environ. Sci. Technol., 41, 4205-4213, 10.1021/Es062303k, 2007.

Galarneau, E., Makar, P. A., Zheng, Q., Narayan, J., Zhang, J., Moran, M. D., Bari, M. A., Pathela, S., Chen, A., and Chlumsky, R.: PAH concentrations simulated with the AURAMS-PAH chemical transport model over Canada and the USA, Atmos. Chem. Phys., 14, 4065-4077, 10.5194/acp-14-4065-2014, 2014.

Gencarelli, C. N., De Simone, F., Hedgecock, I. M., Sprovieri, F., and Pirrone, N.: Development and application of a regional-scale atmospheric mercury model based on WRF/Chem: a Mediterranean area investigation, Environ. Sci. Pollut. R., 21, 4095-4109, 10.1007/s11356-013-2162-3, 2014.

Grell, G. A., and Devenyi, D.: A generalized approach to parameterizing convection combining ensemble and data assimilation techniques, Geophys. Res. Lett., 29, 10.1029/2002gl015311, 2002.

Grell, G. A., Peckham, S. E., Schmitz, R., McKeen, S. A., Frost, G., Skamarock, W. C., and Eder, B.: Fully coupled "online" chemistry within the WRF model, Atmos. Environ., 39, 6957-6975, 10.1016/j.atmosenv.2005.04.027, 2005.

Guenther, A., Karl, T., Harley, P., Wiedinmyer, C., Palmer, P. I., and Geron, C.: Estimates of global terrestrial isoprene emissions using MEGAN (Model of Emissions of Gases and Aerosols from Nature), Atmos. Chem. Phys., 6, 3181-3210, 2006.

Hafner, W. D., Carlson, D. L., and Hites, R. A.: Influence of local human population on atmospheric polycyclic aromatic hydrocarbon concentrations, Environ. Sci. Technol., 39, 7374-7379, 10.1021/es0508673, 2005.

Halsall, C. J., Sweetman, A. J., Barrie, L. A., and Jones, K. C.: Modelling the behaviour of PAHs during atmospheric transport from the UK to the Arctic, Atmos. Environ., 35, 255-267, 10.1016/S1352-2310(00)00195-3, 2001.

Han, J. S., Moon, K. J., Lee, S. J., Kim, Y. J., Ryu, S. Y., Cliff, S. S., and Yi, S. M.: Size-resolved source apportionment of ambient particles by positive matrix factorization at Gosan background site in East Asia, Atmos. Chem. Phys., 6, 211-223, 2006.Hung, H., Blanchard, P., Halsall, C. J., Bidleman, T. F., Stern, G. A., Fellin, P., Muir, D. C. G., Barrie, L. A., Jantunen, L. M., Helm, P. A., Ma, J., and Konoplev, A.: Temporal and spatial variabilities of atmospheric polychlorinated biphenyls (PCBs), organochlorine (OC) pesticides and polycyclic aromatic hydrocarbons (PAHs) in the Canadian Arctic: Results from a decade of monitoring, Sci. Total Environ., 342, 119-144, 10.1016/j.scitotenv.2004.12.058, 2005.

Hansen, K. M., Christensen, J. H., Brandt, J., Frohn, L. M., and Geels, C.: Modelling atmospheric transport of α-hexachlorocyclohexane in the Northern Hemisphere with a 3-D dynamical model: DEHM-POP, Atmos. Chem. Phys., 4, 1125–1137, 2004.

Hylland, K.: Polycyclic aromatic hydrocarbon (PAH) ecotoxicology in marine ecosystems, J. Toxicol. Env. Heal. A., 69, 109-123, 10.1080/15287390500259327, 2006.

Inomata, Y., Kajino, M., Sato, K., Ohara, T., Kurokawa, J. I., Ueda, H., Tang, N., Hayakawa, K., Ohizumi, T., and Akimoto, H.: Emission and Atmospheric Transport of Particulate PAHs in Northeast Asia, Environ. Sci. Technol., 46, 4941-4949, 10.1021/Es300391w, 2012.

Inomata, Y., Kajino, M., Sato, K., Ohara, T., Kurokawa, J., Ueda, H., Tang, N., Hayakawa, K., Ohizumi, T., and Akimoto, H.: Source contribution analysis of surface particulate polycyclic aromatic hydrocarbon concentrations in northeastern Asia by source-receptor relationships, Environ. Pollut., 182, 324-334, 10.1016/j.envpol.2013.07.020, 2013.

Janjic, Z. I.: The Step-Mountain Eta Coordinate Model - Further Developments of the Convection, Viscous Sublayer, and Turbulence Closure Schemes, Mon. Weather. Rev., 122, 927-945, 10.1175/1520-0493(1994)122<0927:Tsmecm>2.0.Co;2, 1994.

Jonker, M. T. O., and Koelmans, A. A.: Sorption of Polycyclic Aromatic Hydrocarbons and Polychlorinated Biphenyls to Soot and Soot-like Materials in the Aqueous Environment: Mechanistic Considerations, Environ. Sci. Technol., 36, 3725-3734, 10.1021/es020019x, 2002.

Jury, W. A., Spencer, W. F., and Farmer, W. J.: Behavior Assessment Model for Trace Organics in Soil .1. Model Description, J. Environ. Qual., 12, 558-564, 1983.

Karickhoff, S. W.: Semi-empirical estimation of sorption of hydrophobic pollutants on natural sediments and soils, Chemosphere, 10, 833-846, 1981.

Keyte, I. J., Harrison, R. M., and Lammel, G.: Chemical reactivity and long-range transport potential of polycyclic aromatic hydrocarbons - a review, Chem. Soc. Rev., 42, 9333-9391, 10.1039/C3cs60147a, 2013.

Kim, J. Y., Ghim, Y. S., Song, C. H., Yoon, S. C., and Han, J. S.: Seasonal characteristics of air masses arriving at Gosan, Korea, using fine particle measurements between November 2001 and August 2003, J. Geophys. Res.-Atmos., 112, 10.1029/2005jd006946, 2007.

Kim, J. Y., Lee, J. Y., Choi, S. D., Kim, Y. P., and Ghim, Y. S.: Gaseous and particulate polycyclic aromatic hydrocarbons at the Gosan background site in East Asia, Atmos. Environ., 49, 311-319, 10.1016/j.atmosenv.2011.11.029, 2012.

Klöpffer W., Wagner B. O., and Steinhäuser K. G.: Atmospheric Degradation of Organic Substances: Persistence, Transport Potential, Spatial Range. Wiley, 2008.

Kwok, E. S. C., Harger, W. P., Arey, J., and Atkinson, R.: Reactions of Gas-Phase Phenanthrene under Simulated Atmospheric Conditions, Environ. Sci. Technol., 28, 521-527, 10.1021/es00052a027, 1994.

Lammel, G., Sehili, A. M., Bond, T. C., Feichter, J., and Grassl, H.: Gas/particle partitioning and global distribution of polycyclic aromatic hydrocarbons - A modelling approach, Chemosphere, 76, 98-106, 10.1016/j.chemosphere.2009.02.017, 2009.

Lang, C., Tao, S., Zhang, G., Fu, J., and Simonich, S.: Outflow of polycyclic aromatic hydrocarbons from Guangdong, Southern China, Environ. Sci. Technol., 41, 8370-8375, 10.1021/es071853v, 2007.

Lang, C., Tao, S., Liu, W. X., Zhang, Y. X., and Simonich, S.: Atmospheric transport and outflow of polycyclic aromatic hydrocarbons from China, Environ. Sci. Technol., 42, 5196-5201, 10.1021/Es800453n, 2008.

Liao, J., Wang, T., Wang, X., Xie, M., Jiang, Z., Huang, X., and Zhu, J.: Impacts of different urban canopy schemes in WRF/Chem on regional climate and air quality in Yangtze River Delta, China, Atmos. Res., 145–146, 226-243, http://dx.doi.org/10.1016/j.atmosres.2014.04.005, 2014.

Lin, Y.-L., Farley, R. D., and Orville, H. D.: Bulk Parameterization of the Snow Field in a Cloud Model, J. Clim. Appl. Meteoro., 22, 1065-1092, 10.1175/1520-0450(1983)022<1065:BPOTSF>2.0.CO;2, 1983.

Liu, S., Tao, S., Liu, W., Liu, Y., Dou, H., Zhao, J., Wang, L., Wang, J., Tian, Z., and Gao, Y.: Atmospheric polycyclic aromatic hydrocarbons in north China: a winter-time study, Environ. Sci. Technol., 41, 8256–8261, 10.1021/es0716249, 2007.

Lohmann, R., and Lammel, G.: Adsorptive and absorptive contributions to the gas-particle partitioning of polycyclic aromatic hydrocarbons: State of knowledge and recommended parametrization for modeling, Environ. Sci. Technol., 38, 3793-3803, 10.1021/Es035337q, 2004.

Lowe, D., Archer-Nicholls, S., Morgan, W., Allan, J., Utembe, S., Ouyang, B., Aruffo, E., Le Breton, M., Zaveri, R. A., Di Carlo, P., Percival, C., Coe, H., Jones, R., and McFiggans, G.: WRF-Chem model predictions of the regional impacts of N_2O_5 heterogeneous processes on night-time chemistry over north-western Europe, Atmos. Chem. Phys., 15, 1385–1409, 2015.

Lu, P. Y., Metcalf, R. L., Plummer, N., and Mandel, D.: The environmental fate of three carcinogens: Benzo-(α)-pyrene, benzidine, and vinyl chloride evaluated in laboratory model ecosystems, Arch. Environ. Contam. Toxicol., 6, 129-142, 10.1007/BF02097756, 1977.

Lu, Z., Zhang, Q., and Streets, D. G.: Sulfur dioxide and primary carbonaceous aerosol emissions in China and India, 1996-2010, Atmos. Chem. Phys., 11, 9839-9864, 10.5194/acp-11-9839-2011, 2011.

Lv, Y., Li, X., Xu, T. T., Cheng, T. T., Yang, X., Chen, J. M., Iinuma, Y., and Herrmann, H.: Size distributions of polycyclic aromatic hydrocarbons in urban atmosphere: sorption mechanism and source contributions to respiratory deposition, Atmos. Chem. Phys., 16, 2971-2983, 10.5194/acp-16-2971-2016, 2016.

Mackay, D., and Paterson, S.: Evaluating the multimedia fate of organic chemicals: a level III fugacity model, Environ. Sci. Technol., 25, 427-436, 10.1021/es00015a008, 1991.

Matthias, V., Aulinger, A., and Quante, M.: CMAQ simulations of the benzo(a)pyrene distribution over Europe for 2000 and 2001, Atmos. Environ., 43, 4078-4086, 10.1016/j.atmosenv.2009.04.058, 2009.

Mlawer, E. J., Taubman, S. J., Brown, P. D., Iacono, M. J., and Clough, S. A.: Radiative transfer for inhomogeneous atmospheres: RRTM, a validated correlated-k model for the longwave, J. Geophys. Res., 102, 16663-16682, 10.1029/97jd00237, 1997.

Mu, Q., Shiraiwa, M., Octaviani, M., Ma, N., Ding, A., Su, H., Lammel, G., Pöschl, U., and Cheng, Y: Temperature effect on phase state and reactivity controls atmospheric multiphase chemistry and transport of PAHs, Sci. Adv., 4, 10.1126/sciadv.aap7314, 2018.

Neu, J. L., and Prather, M. J.: Toward a more physical representation of precipitation scavenging in global chemistry models: cloud overlap and ice physics and their impact on tropospheric ozone, Atmos. Chem. Phys., 12, 3289-3310, 10.5194/acp-12-3289-2012, 2012.

Odabasi, M., Cetin, E., and Sofuoglu, A.: Determination of octanol–air partition coefficients and supercooled liquid vapor pressures of PAHs as a function of temperature: Application to gas–particle partitioning in an urban atmosphere, Atmos. Environ., 40, 6615-6625, http://dx.doi.org/10.1016/j.atmosenv.2006.05.051, 2006.

Prevedouros, K., Jones, K. C., and Sweetman, A. J.: Modelling the atmospheric fate and seasonality of polycyclic aromatic hydrocarbons in the UK, Chemosphere, 56, 195-208, 10.1016/j.chemosphere.2004.02.032, 2004.

Prevedouros, K., Palm-Cousins, A., Gustafsson, O., and Cousins, I. T.: Development of a black carbon-inclusive multi-media model: Application for PAHs in Stockholm, Chemosphere, 70, 607-615, 10.1016/j.chemosphere.2007.07.002, 2008.

Salzmann, M., and Lawrence, M.: Automatic coding of chemistry solvers in WRF-Chem using KPP, 7th WRF Users Workshop, Boulder, Colorado, USA, 2006.

San Jose, R., Perez, J. L., Callen, M. S., Lopez, J. M., and Mastral, A.: BaP (PAH) air quality modelling exercise over Zaragoza (Spain) using an adapted version of WRF-CMAQ model, Environ. Pollut., 183, 151-158, 10.1016/j.envpol.2013.02.025, 2013.

Sandu, A., Daescu, D. N., and Carmichael, G. R.: Direct and adjoint sensitivity analysis of chemical kinetic systems with KPP: Part I - theory and software tools, Atmos. Environ., 37, 5083-5096, 10.1016/j.atmosenv.2003.08.019, 2003.

Sandu, A., and Sander, R.: Technical note: Simulating chemical systems in Fortran90 and Matlab with the Kinetic PreProcessor KPP-2.1, Atmos. Chem. Phys., 6, 187-195, 2006.

Schell, B., Ackermann, I. J., Hass, H., Binkowski, F. S., and Ebel, A.: Modeling the formation of secondary organic aerosol within a comprehensive air quality model system, J. Geophys. Res., 106, 28275-28293, 10.1029/2001jd000384, 2001.

Shen, H. Z., Huang, Y., Wang, R., Zhu, D., Li, W., Shen, G. F., Wang, B., Zhang, Y. Y., Chen, Y. C., Lu, Y., Chen, H., Li, T. C., Sun, K., Li, B. G., Liu, W. X., Liu, J. F., and Tao, S.: Global Atmospheric Emissions of Polycyclic Aromatic Hydrocarbons from 1960 to 2008 and Future Predictions, Environ. Sci. Technol., 47, 6415-6424, 10.1021/Es400857z, 2013.

Sehili, A. M., and Lammel, G.: Global fate and distribution of polycyclic aromatic hydrocarbons emitted from Europe and Russia, Atmos. Environ., 41, 8301-8315, 10.1016/j.almosenv.2007.06.050, 2007.

Shen, H. Z., Tao, S., Liu, J. F., Huang, Y., Chen, H., Li, W., Zhang, Y. Y., Chen, Y. C., Su, S., Lin, N., Xu, Y. Y., Li, B. G., Wang, X. L., and Liu, W. X.: Global lung cancer risk from PAH exposure highly depends on emission sources and individual susceptibility, Sci. Rep., 4, 10.1038/Srep06561, 2014.

Shiraiwa, M., Pfrang, C., and Pöschl, U.: Kinetic multi-layer model of aerosol surface and bulk chemistry (KM-SUB): the influence of interfacial transport and bulk diffusion on the oxidation of oleic acid by ozone, Atmos. Chem. Phys., 10, 3673-3691, 10.5194/acp-10-3673-2010, 2010.

Shiraiwa, M., Sosedova, Y., Rouviere, A., Yang, H., Zhang, Y. Y., Abbatt, J. P. D., Ammann, M., and Pöschl, U.: The role of long-lived reactive oxygen intermediates in the reaction of ozone with aerosol particles, Nat. Chem., 3, 291-295, 10.1038/Nchem.988, 2011.

Shrivastava, M., Lou, S., Zelenyuk, A., Easter, R. C., Corley, R. A., Thrall, B. D., Rasch, P. J., Fast, J. D., Massey Simonich, S. L., Shen, H., and Tao, S.: Global long-range transport and lung cancer risk from polycyclic aromatic hydrocarbons shielded by coatings of organic aerosol, Proceedings of the National Academy of Sciences, 10.1073/pnas.1618475114, 2017.

Stockwell, W. R., Kirchner, F., Kuhn, M., and Seefeld, S.: A new mechanism for regional atmospheric chemistry modeling, J. Geophys. Res., 102, 25847-25879, 10.1029/97jd00849, 1997.

Strand, A., and Hov, Ø.: A model strategy for the simulation of chlorinated hydrocarbon distributions in the global environment, Water Air Soil Poll., 86, 283-316, 10.1007/Bf00279163, 1996.

Teich, M., van Pinxteren, D., Wang, M., Kecorius, S., Wang, Z., Müller, T., Močnik, G., and Herrmann, H.: Contributions of nitrated aromatic compounds to the light absorption of water-soluble and particulate brown carbon in different atmospheric environments in Germany and China, Atmos. Chem. Phys., 17, 1653-1672, 10.5194/acp-17-1653-2017, 2017.

van Jaarsveld, J. A., VanPul, W. A. J., and DeLeeuw, F. A. A. M.: Modelling transport and deposition of persistent organic pollutants in the European region, Atmos. Environ., 31, 1011-1024, 10.1016/S1352-2310(96)00251-8, 1997.

Wesely, M. L.: Parameterization of Surface Resistances to Gaseous Dry Deposition in Regional-Scale Numerical-Models, Atmos. Environ., 23, 1293-1304, 10.1016/0004-6981(89)90153-4, 1989.

WHO (World Health Organization): Polynuclear aromatic hydrocarbons in Drinking-water, Background document for development of WHO Guidelines for Drinking-water Quality, Geneva, 2003.

Wild, O., Zhu, X., and Prather, M. J.: Fast-j: Accurate simulation of in- and below-cloud photolysis in tropospheric chemical models, J. Atmos. Chem., 37, 245-282, 10.1023/A:1006415919030, 2000.

Yaffe, D., Cohen, Y., Arey, J., and Grosovsky, A. J.: Multimedia analysis of PAHs and nitro-PAH daughter products in the Los Angeles basin, Risk Anal., 21, 275-294, 10.1111/0272-4332.212111, 2001.

Yahya, K., Wang, K., Campbell, P., Glotfelty, T., He, J., and Zhang, Y.: Decadal evaluation of regional climate, air quality, and their interactions using WRF/Chem Version 3.6.1, Geosci. Model Dev. Discuss., 8, 6707-6756, 10.5194/gmdd-8-6707-2015, 2016.

Zhang, Y., Pan, Y., Wang, K., Fast, J. D., and Grell, G. A.: WRF/Chem-MADRID: Incorporation of an aerosol module into WRF/Chem and its initial application to the TexAQS2000 episode, J. Geophys. Res., 115, D18202, 10.1029/2009jd013443, 2010.

Zhang, Y. and Tao, S.: Global atmospheric emission inventory of polycyclic aromatic hydrocarbons (PAHs) for 2004, Atmos. Environ., 43, 812–819, 2009.

Zhang, Y., Tao, S., Ma, J., and Simonich, S.: Transpacific transport of benzo[a]pyrene emitted from Asia, Atmos. Chem. Phys., 11, 11993-12006, 10.5194/acp-11-11993-2011, 2011a.

Zhang, Y., Sartelet, K., Wu, S. Y., and Seigneur, C.: Application of WRF/Chem-MADRID and WRF/Polyphemus in Europe - Part 1: Model description, evaluation of meteorological predictions, and aerosol-meteorology interactions, Atmos. Chem. Phys., 13, 6807-6843, 10.5194/acp-13-6807-2013, 2013.

Zhang, Y. X., and Tao, S.: Seasonal variation of polycyclic aromatic hydrocarbons (PAHs) emissions in China, Environ. Pollut., 156, 657-663, 10.1016/j.envpol.2008.06.017, 2008.

Zhang, Y. X., Tao, S., Shen, H. Z., and Ma, J. M.: Inhalation exposure to ambient polycyclic aromatic hydrocarbons and lung cancer risk of Chinese population, P. Natl. Acad. Sci. USA, 106, 21063-21067, 10.1073/pnas.0905756106, 2009.

Zhang, Y. X., Shen, H. Z., Tao, S., and Ma, J. M.: Modeling the atmospheric transport and outflow of polycyclic aromatic hydrocarbons emitted from China, Atmos. Environ., 45, 2820-2827, 10.1016/j.atmosenv.2011.03.006, 2011b.

Zhou, S. M., Shiraiwa, M., McWhinney, R. D., Pöschl, U., and Abbatt, J. P. D.: Kinetic limitations in gas-particle reactions arising from slow diffusion in secondary organic aerosol, Faraday Discuss., 165, 391-406, 10.1039/C3fd00030c, 2013.

Supplementary Material for

"Regional modelling of polycyclic aromatic hydrocarbons: WRF-Chem-PAH model development and East Asia case studies"

Qing Mu, Gerhard Lammel, Christian N. Gencarelli, Ian M. Hedgecock, Ying Chen, Petra Přibylová, Yuxuan Zhang, Guangjie Zheng, Qiang Zhang, Manabu Shiraiwa, Peter Spichtinger, Hang Su, Ulrich Pöschl, Yafang Cheng

Table of Contents

Text S1. Overview of the heterogeneous degradation of BaP.

Text S2. Sampling at the Xianghe site and data quality control.

Table S5. Field blank concentrations (G: gas phase; P: particulate phase) and number of samples >LOQ out of total samples.

Table S1. Configurations of WRF-Chem v3.6.1.

Physics	WRF option
Microphysics	Lin scheme
Surface layer	Eta Monin–Obukhov (Janjic) scheme
Planetary boundary layer	Mellor–Yamada–Janjic (MJY) TKE scheme
Cumulus parameterisation	Grell 3-D ensemble scheme
Land-surface model	Unified Noah land-surface model
Shortwave radiation	Goddard scheme
Longwave radiation	RRTMG scheme
Chemistry	**Chem option**
Gas-phase mechanism	RACM with aqua-phase reactions
Aerosol module	MADE/SORGAM
Photolytic rate	Fast-J photolysis scheme

Table S2. Parameterization of heterogeneous reaction rate for the ozonolysis of BaP. First-order reaction rate coefficients k (s^{-1}) are given by the Hill equation $k = base + \frac{max-base}{1+(\frac{xhalf}{[O_3]})^{rate}}$ with $[O_3]$ in ppbv. For each grid cell, the parameters are read from the look-up table with temperature and relative humidity (RH) closest to the temperature and humidity of the grid cell. When equally close, the smaller parameter value is adopted.

70% RH				
Temperature (°C)	base	max	rate	xhalf
40	1.67e-4	1.29e-2	0.682	1.25e3
35	1.19e-4	1.29e-2	0.682	1.25e3
30	8.52e-5	9.02e-3	0.696	1.23e3
25	5.94e-5	6.33e-3	0.707	1.27e3
23	4.84e-5	5.14e-3	0.700	1.25e3
15	2.55e-5	2.72e-3	0.711	1.29e3
10	1.58e-5	1.68e-3	0.706	1.27e3
5	9.49e-6	1.00e-3	0.698	1.24e3
0	6.85e-6	5.64e-4	0.704	1.11e3
-5	5.31e-6	3.10e-4	0.713	1.01e3
-10	3.83e-6	1.48e-4	0.731	7.33e2
-15	8.93e-7	1.05e-4	0.580	1.88e3
-20	1.16e-6	2.58e-5	0.673	3.35e2

50% RH				
Temperature (°C)	base	max	rate	xhalf
40	1.65e-4	1.80e-2	0.672	1.21e3
35	1.16e-4	1.27e-2	0.678	1.24e3
30	8.24e-5	8.68e-3	0.688	1.22e3
25	5.44e-5	5.71e-3	0.688	1.21e3
23	2.64e-5	3.08e-3	0.618	7.97e2
15	2.20e-6	1.10e-3	0.544	5.83e2
10	7.84e-7	2.60e-4	0.559	7.50e1
5	-4.79e-7	7.19e-5	0.564	1.31e1
0	-7.02e-6	2.18e-5	0.464	1.05e0
-5	-4.06e-6	6.54e-6	0.459	1.24e-1
-10	-1.89e-6	2.02e-6	0.429	1.44e-2
-15	2.58e-7	7.22e-7	0.175	1.28e-1
-20	1.79e-7	2.60e-7	0.689	1.11e3

Dry				
Temperature (°C)	base	max	rate	xhalf
40	1.61e-4	1.74e-2	0.667	1.19e3
35	1.10e-4	1.19e-2	0.667	1.21e3
30	6.75e-5	7.31e-3	0.653	1.11e3
25	2.3e-5	3.10e-3	0.586	7.02e2
23	-1.90e-5	9.28e-4	0.446	1.59e2
15	-2.65e-5	3.09e-4	0.341	8.38e1
10	-4.28e-5	1.03e-4	0.191	4.41e0
5	-1.12e-5	3.49e-5	0.142	4.33e0
0	3.39e-6	1.03e-5	0.382	8.85e2
-5	1.37e-6	5.67e-6	0.780	2.96e3

-10	4.53e-7	1.57e-6	0.979	1.63e3
-15	1.44e-7	2.10e-6	0.924	1.39e4

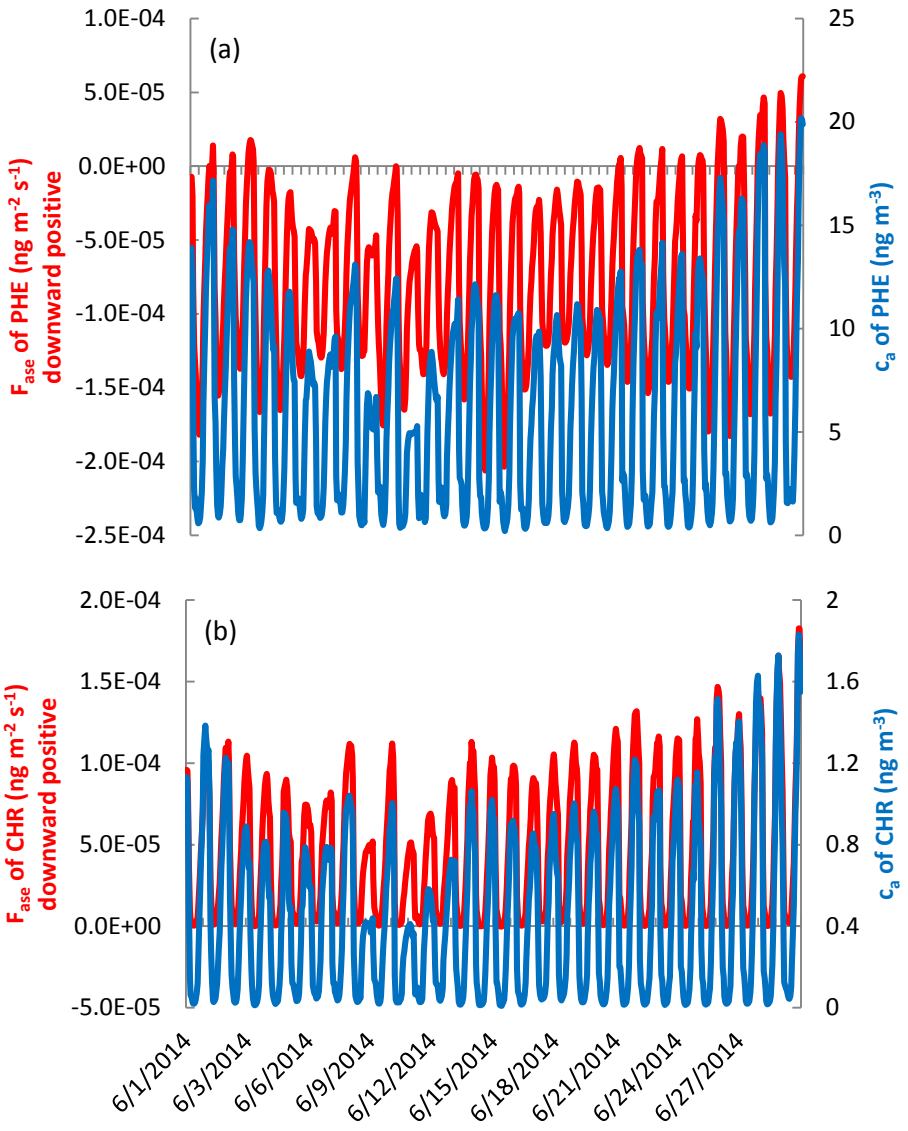

Figure S1. Air-soil gas exchange flux (F_{ase}, positive is defined downward, negative is defined upward) and near-ground air concentration (c_a) at a receptor site.

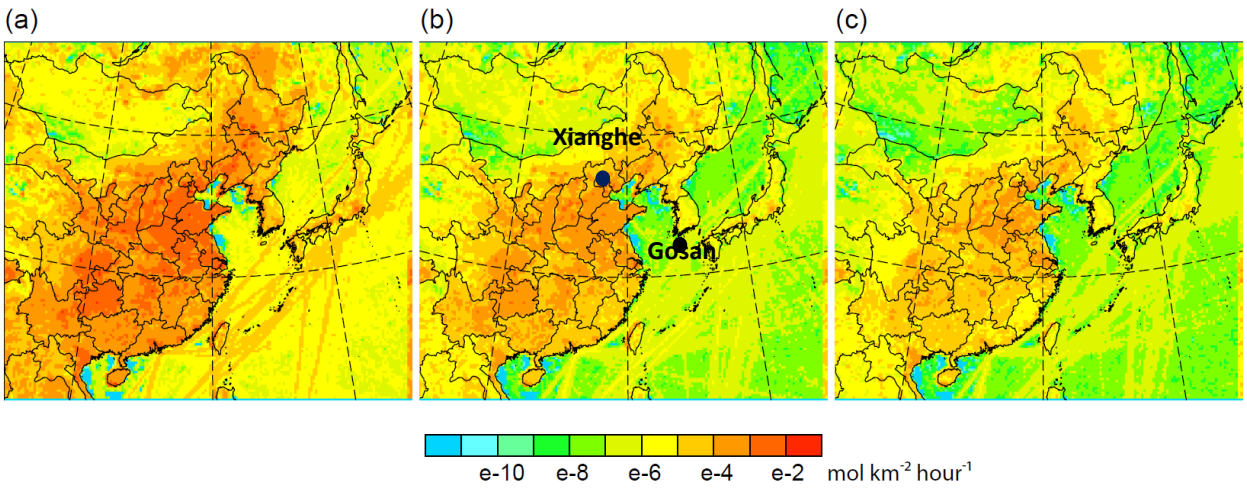

Figure S2. Emissions of (a) PHE, (b) CHR and (c) BaP in July 2013. The locations of Xianghe and Gosan are also shown.

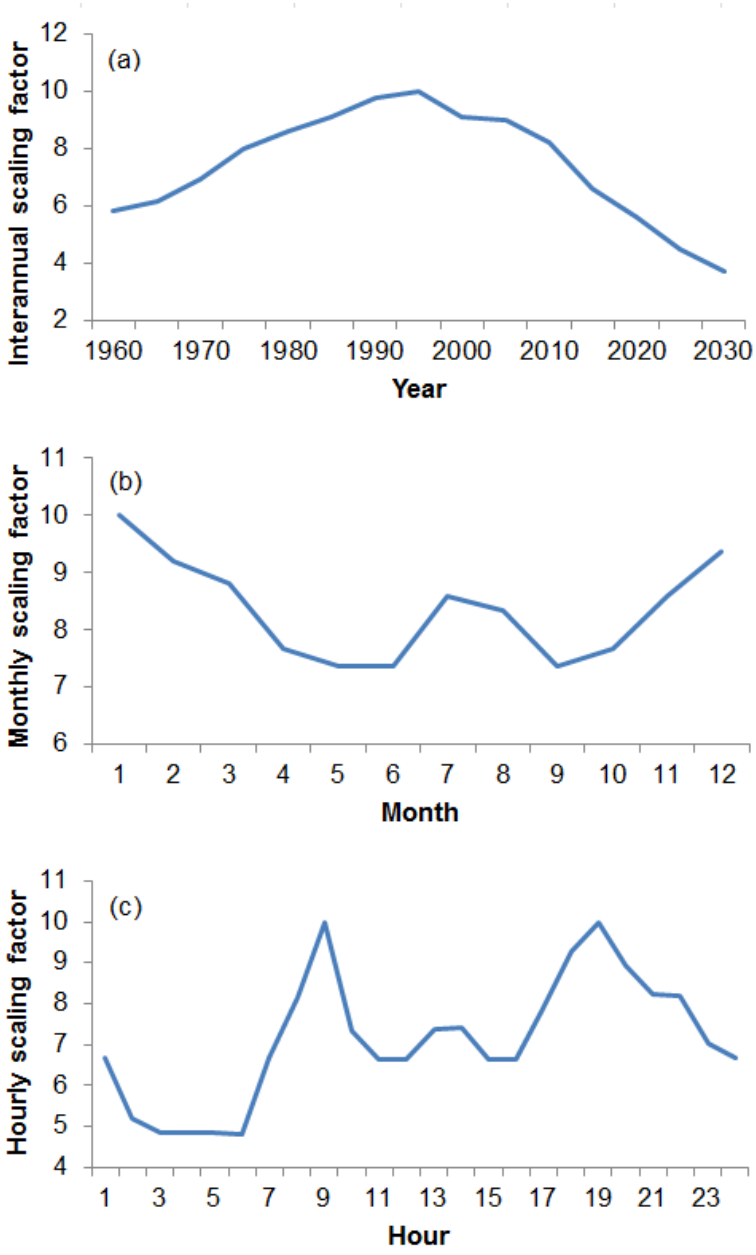

Figure S3. (a) Interannual, (b) monthly and (c) hourly scaling factors of PAH emissions.

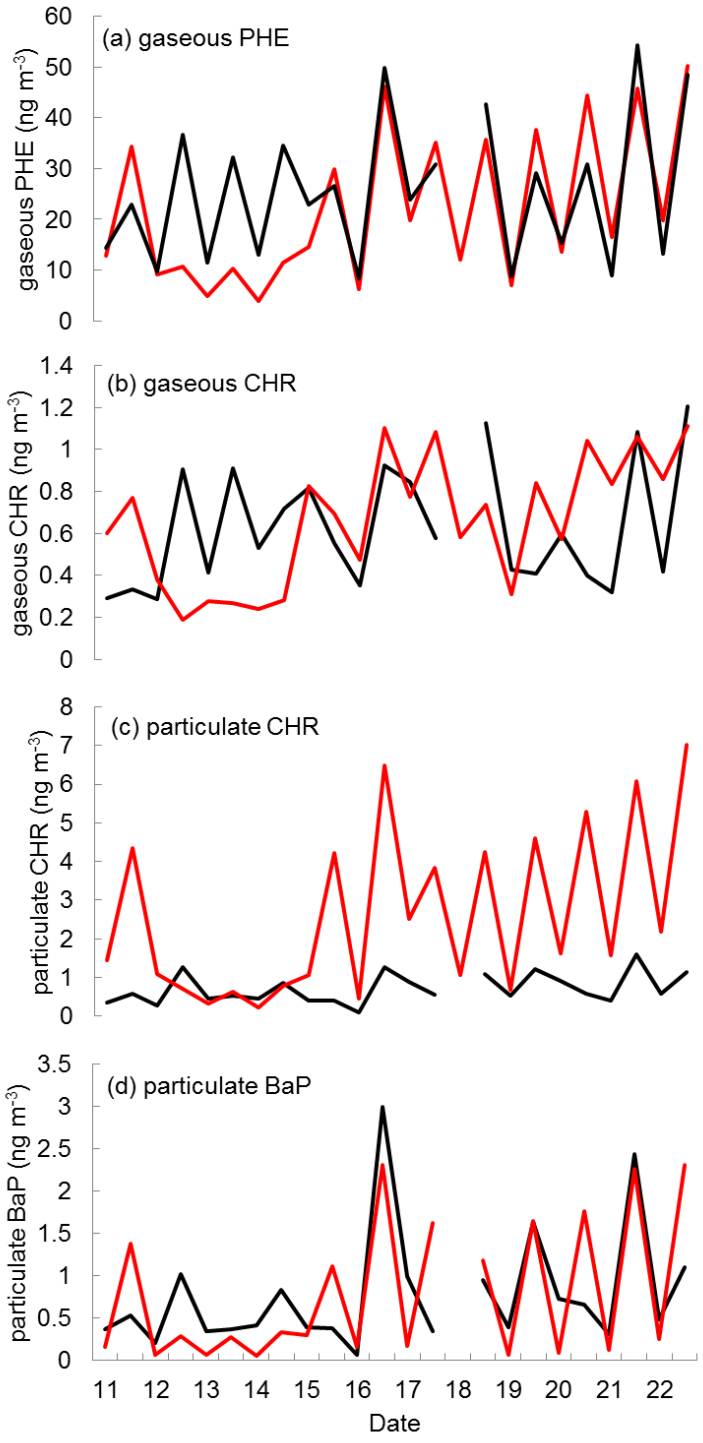

Figure S4. Simulated (red) and observed (black) concentrations of (a) gaseous PHE, (b) gaseous CHR, (c) particulate CHR and (d) particulate BaP at the Xianghe site during 11–22 July, 2013.

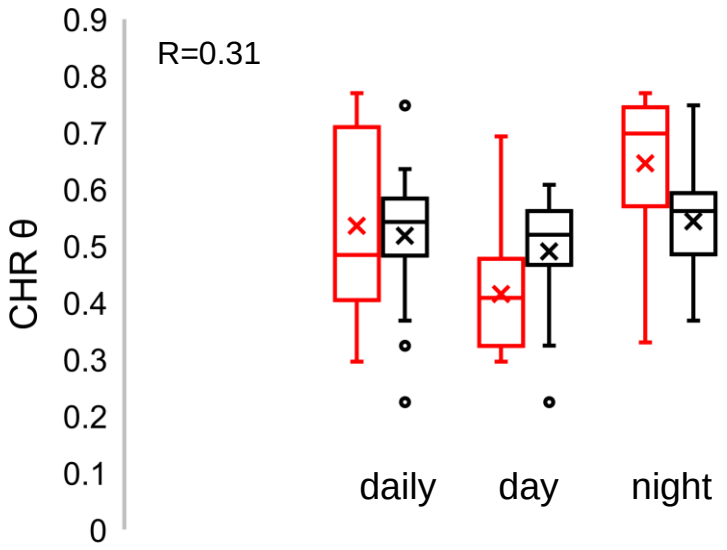

Figure S5. Simulated (red) and observed (black) daily, day and night particulate mass fraction of CHR at the Xianghe site during 11–22 July, 2013. The line and "X" in each box are the median and mean, while the boxes represent the 25th and 75th percentiles. Upper whisker is quartile 3 (Q3) + 1.5 × interquartile range (IQR) or maximum value, whichever is smaller; lower whisker is quartile 1 (Q1) - 1.5 × IQR or minimum value, whichever is larger. The Spearman's rank correlation coefficients R use combined daytime and nighttime data sets.

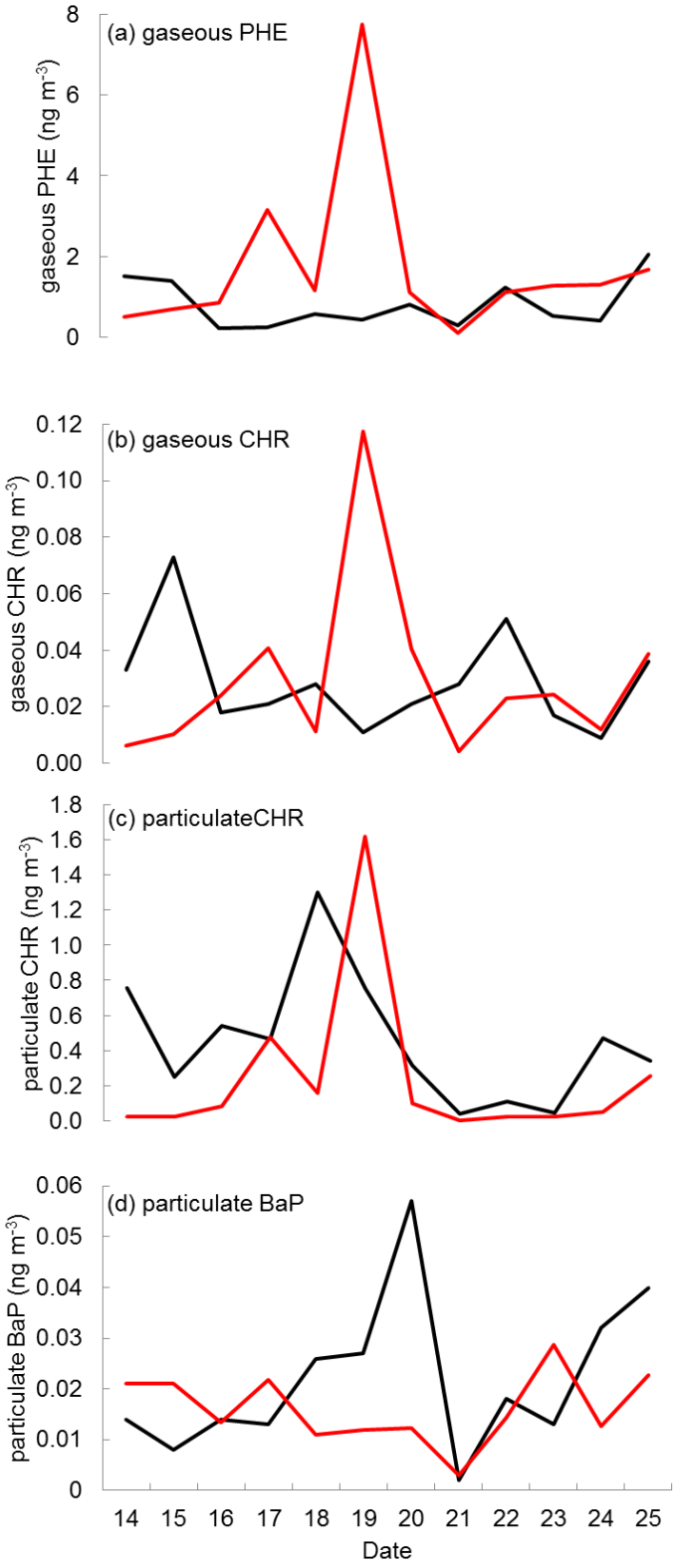

Figure S6. Simulated (red) and observed (black) concentrations of (a) gaseous PHE, (b) gaseous CHR, (c) particulate CHR and (d) particulate BaP at the Gosan site during 14–25 February, 2003.

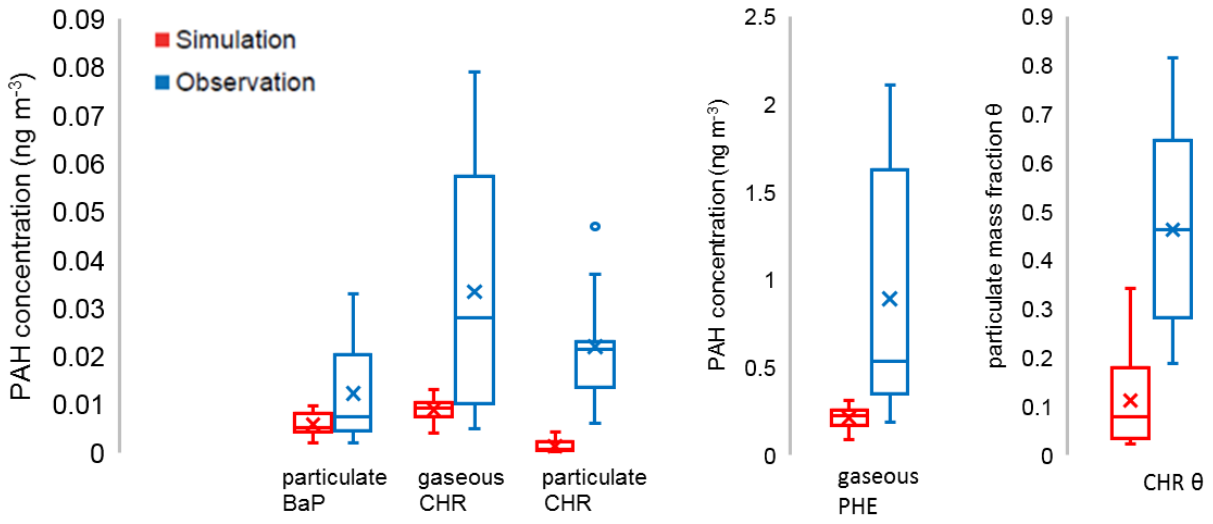

Figure S7. Simulated (red) and observed (blue) concentrations of gaseous PHE and CHR, particulate BaP and CHR, and particulate mass fraction of CHR at the Gosan site averaged over 6–17 June 2003 (summer case). The line and "X" in each box are the median and mean, while the boxes represent the 25th and 75th percentiles. Upper whisker is quartile 3 (Q3) + 1.5 × interquartile range (IQR) or maximum value, whichever is smaller; lower whisker is quartile 1 (Q1) - 1.5 × IQR or minimum value, whichever is larger.

Table S3. Observed (obs) and simulated (sim) median, mean bias (MB), root mean square error (RMSE), mean absolute deviation (MAD) in unit ng m^{-3} and Spearman's rank correlation coefficient (R) at the Xianghe site averaged over 11–22 July, 2013. R use combined daytime and nighttime data sets.

gaseous PHE												
	daily				day				night			
	obs	sim	sim-obs	(sim-obs)/obs	obs	sim	sim-obs	(sim-obs)/obs	obs	sim	sim-obs	(sim-obs)/obs
Median	23.9	15.5	-8.5	-35.5%	13.0	12.5	-0.5	-4.2%	33.3	35.3	2.0	6.0%
MB	-3.0				-2.0				-3.9			
RMSE	10.5				5.4				13.6			
MAD	7.9				4.5				11.1			
R	0.69											
gaseous CHR												
	daily				day				night			
	obs	sim	sim-obs	(sim-obs)/obs	obs	sim	sim-obs	(sim-obs)/obs	obs	sim	sim-obs	(sim-obs)/obs
Median	0.56	1.08	0.52	94.0%	0.42	0.61	0.19	45.5%	0.81	1.98	1.17	143.8%
MB	0.67				0.16				1.14			
RMSE	0.97				0.35				1.31			
MAD	0.74				0.30				1.14			
R	0.42											
particulate CHR												
	daily				day				night			

	obs	sim	sim-obs	(sim-obs)/obs	obs	sim	sim-obs	(sim-obs)/obs	obs	sim	sim-obs	(sim-obs)/obs
Median	0.58	0.98	0.40	69.1%	0.45	0.45	0.00	0.7%	0.97	4.89	3.92	404.4%
MB	1.83				0.03				3.48			
RMSE	3.07				0.46				4.23			
MAD	2.00				0.35				3.51			
R	0.54											

particulate BaP

	daily				day				night			
	obs	sim	sim-obs	(sim-obs)/obs	obs	sim	sim-obs	(sim-obs)/obs	obs	sim	sim-obs	(sim-obs)/obs
Median	0.49	0.29	-0.20	-41.1%	0.39	0.13	-0.26	-67.1%	1.50	0.89	-0.61	-40.6%
MB	0.002				-0.29				0.27			
RMSE	0.61				0.38				0.76			
NMB	0.48				0.31				0.63			
R	0.62											

Table S4. Same as SI Table S3 but at the Gosan site averaged over 14–25 February, 2003.

gaseous PHE				
	obs	sim	sim-obs	(sim-obs)/obs
Median	0.54	1.14	0.60	109.8%
MB	0.92			
RMSE	2.35			
MAD	1.32			
gaseous CHR				
	obs	sim	sim-obs	(sim-obs)/obs
Median	0.02	0.02	0.00	-4.6%
MB	0.00			
RMSE	0.04			
MAD	0.03			
particulate CHR				
	obs	sim	sim-obs	(sim-obs)/obs
Median	0.40	0.06	-0.34	-84.1%
MB	-0.21			
RMSE	0.51			
MAD	0.36			
particulate BaP				
	obs	sim	sim-obs	(sim-obs)/obs
Median	0.016	0.018	0.002	13.8%
MB	0.000			
RMSE	0.021			
MAD	0.016			

Text S1. Overview of the heterogeneous degradation of BaP.

In the atmosphere, BaP resides almost entirely in the particle phase of aerosols and undergoes heterogeneous reaction with ozone, but the reactivity is not well characterized for particles of complex composition and morphology. Laboratory experiments have shown that the reaction with ozone is fast on the surface of solid particles but decreases substantially on liquid substrates and in the presence of coatings that can shield BaP from the oxidant (Pöschl et al., 2001; Kwamena et al., 2004; Kahan et al., 2006; Shiraiwa et al., 2009; Zhou et al., 2012; Zhou et al., 2013). So far, however, laboratory data are available only at room temperature and some of the experiments were performed at unrealistically high ozone concentrations (up to 3 orders of magnitude above tropospheric levels). Field experiments indicate substantial but not very fast degradation of BaP on aerosols in ambient air (Schauer et al. 2003), and recent studies suggest that the phase state can strongly influence the rates of gas uptake, oxidation, and chemical aging of organic aerosol particles depending on temperature and relative humidity (e.g., Shiraiwa et al. 2011, Berkemeier et al. 2016). Following up on the laboratory experiments of Zhou et al. (2012) and Zhou et al. (2013), Shrivastava et al. (2017) applied a highly simplified parameterization to investigate the influence of temperature and humidity on the atmospheric degradation and transport of BaP and concluded that organic aerosol coatings can have a strong influence on lung cancer risks.

Text S2. Sampling at the Xianghe site and data quality control.

Particulate- and gas-phase samples were collected twice a day (day time samples 8:00 – 18:00 LT, night time samples 20:00 – 6:00 LT) during 11–22 July 2013 using a low volume sampler at a flow rate of 2.3 m^3 h^{-1} (Leckel LVS, PM_{10} inlet) equipped with a quartz filter (Whatman QMA 47 mm) and 2 polyurethane foam (PUF) plugs (Gumotex Břeclav, density 0.030 g cm^{-3}, 55 mm diameter, total depth 10 cm, cleaned by extraction in acetone and dichloromethane, 8 h each, placed in a glass cartridge) in series. Field blanks were prepared (4 for particulate phase and 3 for gas-phase) following the standard protocol for mounting QFF and PUF plugs without turning on the sampler. PAHs were analyzed using gas-chromatography coupled to a mass spectrometer operated in the electron impact ionization mode. Breakthrough of the PUFs was not expected based on estimation of the safe sample volume (Kamprad and Goss, 2007; Melymuk et al., 2016), but nevertheless was controlled by separate analysis of PUF plugs in series and confirmed to not occur.

Limits of quantification (LOQ) were calculated based on instrument detection limits, which in turn are determined using 3 times the chromatogram baseline noise level: LOQ = mean blank concentrations + 3 * standard deviations (SD). PAH concentrations are reported after subtraction of the mean field blank level (see Table S5). Only data points for which the concentrations exceeded the LOQ were considered. Therefore, gaseous PHE and CHR, and particulate phase CHR and BaP were used for the model evaluation, when all the samples with concentration exceeding LOQ. The field blank level of selected species corresponded to about 3-10% of the amounts collected in samples.

Table S5. Field blank concentrations (G: gas-phase; P: particulate phase; based on typical sampling volume) and percentage of samples with concentrations exceeding LOQ.

Species	Field blank concentrations (ng m^{-3}) Mean ± SD	Percentage of samples >LOQ
PHE	G: 2.46 ± 0.57	100%
	P: 0.56 ± 0.06	34%
CHR	G: 0.07 ± 0.006	100%
	P: 0.03 ± 0.004	100%
BaP	G: 0.03	0
	P: < 0.03	100%

Text References:

Berkemeier, T., Steimer, S. S., Krieger, U. K., Peter, T., Pöschl, U., Ammann, M., and Shiraiwa, M.: Ozone uptake on glassy, semi-solid and liquid organic matter and the role of reactive oxygen intermediates in atmospheric aerosol chemistry, Phys. Chem. Chem. Phys., 18, 12662-12674, 10.1039/c6cp00634e, 2016.

Kahan, T. F., Kwamena, N. O. A., and Donaldson, D. J.: Heterogeneous ozonation kinetics of polycyclic aromatic hydrocarbons on organic films, Atmos. Environ., 40, 3448-3459, 10.1016/j.atmosenv.2006.02.004, 2006.

Kamprad, I. and Goss, K.: Systematic Investigation of the Sorption Properties of Polyurethane Foams for Organic Vapors, Analytical Chemistry, 79, 4222-4227, 2007.

Kwamena, N. O. A., Thornton, J. A., and Abbatt, J. P. D.: Kinetics of surface-bound benzo[a]pyrene and ozone on solid organic and salt aerosols, J. Phys. Chem. A, 108, 11626-11634, 10.1021/Jp046161x, 2004.

Melymuk, L., Bohlin-Nizzetto, P., Prokeš, R., Kuku˘cka, P., and Klánová, J.: Sampling artifacts in active air sampling of semivolatile organic contaminants: Comparing theoretical and measured artifacts and evaluating implications for monitoring networks, Environ. Pollut., 217, 97–106, 2016.

Pöschl, U., Letzel, T., Schauer, C., and Niessner, R.: Interaction of ozone and water vapor with spark discharge soot aerosol particles coated with benzo[a]pyrene: O-3 and H2O adsorption, benzo[a]pyrene degradation, and atmospheric implications, J. Phys. Chem. A, 105, 4029-4041, 10.1021/Jp004137n, 2001.

Schauer, C., Niessner, R., and Pöschl, U.: Polycyclic aromatic hydrocarbons in urban air particulate matter: Decadal and seasonal trends, chemical degradation, and sampling artifacts, Environ. Sci. Technol., 37, 2861-2868, 10.1021/es034059s, 2003.

Shiraiwa, M., Garland, R. M., and Pöschl, U.: Kinetic double-layer model of aerosol surface chemistry and gas-particle interactions (K2-SURF): Degradation of polycyclic aromatic hydrocarbons exposed to O3, NO2, H2O, OH and NO3, Atmos. Chem. Phys., 9, 9571-9586, 10.5194/acp-9-9571-2009, 2009.

Shiraiwa, M., Ammann, M., Koop, T., and Pöschl, U.: Gas uptake and chemical aging of semisolid organic aerosol particles, Proc. Natl. Acad. Sci. USA, 108, 11003-11008, 10.1073/pnas.1103045108, 2011.

Shrivastava, M., Lou, S., Zelenyuk, A., Easter, R. C., Corley, R. A., Thrall, B. D., Rasch, P. J., Fast, J. D., Massey Simonich, S. L., Shen, H., and Tao, S.: Global long-range transport and lung cancer risk from polycyclic aromatic hydrocarbons shielded by coatings of organic aerosol, Proceedings of the National Academy of Sciences, 10.1073/pnas.1618475114, 2017.

Zhou, S., Lee, A. K. Y., McWhinney, R. D., and Abbatt, J. P. D.: Burial Effects of Organic Coatings on the Heterogeneous Reactivity of Particle-Borne Benzo[a]pyrene (BaP) toward Ozone, J. Phys. Chem. A, 116, 7050-7056, 10.1021/Jp3030705, 2012.

Zhou, S. M., Shiraiwa, M., McWhinney, R. D., Pöschl, U., and Abbatt, J. P. D.: Kinetic limitations in gas-particle reactions arising from slow diffusion in secondary organic aerosol, Faraday Discuss., 165, 391-406, 10.1039/C3fd00030c, 2013.

B.2 Mu et al., Sci. Adv., 2018

Temperature effect on phase state and reactivity controls atmospheric multiphase chemistry and transport of PAHs

Qing Mu[1], Manabu Shiraiwa[1,2], Mega Octaviani[1], Nan Ma[3,1], Aijun Ding[4,5], Hang Su[3,1], Gerhard Lammel[1,6], Ulrich Pöschl[1,7], Yafang Cheng[1,3]

[1] Multiphase Chemistry Department, Max Planck Institute for Chemistry, P.O. Box 3060, 55128 Mainz, Germany

[2] Department of Chemistry, University of California, Irvine, 92697-2025 California, USA

[3] Institute for Environmental and Climate Research, Jinan University, 511443 Guangzhou, China

[4] Joint International Research Laboratory of Atmospheric and Earth System Sciences, School of Atmospheric Sciences, Nanjing University, 210023, Nanjing, China

[5] Jiangsu Provincial Collaborative Innovation Center of Climate Change, 210023, Nanjing, China

[6] Research Centre for Toxic Compounds in the Environment, Masaryk University, 62500 Brno, Czech Republic

[7] Johannes Gutenberg University Mainz, 55122 Mainz, Germany

Author contributions

Y.C., H.S., U.P. and G.L. conceived the study. M.S., Y.C., H.S. and U.P. developed the temperature dependent ROI-T scheme for model implementation. Q.M. incorporated new PAH module into the regional model WRF-Chem and performed the model simulation and data analyses. M.O. incorporated new PAH module into the global model EMAC and performed the model simulation and data analyses. Y.C., H.S. and Q.M. analyzed and interpreted results. N.M. contributed to data analysis and visualization. A. D. contributed to the transport process analysis and relevant discussion in the SI. All coauthors discussed the results. H.S., Y.C. and Q.M. wrote the manuscript with input from all coauthors.

ATMOSPHERIC SCIENCE

Temperature effect on phase state and reactivity controls atmospheric multiphase chemistry and transport of PAHs

Qing Mu,[1]* Manabu Shiraiwa,[1,2] Mega Octaviani,[1]* Nan Ma,[3,1] Aijun Ding,[4,5] Hang Su,[3,1]† Gerhard Lammel,[1,6†] Ulrich Pöschl,[1,7] Yafang Cheng[1,3†]

Polycyclic aromatic hydrocarbons like benzo(*a*)pyrene (BaP) in atmospheric particulate matter pose a threat to human health because of their high carcinogenicity. In the atmosphere, BaP is mainly degraded through a multiphase reaction with ozone, but the fate and atmospheric transport of BaP are poorly characterized. Earlier modeling studies used reaction rate coefficients determined in laboratory experiments at room temperature, which may overestimate/underestimate degradation rates when applied under atmospheric conditions. Moreover, the effects of diffusion on the particle bulk are not well constrained, leading to large discrepancies between model results and observations. We show how regional and global distributions and transport of BaP can be explained by a new kinetic scheme that provides a realistic description of the temperature and humidity dependence of phase state, diffusivity, and reactivity of BaP-containing particles. Low temperature and humidity can substantially increase the lifetime of BaP and enhance its atmospheric dispersion through both the planetary boundary layer and the free troposphere. The new scheme greatly improves the performance of multiscale models, leading to better agreement with observed BaP concentrations in both source regions and remote regions (Arctic), which cannot be achieved by less-elaborate degradation schemes (deviations by multiple orders of magnitude). Our results highlight the importance of considering temperature and humidity effects on both the phase state of aerosol particles and the chemical reactivity of particulate air pollutants.

INTRODUCTION

Polycyclic aromatic hydrocarbons (PAHs) are derived from combustion processes. High health risks are associated with exposure to PAHs, among which benzo(*a*)pyrene (BaP) is one of the most carcinogenic species (*1*, *2*). Because BaP resides almost entirely in the particulate phase, the distribution and long-range atmospheric transport of BaP are largely controlled by its multiphase degradation, mainly the reaction of particulate BaP with gaseous ozone (*3*). Laboratory studies showed rapid BaP degradation on the surface of soot, ammonium sulfate, and organic aerosol (OA) particles (*4*–*6*), whereas atmospheric observations revealed a much longer lifetime and persistence of BaP especially toward remote and polar regions (*7*, *8*). Recent laboratory and kinetic studies have shown that OA coatings can effectively shield BaP from oxidants and that the OA phase state may strongly influence the rate of degradation (*9*–*13*). However, key factors controlling the multiphase degradation and the fate of BaP in aerosols under real atmosphere conditions are still not resolved (*14*). In particular, the laboratory-derived degradation schemes of BaP that have been applied in previous model studies (Fig. 1A and table S1) (*14*–*21*) do not fully account for dependence on environmental conditions/parameters.

Temperature (T) and relative humidity (RH) in the atmosphere cover a wide range, which influence not only the phase state and diffusivity of OA (*12*) but also the chemical reactivity of organic compounds. Because most modeling studies used degradation rates determined at room temperature (that is, 296 to 298 K) in laboratory experiments, they may overestimate degradation rates when applied in colder atmospheric environments. On the basis of the study of Zhou *et al.* (*11*), Shrivastava *et al.* (*14*) introduced a threshold temperature below which the OA coating was assumed to shut off the multiphase degradation of BaP. This shielding effect improved agreement between model predictions and observations and was very sensitive to choice of threshold temperature. A simple threshold value, however, does not resolve the actual temperature dependence of multiphase reactions because both the molecular diffusivity and the chemical reactivity of BaP are expected to exhibit a continuous change in response to changing temperature rather than following a step function (*13*).

Moreover, the effects of diffusion and reaction on the particle bulk are not well characterized in earlier studies. For example, most laboratory experiments (*4*, *5*, *11*, *22*) were carried out under excessively high ozone concentrations (up to three orders of magnitude above tropospheric levels), and often, surface reaction rate equations were used to extrapolate the laboratory results for application in atmospheric models. The use of surface reaction rate equations without considering bulk processes, however, can result in inconsistent dependencies of BaP degradation rates on RH and ozone concentration (text S1).

Here, we use an advanced kinetic model framework to develop an elaborate kinetic scheme for better representation of multiphase degradation of BaP in regional and global models. This new scheme has incorporated three major improvements compared to previous schemes: (i) considering the formation of reactive oxygen intermediates (ROIs), (ii) including temperature and humidity effects on phase state of OA and temperature-dependent chemical reactivity, and (iii) using a model

[1]Multiphase Chemistry Department, Max Planck Institute for Chemistry, P.O. Box 3060, 55128 Mainz, Germany. [2]Department of Chemistry, University of California, Irvine, Irvine, CA 92697–2025, USA. [3]Institute for Environmental and Climate Research, Jinan University, 511443 Guangzhou, China. [4]Joint International Research Laboratory of Atmospheric and Earth System Sciences, School of Atmospheric Sciences, Nanjing University, 210023 Nanjing, China. [5]Jiangsu Provincial Collaborative Innovation Center of Climate Change, 210023 Nanjing, China. [6]Research Centre for Toxic Compounds in the Environment, Masaryk University, 62500 Brno, Czech Republic. [7]Johannes Gutenberg University Mainz, 55122 Mainz, Germany.
*These authors contributed equally to this work.
†Corresponding author. Email: yafang.cheng@mpic.de (Y.C.); g.lammel@mpic.de (G.L.); h.su@mpic.de (H.S.)

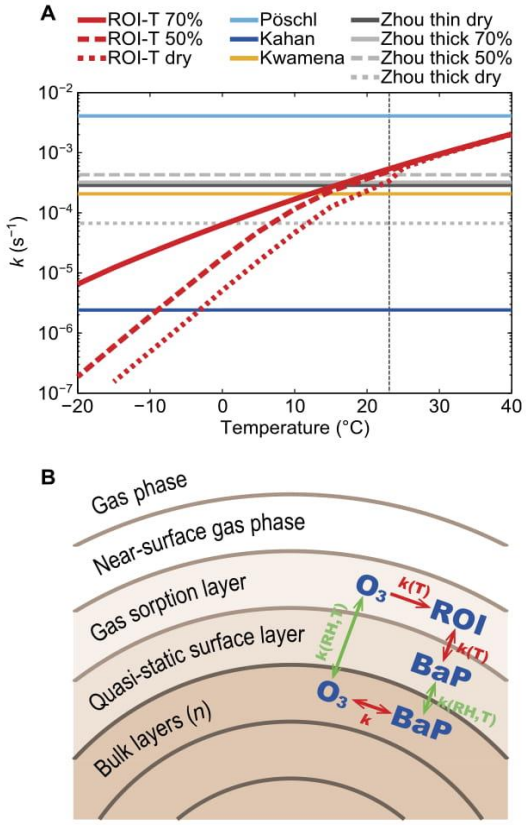

Fig. 1. Kinetic scheme ROI-T. (**A**) First-order multiphase degradation rate coefficient k (s^{-1}) for laboratory schemes of Pöschl *et al.* (*4*), Kahan *et al.* (*22*), Kwamena *et al.* (*5*), and Zhou *et al.* (*11*) (table S1) and the kinetic scheme ROI-T at 50 ppb O_3. Vertical dashed line denotes 23°C. (**B**) Model framework of the multilayer kinetic scheme ROI-T. Red arrows show the reactions: O_3 is decomposed and forms ROI in the gas sorption layer, BaP reacts with ROI between gas sorption and surface layer, and BaP reacts with O_3 in the bulk. Green arrows show the RH/T-dependent mass transport: O_3 from gas sorption to bulk layer, BaP from bulk to surface layer.

framework that considers both bulk diffusion/reaction and surface reaction to interpret laboratory results for application in models and comparison to field measurements. We find that the new ROI-T scheme can be a good predictor of BaP concentrations from regional to global scales. Our results highlight the importance of temperature in BaP multiphase degradation from a kenitic view and demonstrate a universal scheme that can be applied for various atmospheric conditions and geolocations. Because of the common existence of OA coating, similar temperature effects are expected for other multiphase reactions, which can be determined from laboratory studies by the general modeling framework and approaches proposed here.

RESULTS

BaP degradation kinetic scheme

In the new kinetic scheme ROI-T, the multiphase degradation of BaP with ozone is treated in multiple compartments as shown in Fig. 1B, which has not yet been fully considered by previous schemes. The reaction involves the decomposition of surface ozone and formation of ROI (*23*). To account for mass transport and reactions of gaseous and particle-bound chemical species at the surface and in the bulk phase, we apply the kinetic multilayer model of aerosol surface and bulk chemistry (KM-SUB) (*24*) (see KM-SUB model in Materials and Methods), which is based on the Pöschl-Rudich-Ammann framework (*25*). Secondary OA (SOA) formed from α-pinene oxidation was chosen to represent the OA coating (*11*). With the kinetic parameters in table S2, the new kinetic scheme ROI-T can effectively explain the kinetics of multiphase degradation of BaP and successfully reproduce the results of the Zhou's experimental data (*11*) for both thin and thick coating cases (8 and 40 nm) at different RH (that is, dry, 50% and 70%). In further regional/global model applications, the thick coating scenario is adopted, because the global simulation has found that the OA shielding on BaP is generally thick (*14*). As shown in Fig. 1A, rather than a fixed degradation rate, the rate coefficients of the ROI-T scheme show a monotonic increase with increasing temperature and systematically smaller degradation rate of BaP at lower RH.

The temperature and RH dependence of diffusivity and BaP chemical reactivity both control the degradation rate of BaP. In the new ROI-T scheme, on the one hand, temperature influences OA diffusivity and its phase state, that is, the diffusion coefficients of ozone and BaP are assumed to decrease by one order of magnitude upon a temperature decrease of 10°C (*26*) (see KM-SUB model in Materials and Methods). On the other hand, temperature influences the chemical reactivity of BaP with ROI following the Arrhenius equation (see KM-SUB model in Materials and Methods). Considering both effects, the degradation rates of BaP at 253 K are three to four orders of magnitude smaller than those at 313 K (Fig. 1A).

To demonstrate the advantages of the new ROI-T scheme, we have also included other commonly used degradation schemes of BaP: Kwamena *et al.* (*5*), Kahan *et al.* (*22*), and Pöschl *et al.* (*4*) schemes refer to ozonolysis of uncoated BaP on azelaic acid, liquid substrates, and soot, respectively; the Zhou *et al.* (*11*) scheme refers to ozonolysis of OA-coated BaP. As shown in Fig. 1A, these schemes show different degradation rates due to the substrate and shielding effects summarized in table S1.

Model versus observation

Other BaP degradation schemes provide reliable predictions only at specific characteristic distances from sources or geolocations but are less at others. For example, the Kwamena scheme shows the best agreement with observations at mid-latitude, whereas the optimum scheme for the Arctic is the scheme that predicts the slowest degradation rates, that is, the Kahan scheme (Fig. 1A) (*17*, *19*). The ROI-T scheme, on the contrary, can account for the different temperature/RH regimes at different locations and transport distances.

In Fig. 2A, we compare the performance of the kinetic ROI-T scheme and the most commonly used Kwamena scheme (*15*, *18*, *21*, *27*) in multiscale model simulations (see Model setup and BaP extension in Materials and Methods). The model results from the Pöschl scheme (the fastest) and the Kahan scheme (the slowest) (Fig. 1A) are also included as references. The observational data used for model evaluation cover a wide range of source/receptor sites over a large span of latitudes (33° to 83°N; see Observational data of BaP in Materials and Methods). Compared with other schemes, the ROI-T scheme consistently provides better predictions at all types of sites, from near-source, mid-latitude, remote background sites to the Arctic (table S4). It improves

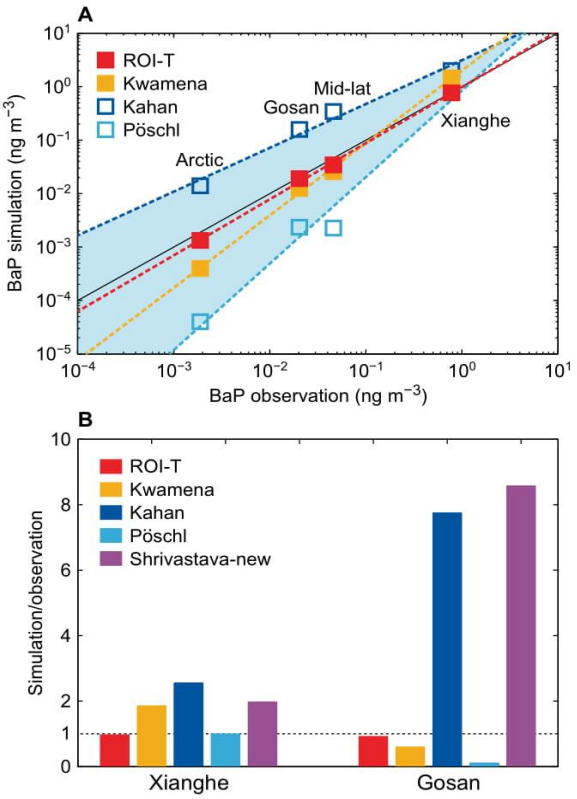

Fig. 2. Comparisons of the ROI-T scheme and previous laboratory-derived schemes with observations. (**A**) Simulated concentrations of BaP (ng m^{-3}) by the ROI-T, Kwamena, Kahan, and Pöschl schemes at the Xianghe site, the Gosan site, other mid-latitude sites, and the Arctic sites. The solid black line is a 1:1 line of simulation and observation. The dashed lines are fitted by respective simulations. The shaded area is constrained by the Pöschl and Kahan schemes. (**B**) The ratios of simulated and observed BaP concentrations with different schemes at the Xianghe site and the Gosan site.

the BaP simulation most significantly at the Arctic sites, where air masses underwent the longest and coldest transport processes. For example, simulated BaP levels at the Alert and Spitsbergen sites are improved by more than one order of magnitude with the ROI-T scheme compared with the Kwamena scheme (table S4A).

To further elucidate the advantages of the ROI-T scheme, we focus on two cases with contrasting temperature/RH conditions (Fig. 2B): a near-source site Xianghe (39.80°N, 116.96°E, 45 km southeast of Beijing, China), representing the local surface transport in hot/humid environment in July, and a remote background site Gosan (33.28°N, 126.17°E on the Jeju Island, about 100 km south of the Korean peninsula), representing long-range transport in cold/dry air in February. The results show that it is impossible to reproduce observations for both cases by a fixed degradation rate. The Kwamena scheme is either too slow for the Xianghe summer case or too fast for the Gosan winter case, suggesting strong temperature and humidity effects on the diffusivity and reactivity. The model performance cannot be improved by simply changing for another degradation rate, because a higher (lower) degradation rate will reduce (increase) the BaP concentrations at both sites. As shown in Fig. 2 (A and B), a scheme with faster degradation rates, such as Pöschl scheme, reduces the BaP concentration to the same level as observations for the Xianghe case but shows a larger underestimation for the Gosan case. We also test the step function setting of the Zhou scheme as in Shrivastava *et al.* (*14*). It cannot reproduce BaP observations over both cases either, with a very similar performance as the Kahan scheme (the slowest) (Fig. 2B).

By unifying the impact of temperature and RH on diffusivity and reactivity under an elaborate kinetic framework (Fig. 1B), the ROI-T scheme solves the problem with changing BaP degradation rates in response to the changes of environmental conditions (Fig. 1A). Under the new scheme, the hot/humid conditions increase the diffusivity/reactivity and the BaP degradation rate, whereas it is the other way around in the cold/dry environment. Compared with the Kwamena scheme, our ROI-T scheme leads to reduced BaP concentrations at the Xianghe site and elevated BaP concentration at the Gosan site, finally showing good agreements for both cases. The changes in both diffusivity and chemical reactivity contribute to the changes of degradation rate in the new ROI-T scheme. To decouple their effects, we perform sensitivity studies by turning on/off the temperature/RH dependence of diffusivity. At the Gosan site, a fixed degradation rate in ROI-T scheme at room temperature 296 K leads to an underestimation of BaP concentration by a factor of 3. Further tests show that the temperature/RH-induced change of diffusivity would account for ~50% of the improvement in the predicted BaP concentrations, whereas the change of reactivity further contributes to the rest of the ~50% (as shown by the comparison between the "ROI-T at 296 K" and "ROI-T with fixed diffusivity" cases in fig. S1).

East Asia outflow

As one of the largest source regions, the outflow of BaP from East Asia to the downwind regions and remote Pacific Ocean is of international concern (*28*, *29*). Figure 3 (A and B) shows a typical outflow transport of BaP from East Asia in winter (24 February 2003). With the Kwamena scheme, most BaP is bounded in the boundary layer due to fast degradation with an average lifetime of ~2 to 3 hours throughout the whole domain (fig. S2), resulting in very low concentrations above 1 km (Fig. 3A). However, the decrease of degradation rate, which results from the change in temperature and RH during air mass rising (see temperature and RH distribution in fig. S3), is not accounted for. Even when BaP is able to escape out of the boundary layer by large-scale advections associated with cyclones or by convections in mid-latitudes (that is, 35° to 45°N), fast degradation limits dispersion and transport of BaP to the vicinity of the source region. Thus, the transport of BaP with the Kwamena scheme is constrained within the boundary layer, and the long-range transport impacts are limited.

The ROI-T scheme shows a different spatial distribution and transport pathway of BaP, with more BaP distributed at higher altitude. This is because low temperature reduces OA diffusivity and reaction rate of BaP with ROI ["freezing effect"; see three-dimensional (3D) degradation rate k in fig. S2] and thus leads to a much longer lifetime of BaP above 1 km (~2 to 3 hours to more than 20 days; fig. S2), making transport in the free troposphere an efficient pathway. Compared with the Kwamena scheme, 15 times more BaP is lifted by frontal activities and convection to middle troposphere, where strong westerlies/jets cause a fast transport of the plumes to downwind areas (figs. S5 and S6 and text S2) and toward polar region, resulting in much stronger global impacts. At the cross section of 126°E (Fig. 3, A and B), the BaP outflow toward the ocean shows a maximum zonal net flux of ~35 ng m^{-2} s^{-1} in

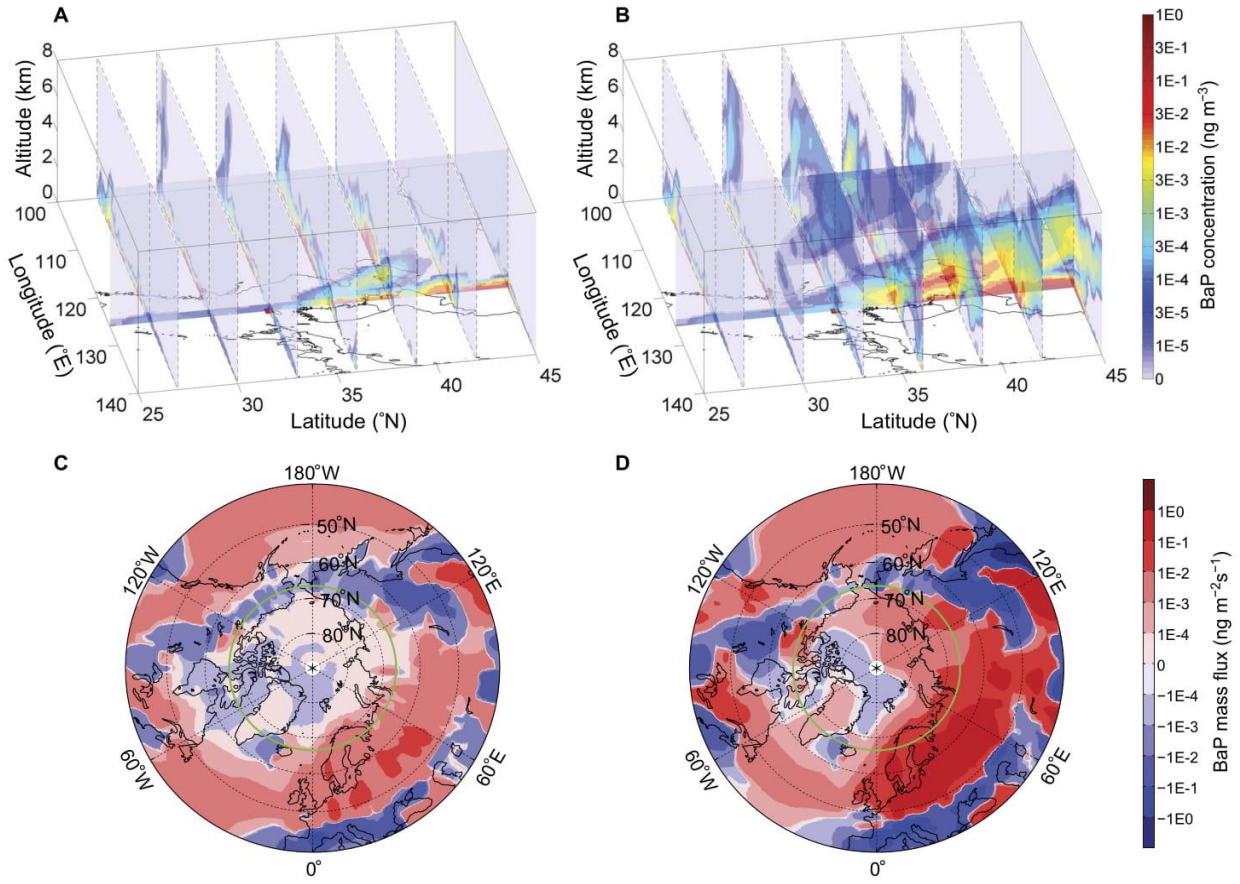

Fig. 3. Implications on the transport. Average concentrations of BaP (ng m^{-3}) in a strong East Asia outflow episode on 24 February 2003 are shown for the (**A**) Kwamena scheme and the (**B**) ROI-T scheme. Longitude cross section locates at 126°E. BaP net meridional flux (ng m^{-2} s^{-1}) averaged over years 2007–2009 are shown for the (**C**) Kwamena scheme and the (**D**) ROI-T scheme. Northward has positive values (red), and southward has negative values (blue). Green circle marks the Arctic Circle at 66.56°N.

the ROI-T scheme but only ~10 ng m^{-2} s^{-1} in the Kwamena scheme (fig. S4, A and B). It is also clear that the vertical center of the BaP column mass in the ROI-T scheme is higher than that in the Kwamena scheme, that is, ~0.6 and 0.3 km, respectively (fig. S4, C and D).

Transport to the Arctic

BaP emitted in source regions can undergo intercontinental transport, allowing them to distribute and accumulate even in the polar regions (*7*, *30*). The concentration level of BaP in the Arctic arouses high interest, because BaP is not only a good indicator of human contamination (*30*) but also responsible for the severe bioconcentrate effect in the Arctic (*31*) where the ecosystem is most vulnerable, bioaccumulation along marine and terrestrial food chains (*31*–*33*). As shown in the East Asia outflow case, the "freezing effect" may make the intercontinental transport of BaP from source regions to the Arctic at high-altitude or low-temperature regions more efficient than previously thought.

As shown in Fig. 3 (C and D), BaP in the Arctic is mainly transported from Europe, North America, and Asia, similar to long-lived halogenated pollutants (*34*). The 2007–2009 average total meridional net flux of BaP toward the Arctic (integrated over 1000 to 10 hPa at 65°N) is 1.97 ng m^{-2} s^{-1} with the ROI-T scheme but only 0.12 ng m^{-2} s^{-1} with the Kwamena scheme (fig. S4E), which is about 16 times lower. The larger fluxes of BaP with the ROI-T scheme can be attributed to a longer lifetime of BaP caused by the "freezing effect" (fig. S2), because the pollutant is transported significantly higher. The average vertical center of the BaP column mass transported across 65°N during 2007–2009 is 2 km for the ROI-T scheme but only 0.5 km for the Kwamena scheme (fig. S4F), showing a more prominent difference in height than that in the East Asian outflow case.

DISCUSSION

The strong temperature/RH effects on fate and global transport of BaP advance the understanding and challenge the traditional view of modeling the multiphase degradation of reactive pollutants (for example, BaP) in OAs. In warm/humid environments (for example, tropical rainforests), aerosol particles tend to be liquid, whereas in cold environments, aerosols are found to be in an amorphous solid phase, most probably a glassy state (*12*). The phase state and degradation rate of BaP may vary largely depending on temperature/RH

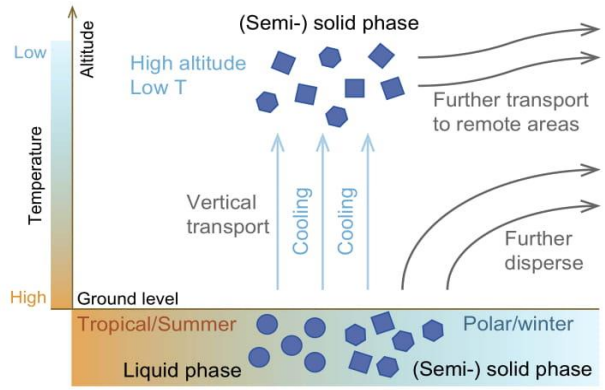

Fig. 4. Diagram of temperature/RH effects on BaP transport in ambient air. OA diffusivity and chemical reactivity are both reduced in response to changes in season (summer to winter), latitude (tropical to polar), and altitude (surface to high altitude), when OA phase state also changes from liquid to (semi-) solid phase. With a slower degradation rate and hence prolonged lifetime, BaP can be further dispersed and transported.

and hence the season (summer versus winter), altitude (surface versus high altitude), and latitude (tropical versus polar) (Fig. 4). It also emphasizes the importance of higher altitude or cold season/region pathway for the long-range transport, that is, the low temperature helps OA and reactive compounds within it survive from the multiphase chemistry, remaining undergrated and being transported further.

The ROI-T scheme is based on the kinetic data observed on the ozonolysis of BaP coated by α-pinene SOA. Recent studies have suggested that α-pinene SOA is less viscous than aromatic SOA and is more viscous than isoprene SOA (*35*, *36*). SOA particles are also often internally mixed with inorganic components, which may affect particle phase state, nonideal mixing and morphology, and hence the multiphase reaction rates (*37*). Therefore, the effects of different SOA precursors and inorganic interactions should be further explored. Partitioning of PAHs to other OAs, such as bioparticles, is less efficient than partitioning to liquid and semisolid SOA (*38*). The presence of more viscous bioparticles will lead to less reactive PAHs and therefore an even higher long-range transport potential.

The large impact of temperature/RH on the diffusivity/reactivity is not limited to the degradation of BaP but has general implications for all kinds of multiphase reactions in aerosols, clouds, and fog droplets relevant for atmospheric chemistry and transport (*9*, *12*, *39*, *40*). The impact is particularly important for the northern hemisphere, where efficient large-scale advection/convection associated with cyclones and strongest anthropogenic emissions exist. Our results demonstrate that it is important to perform laboratory kinetic studies on the large temperature/RH span relevant for atmospheric conditions. Our modeling scheme provides an advanced physicochemical-based framework for the representation of multiphase reaction in atmospheric models and can be readily modified to include other hazardous air pollutants and OA species once the kinetic data are available.

MATERIALS AND METHODS

Model setup

The ROI-T scheme was incorporated as a look-up table (table S3) into two state-of-the-art models with BaP extension for further application.

Regional model

The open-source community model WRF-Chem (Weather Research and Forecasting model coupled with Chemistry), an "online" regional model with coupled meteorology and chemistry (*41*, *42*), has higher spatial resolution and greater advantages in determining the fine structures of transport process, especially the vertical transport within and out of the boundary layer. The PAH extension was based on the model version 3.6.1.

The physics schemes of the regional WRF-Chem model used here were as follows (*42*): microphysics and cumulus parameterizations followed the Purdue-Lin scheme and the Grell 3D ensemble scheme, respectively. The longwave and shortwave radiations were calculated by the online rapid radiative transfer model and the Goddard scheme, respectively. The planetary boundary layer was based on the Mellor-Yamada-Janjic scheme, along with the Eta similarity surface layer scheme. The implemented air-soil gas exchange was coupled with the Noah land surface model. Photolysis rates used the Fast-J photolysis scheme. As for the chemistry schemes, we used the Regional Atmospheric Chemistry Mechanism (RACM) for homogeneous gas-phase reactions. The aerosol module included the inorganic fraction Modal Aerosol Dynamics model for Europe (MADE) and organic fraction Secondary Organic Aerosol Model (SORGAM).

Global model

The global model EMAC (ECHAM/MESSy Atmospheric Chemistry) covered intercontinental transport, such as from source areas to the Arctic. It was a combination of the ECHAM5 general circulation model (*43*) and MESSy (Modular Earth Submodel System, version 2.5) (*44*). MESSy provided infrastructure to couple the base model ECHAM5 and different components (or submodels) that represent various processes of the Earth system.

The model simulations included the following MESSy submodels (*44*): CLOUD described cloud scheme and precipitation. Convection parameterization and radiation were in submodels CONVECT and RAD. Air-sea exchange was parameterized by AIRSEA. Wet and dry depositions were described by SCAV and DDEP. Prescribed emissions were calculated by OFFLEM, whereas online emissions were calculated by ONLEM. As for chemistry, MECCA was responsible for gas-phase chemistry, JVAL took care of photolysis rate, and GMXe was the submodel for aerosol microphysics and semivolatile inorganic partitioning.

Simulation

We performed regional (global) simulations at a grid spacing of 27 km × 27 km (1.9° × 2.5°) with 39 (19) vertical levels from the surface to 100 hPa (10 hPa). Simulations were conducted during 11 to 22 July 2013 for Xianghe case and 14 to 25 February 2003 for Gosan case over East Asia domain (15° to 55°N, 95° to 155°E) by the regional model, and 2007 to 2009 for mid-latitude and Arctic sites by the global model, respectively.

BaP extension

The following processes of BaP were included: emission, gas-particle partitioning, gas-phase and multiphase reactions, air-soil gas exchange, and wet and dry depositions.

Emissions

Anthropogenic BaP emissions were regridded from a 0.1° × 0.1° global annual PAH emission inventory, with 69 detailed source types (*45*). Monthly variation was based on black carbon (BC) emission seasonality of HTAP_v2.2 (*46*). For regional simulations, annual scaling factors (*45*) and diurnal cycle (following BC) of the PAH emissions were also applied. Biogenic contributions to PAH emission have been neglected.

Gas-particle partitioning

Gas-particle partitioning of BaP used in the regional model followed an equilibrium partitioning expression that accounted for the absorption into organic matter and adsorption onto BC (*47*, *48*). In the global model, polyparameter linear free energy relationships were applied, which accounted for BaP absorption into organic matter and adsorption to soot and inorganic salts (*38*).

Gas-phase reaction

The second-order rate coefficients for reactions of gaseous BaP with OH, NO_3, and O_3 are 1.5×10^{-10}, 5.4×10^{-11}, and 2.6×10^{-17} cm^3 $molecules^{-1}$ s^{-1}, respectively (*49*).

Wet/dry depositions

The original regional/global model routines have been adapted to include the deposition of gas-phase and particulate-phase BaP using corresponding deposition parameterizations.

Air-soil gas exchange

Air-soil gas exchange of BaP was parameterized (*50*) on the basis of air/soil concentrations and properties of BaP. The concentrations of BaP in soil were initialized by the global multicompartmental model ECHAM5-HAM: BaP has been globally simulated over 10 years with $2.8° \times 2.8°$ horizontal resolution (*51*). A steady state of BaP concentrations in the soil compartment was safely reached.

KM-SUB model

The KM-SUB model treats mass transport and chemical reactions at the surface and in the particle bulk (*24*). KM-SUB was composed of the following compartments: gas phase, near-surface gas phase, sorption layer, quasi-static surface layer, near-surface bulk layer, and a number of bulk layers. The model resolved the following processes explicitly: gas-phase diffusion, reversible adsorption of O_3, surface reaction involving decomposition of O_3 and formation of long-lived ROIs, bulk diffusion of O_3 and BaP in OA coating, and bulk reaction between O_3 and BaP. Note that heat transfer was not treated in the model because heat released by trace gas uptake and reactions can be efficiently buffered by the ambient gas and did not lead to a substantial increase of particle-surface temperature (*52*). KM-SUB can simulate the evolution of species at the particle surface and in the particle bulk, along with surface concentrations and gas uptake coefficients. Core-shell morphology was assumed with an organic phase embedding BaP as particle shell and an inorganic phase as particle core (*37*). The required kinetic parameters were summarized in table S2, and the values were on the basis of previous studies of KM-SUB applications to experimental data of Zhou *et al.* (*11*).

The ROI-T considered the temperature dependence of bulk diffusivity and chemical reactivity. The diffusion coefficients of ozone and PAH were assumed to decrease by one order of magnitude upon a decrease of temperature by 10°C based on the Vogel-Fulcher-Tamman approach (*26*, *35*). Temperature dependence of rate coefficients k was considered by the Arrhenius equation using the activation energies of surface reactions as listed in table S2. KM-SUB simulations were conducted in the temperature range of −20° to 40°C with gas-phase ozone concentrations of 0 to 200 parts per billion (ppb). The obtained first-order decay rate of PAH was then fitted with the Hill equation as shown in table S3, so that the parameterizations can be efficiently incorporated in regional and global transport models.

Observational data of BaP

The near-source observation data of BaP were collected at the Xianghe Atmospheric Observatory (39.80°N, 116.96°E). The Xianghe site is a suburban site, located 45 km southeast of Beijing and 70 km northwest of Tianjin. Particulate- and gas-phase samples were collected for daytime (8:00 to 18:00 local time) and nighttime (20:00 to 6:00 local time), respectively, during 11 to 22 July 2013.

The outflow observation data of BaP were measured at the Gosan site (33.28°N, 126.17°E) on Jeju Island. The site was 72 m above sea level and about 100 km south of the Korean peninsula. Gosan is a representative background station in East Asia to study outflow of air pollutants from land to ocean. Intensive daily measurements (8:00 to 8:00 local time in the following morning) of particulate phase BaP were carried out during a pollution period 14 to 25 February 2003. Details of sampling and analysis methods were given in the study of Kim *et al.* (*53*).

The mid-latitude observation data of BaP were taken from 18 stations of the European Monitoring and Evaluation Programme (EMEP) (*54*), the Integrated Atmospheric Deposition Network (*55*), and Arctic Monitoring and Assessment Programme (AMAP) (*56*). Three Arctic sites (that is, north of 66.5°N) are as follows: Alert in Canada (AMAP; 62.3°W, 82.5°N), Spitsbergen in Norway (EMEP; 11.9°E, 78.9°N), and Pallas in Finland (EMEP; 24.3°E, 68.0°N). The concentration of BaP during 2007–2009 was averaged over all months, with at least 1 weekly measurement reported.

SUPPLEMENTARY MATERIALS

Supplementary material for this article is available at http://advances.sciencemag.org/cgi/content/full/4/3/eaap7314/DC1

text S1. Problems without considering bulk processes.
text S2. Warm conveyor belts (WCBs) and BaP transport in Gosan winter case.
table S1. Flow tube experiments of multiphase degradation of BaP with ozone.
table S2. Kinetic parameters used in the KM-SUB simulation for the ozonolysis of BaP to reproduce experiment results of the Zhou scheme.
table S3. Parameterization of multiphase degradation rate for the ozonolysis of BaP.
table S4. Comparisons of observed and predicted BaP concentrations in the regional WRF-Chem model and the global EMAC model.
fig. S1. Same as Fig. 2B but with three more sensitivity studies.
fig. S2. Multiphase degradation rate and chemical lifetime.
fig. S3. BaP concentrations and multiphase degradation rate.
fig. S4. Net meridional mass flux and vertical center of column mass for BaP in different cases.
fig. S5. BaP transport due to WCB and frontal activities associated with mid-latitude cyclones for the Gosan winter case.
fig. S6. A conceptual scheme for air pollution transport due to middle-latitude cyclone.
References (*57*–*60*)

REFERENCES AND NOTES

1. F. P. Perera, Environment and cancer: Who are susceptible? *Science* **278**, 1068–1073 (1997).
2. P. Boffetta, N. Jourenkova, P. Gustavsson, Cancer risk from occupational and environmental exposure to polycyclic aromatic hydrocarbons. *Cancer Causes Control* **8**, 444–472 (1997).
3. I. J. Keyte, R. M. Harrison, G. Lammel, Chemical reactivity and long-range transport potential of polycyclic aromatic hydrocarbons—A review. *Chem. Soc. Rev.* **42**, 9333–9391 (2013).
4. U. Pöschl, T. Letzel, C. Schauer, R. Niessner, Interaction of ozone and water vapor with spark discharge soot aerosol particles coated with benzo[*a*]pyrene: O_3 and H_2O adsorption, benzo[*a*]pyrene degradation, and atmospheric implications. *J. Phys. Chem. A* **105**, 4029–4041 (2001).
5. N.-O. A. Kwamena, J. A. Thornton, J. P. D. Abbatt, Kinetics of surface-bound benzo[*a*]pyrene and ozone on solid organic and salt aerosols. *J. Phys. Chem. A* **108**, 11626–11634 (2004).
6. S. Zhou, A. K. Y. Lee, R. D. McWhinney, J. P. D. Abbatt, Burial effects of organic coatings on the heterogeneous reactivity of particle-borne benzo[*a*]pyrene (BaP) toward ozone. *J. Phys. Chem. A* **116**, 7050–7056 (2012).
7. C. J. Halsall, L. A. Barrie, P. Fellin, D. C. G. Muir, B. N. Billeck, L. Lockhart, F. Ya. Rovinsky, E. Ya. Kononov, B. Pastukhov, Spatial and temporal variation of polycyclic aromatic hydrocarbons in the Arctic atmosphere. *Environ. Sci. Technol.* **31**, 3593–3599 (1997).

8. C. Schauer, R. Niessner, U. Pöschl, Polycyclic aromatic hydrocarbons in urban air particulate matter: Decadal and seasonal trends, chemical degradation, and sampling artifacts. *Environ. Sci. Technol.* **37**, 2861–2868 (2003).
9. M. Shiraiwa, M. Ammann, T. Koop, U. Pöschl, Gas uptake and chemical aging of semisolid organic aerosol particles. *Proc. Natl. Acad. Sci. U.S.A.* **108**, 11003–11008 (2011).
10. T. Berkemeier, S. S. Steimer, U. K. Krieger, T. Peter, U. Pöschl, M. Ammann, M. Shiraiwa, Ozone uptake on glassy, semi-solid and liquid organic matter and the role of reactive oxygen intermediates in atmospheric aerosol chemistry. *Phys. Chem. Chem. Phys.* **18**, 12662–12674 (2016).
11. S. Zhou, M. Shiraiwa, R. D. McWhinney, U. Pöschl, J. P. D. Abbatt, Kinetic limitations in gas-particle reactions arising from slow diffusion in secondary organic aerosol. *Faraday Discuss.* **165**, 391–406 (2013).
12. M. Shiraiwa, Y. Li, A. P. Tsimpidi, V. A. Karydis, T. Berkemeier, S. N. Pandis, J. Lelieveld, T. Koop, U. Pöschl, Global distribution of particle phase state in atmospheric secondary organic aerosols. *Nat. Commun.* **8**, 15002 (2017).
13. T. Koop, J. Bookhold, M. Shiraiwa, U. Pöschl, Glass transition and phase state of organic compounds: Dependency on molecular properties and implications for secondary organic aerosols in the atmosphere. *Phys. Chem. Chem. Phys.* **13**, 19238–19255 (2011).
14. M. Shrivastava, S. Lou, A. Zelenyuk, R. C. Easter, R. A. Corley, B. D. Thrall, P. J. Rasch, J. D. Fast, S. L. Massey Simonich, H. Shen, S. Tao, Global long-range transport and lung cancer risk from polycyclic aromatic hydrocarbons shielded by coatings of organic aerosol. *Proc. Natl. Acad. Sci. U.S.A.* **114**, 1246–1251 (2017).
15. V. Matthias, A. Aulinger, M. Quante, CMAQ simulations of the benzo(a)pyrene distribution over Europe for 2000 and 2001. *Atmos. Environ.* **43**, 4078–4086 (2009).
16. A. Aulinger, V. Matthias, M. Quante, An approach to temporally disaggregate benzo(a) pyrene emissions and their application to a 3D Eulerian atmospheric chemistry transport model. *Water Air Soil Pollut.* **216**, 643–655 (2011).
17. C. L. Friedman, N. E. Selin, Long-range atmospheric transport of polycyclic aromatic hydrocarbons: A global 3-D model analysis including evaluation of Arctic sources. *Environ. Sci. Technol.* **46**, 9501–9510 (2012).
18. R. San José, J. L. Pérez, M. S. Callén, J. M. Lopez, A. Mastral, BaP (PAH) air quality modelling exercise over Zaragoza (Spain) using an adapted version of WRF-CMAQ model. *Environ. Pollut.* **183**, 151–158 (2013).
19. C. L. Friedman, J. R. Pierce, N. E. Selin, Assessing the influence of secondary organic versus primary carbonaceous aerosols on long-range atmospheric polycyclic aromatic hydrocarbon transport. *Environ. Sci. Technol.* **48**, 3293–3302 (2014).
20. C. L. Friedman, Y. Zhang, N. E. Selin, Climate change and emissions impacts on atmospheric PAH transport to the Arctic. *Environ. Sci. Technol.* **48**, 429–437 (2014).
21. C. I. Efstathiou, J. Matejovičová, J. Bieser, G. Lammel, Evaluation of gas-particle partitioning in a regional air quality model for organic pollutants. *Atmos. Chem. Phys.* **16**, 15327–15345 (2016).
22. T. F. Kahan, N.-O. A. Kwamena, D. J. Donaldson, Heterogeneous ozonation kinetics of polycyclic aromatic hydrocarbons on organic films. *Atmos. Environ.* **40**, 3448–3459 (2006).
23. M. Shiraiwa, Y. Sosedova, A. Rouvière, H. Yang, Y. Zhang, J. P. D. Abbatt, M. Ammann, U. Pöschl, The role of long-lived reactive oxygen intermediates in the reaction of ozone with aerosol particles. *Nat. Chem.* **3**, 291–295 (2011).
24. M. Shiraiwa, C. Pfrang, U. Pöschl, Kinetic multi-layer model of aerosol surface and bulk chemistry (KM-SUB): The influence of interfacial transport and bulk diffusion on the oxidation of oleic acid by ozone. *Atmos. Chem. Phys.* **10**, 3673–3691 (2010).
25. U. Pöschl, Y. Rudich, M. Ammann, Kinetic model framework for aerosol and cloud surface chemistry and gas-particle interactions? Part 1: General equations, parameters, and terminology. *Atmos. Chem. Phys.* **7**, 5989–6023 (2007).
26. A. M. Arangio, J. H. Slade, T. Berkemeier, U. Pöschl, D. A. Knopf, M. Shiraiwa, Multiphase chemical kinetics of OH radical uptake by molecular organic markers of biomass burning aerosols: Humidity and temperature dependence, surface reaction, and bulk diffusion. *J. Phys. Chem. A* **119**, 4533–4544 (2015).
27. A. Aulinger, V. Matthias, M. Quante, Introducing a partitioning mechanism for PAHs into the Community Multiscale Air Quality modeling system and its application to simulating the transport of benzo(a)pyrene over Europe. *J. Appl. Meteorol. Climatol.* **46**, 1718–1730 (2007).
28. Y. Zhang, S. Tao, J. Ma, S. Simonich, Transpacific transport of benzo[a]pyrene emitted from Asia. *Atmos. Chem. Phys.* **11**, 11993–12006 (2011).
29. Y. Zhang, H. Shen, S. Tao, J. Ma, Modeling the atmospheric transport and outflow of polycyclic aromatic hydrocarbons emitted from China. *Atmos. Environ.* **45**, 2820–2827 (2011).
30. V. Hoyau, J. L. Jaffrezo, Ph. Garrigues, M. P. Clain, P. Masclet, Deposition of aerosols in polar regions-contamination of the ice sheet by polycyclic aromatic hydrocarbons. *Polycycl. Aromat. Compd.* **8**, 35–44 (1996).
31. R. W. Macdonald, J. M. Bewers, Contaminants in the arctic marine environment: Priorities for protection. *Ices J. Mar. Sci.* **53**, 537–563 (1996).
32. R. K. Achazi, C. A. M. Van Gestel, Uptake and Accumulation of PAHs by Terrestrial Invertebrates, in *PAHs: An Ecotoxicological Perspective*, P. E. T. Douben, Ed. (Wiley, 2003), pp. 173–190.
33. J. P. Meador, J. E. Stein, W. L. Reichert, U. Varanasi, Bioaccumulation of polycyclic aromatic hydrocarbons by marine organisms. *Rev. Environ. Contam. Toxicol.* **143**, 79–165 (1995).
34. M. Octaviani, I. Stemmler, G. Lammel, H. F. Graf, Atmospheric transport of persistent organic pollutants to and from the Arctic under present-day and future climate. *Environ. Sci. Technol.* **49**, 3593–3602 (2015).
35. T. Berkemeier, M. Shiraiwa, U. Pöschl, T. Koop, Competition between water uptake and ice nucleation by glassy organic aerosol particles. *Atmos. Chem. Phys.* **14**, 12513–12531 (2014).
36. M. Song, P. F. Liu, S. J. Hanna, Y. J. Li, S. T. Martin, A. K. Bertram, Relative humidity-dependent viscosities of isoprene-derived secondary organic material and atmospheric implications for isoprene-dominant forests. *Atmos. Chem. Phys.* **15**, 5145–5159 (2015).
37. M. Shiraiwa, A. Zuend, A. K. Bertram, J. H. Seinfeld, Gas–particle partitioning of atmospheric aerosols: Interplay of physical state, non-ideal mixing and morphology. *Phys. Chem. Chem. Phys.* **15**, 11441–11453 (2013).
38. P. Shahpoury, G. Lammel, A. Albinet, A. Sofuoğlu, Y. Dumanoğlu, S. C. Sofuoğlu, Z. Wagner, V. Zdimal, Evaluation of a conceptual model for gas-particle partitioning of polycyclic aromatic hydrocarbons using polyparameter linear free energy relationships. *Environ. Sci. Technol.* **50**, 12312–12319 (2016).
39. Y. Cheng, H. Su, T. Koop, E. Mikhailov, U. Pöschl, Size dependence of phase transitions in aerosol nanoparticles. *Nat. Commun.* **6**, 5923 (2015).
40. Y. Cheng, G. Zheng, C. Wei, Q. Mu, B. Zheng, Z. Wang, M. Gao, Q. Zhang, K. He, G. Carmichael, U. Pöschl, H. Su, Reactive nitrogen chemistry in aerosol water as a source of sulfate during haze events in China. *Sci. Adv.* **2**, e1601530 (2016).
41. G. A. Grell, S. E. Peckham, R. Schmitz, S. A. McKeen, G. Frost, W. C. Skamarock, B. Eder, Fully coupled "online" chemistry within the WRF model. *Atmos. Environ.* **39**, 6957–6975 (2005).
42. *WRF-Chem Version 3.6.1 User's Guide* (National Center for Atmospheric Research, 2014)
43. E. Roeckner, G. Bäuml, L. Bonaventura, R. Brokopf, M. Esch, M. Giorgetta, S. Hagemann, I. Kirchner, L. Kornblueh, E. Manzini, A. Rhodin, U. Schlese, U. Schulzweida, A. Tompkins, *"The atmospheric general circulation model ECHAM 5. Part I: Model description"* (MPI-Report No. 349, Max Planck Institute for Meteorology, 2003).
44. P. Jöckel, A. Kerkweg, A. Pozzer, R. Sander, H. Tost, H. Riede, A. Baumgaertner, S. Gromov, B. Kern, Development cycle 2 of the Modular Earth Submodel System (MESSy2). *Geosci. Model Dev.* **3**, 717–752 (2010).
45. H. Shen, Y. Huang, R. Wang, D. Zhu, W. Li, G. Shen, B. Wang, Y. Zhang, Y. Chen, Y. Lu, H. Chen, T. Li, K. Sun, B. Li, W. Liu, J. Liu, S. Tao, Global atmospheric emissions of polycyclic aromatic hydrocarbons from 1960 to 2008 and future predictions. *Environ. Sci. Technol.* **47**, 6415–6424 (2013).
46. G. Janssens-Maenhout, M. Crippa, D. Guizzardi, F. Dentener, M. Muntean, G. Pouliot, T. Keating, Q. Zhang, J. Kurokawa, R. Wankmüller, H. Denier van der Gon, J. J. P. Kuenen, Z. Klimont, G. Frost, S. Darras, B. Koffi, M. Li, HTAP_v2.2: A mosaic of regional and global emission grid maps for 2008 and 2010 to study hemispheric transport of air pollution. *Atmos. Chem. Phys.* **15**, 11411–11432 (2015).
47. R. Lohmann, G. Lammel, Adsorptive and absorptive contributions to the gas-particle partitioning of polycyclic aromatic hydrocarbons: State of knowledge and recommended parametrization for modeling. *Environ. Sci. Technol.* **38**, 3793–3803 (2004).
48. E. Galarneau, P. A. Makar, Q. Zheng, J. Narayan, J. Zhang, M. D. Moran, M. A. Bari, S. Pathela, A. Chen, R. Chlumsky, PAH concentrations simulated with the AURAMS-PAH chemical transport model over Canada and the USA. *Atmos. Chem. Phys.* **14**, 4065–4077 (2014).
49. W. Klöpffer, B. O. Wagner, K. G. Steinhäuser, *Atmospheric Degradation of Organic Substances: Persistence, Transport Potential, Spatial Range* (Wiley, 2008).
50. W. A. Jury, W. F. Spencer, W. J. Farmer, Behavior assessment model for trace organics in soil: I. Model description. *J. Environ. Qual.* **12**, 558–564 (1983).
51. G. Lammel, A. M. Sehili, T. C. Bond, J. Feichter, H. Grassl, Gas/particle partitioning and global distribution of polycyclic aromatic hydrocarbons—A modelling approach. *Chemosphere* **76**, 98–106 (2009).
52. M. Shiraiwa, C. Pfrang, T. Koop, U. Pöschl, Kinetic multi-layer model of gas-particle interactions in aerosols and clouds (KM-GAP): Linking condensation, evaporation and chemical reactions of organics, oxidants and water. *Atmos. Chem. Phys.* **12**, 2777–2794 (2012).
53. J. Y. Kim, J. Y. Lee, S.-D. Choi, Y. P. Kim, Y. S. Ghim, Gaseous and particulate polycyclic aromatic hydrocarbons at the Gosan background site in East Asia. *Atmos. Environ.* **49**, 311–319 (2012).
54. K. Tørseth, W. Aas, K. Breivik, A. M. Fjæraa, M. Fiebig, A. G. Hjellbrekke, C. Lund Myhre, S. Solberg, K. E. Yttri, Introduction to the European Monitoring and Evaluation Programme (EMEP) and observed atmospheric composition change during 1972–2009. *Atmos. Chem. Phys.* **12**, 5447–5481 (2012).

55. E. Galarneau, T. F. Bidleman, P. Blanchard, Seasonality and interspecies differences in particle/gas partitioning of PAHs observed by the Integrated Atmospheric Deposition Network (IADN). *Atmos. Environ.* **40**, 182–197 (2006).
56. H. Hung, R. Kallenborn, K. Breivik, Y. Su, E. Brorström-Lundén, K. Olafsdottir, J. M. Thorlacius, S. Leppänen, R. Bossi, H. Skov, S. Manø, G. W. Patton, G. Stern, E. Sverko, P. Fellin, Atmospheric monitoring of organic pollutants in the Arctic under the Arctic Monitoring and Assessment Programme (AMAP): 1993–2006. *Sci. Total Environ.* **408**, 2854–2873 (2010).
57. A. Ding, X. Huang, C. Fu, *Air pollution and weather interaction in East Asia* (Oxford Research Encyclopedia of Environmental Science, 2017).
58. A. Ding, T. Wang, L. Xue, J. Gao, A. Stohl, H. Lei, D. Jin, Y. Ren, X. Wang, X. Wei, Y. Qi, J. Liu, X. Zhang, Transport of north China air pollution by midlatitude cyclones: Case study of aircraft measurements in summer 2007. *J. Geophys. Res.* **114**, D08304 (2009).
59. A. Stohl, Z. Klimont, S. Eckhardt, K. Kupiainen, V. P. Shevchenko, V. M. Kopeikin, A. N. Novigatsky, Black carbon in the Arctic: The underestimated role of gas flaring and residential combustion emissions. *Atmos. Chem. Phys.* **13**, 8833–8855 (2013).
60. P. Winiger, A. Andersson, S. Eckhardt, A. Stohl, Ö. Gustafsson, The sources of atmospheric black carbon at a European gateway to the Arctic. *Nat. Commun.* **7**, 12776 (2016).

Acknowledgments: We thank Q. Zhang, Y. Zhang, and G. Zheng (Tsinghua University, China) for sampling, and P. Příbylová and O. Audy (Masaryk University, Czech Republic) for chemical analysis at the Xianghe site. We also acknowledge Y.-S. Ghim (Hankuk University of Foreign Studies, Korea) for sharing of BaP concentration data at the Gosan site. **Funding:** We acknowledge the National Natural Science Foundation of China (91644218 and 41330635), NSF (AGS-1654104), U.S. Department of Energy (DE-SC0018349), and Czech Science Foundation (P503 16-11537S). This work was supported by the Max Planck Society (MPG). Y.C. would also like to thank the Minerva Program of MPG. **Author contributions:** Y.C., H.S., U.P., and G.L. conceived the study. M.S., Y.C., H.S., and U.P. developed the temperature-dependent ROI-T scheme for model implementation. Q.M. incorporated new PAH module into the regional model WRF-Chem and performed the model simulation and data analyses. M.O. incorporated new PAH module into the global model EMAC and performed the model simulation and data analyses. Y.C., H.S., and Q.M. analyzed and interpreted results. N.M. contributed to data analysis and visualization. A.D. contributed to the transport process analysis and relevant discussion in the Supplementary Materials. All coauthors discussed the results. H.S., Y.C., and Q.M. wrote the manuscript with input from all coauthors. **Competing interests:** The authors declare that they have no competing interests. **Data and materials availability:** All data needed to evaluate the conclusions in the paper are present in the paper and/or the Supplementary Materials. Additional data related to this paper may be requested from the authors.

Submitted 21 August 2017
Accepted 9 February 2018
Published 21 March 2018
10.1126/sciadv.aap7314

Citation: Q. Mu, M. Shiraiwa, M. Octaviani, N. Ma, A. Ding, H. Su, G. Lammel, U. Pöschl, Y. Cheng, Temperature effect on phase state and reactivity controls atmospheric multiphase chemistry and transport of PAHs. *Sci. Adv.* **4**, eaap7314 (2018).

Science Advances

AAAS

advances.sciencemag.org/cgi/content/full/4/3/eaap7314/DC1

Supplementary Materials for

Temperature effect on phase state and reactivity controls atmospheric multiphase chemistry and transport of PAHs

Qing Mu, Manabu Shiraiwa, Mega Octaviani, Nan Ma, Aijun Ding, Hang Su, Gerhard Lammel, Ulrich Pöschl, Yafang Cheng

Published 21 March 2018, *Sci. Adv.* **4**, eaap7314 (2018)
DOI: 10.1126/sciadv.aap7314

This PDF file includes:

text S1. Problems without considering bulk processes.

The use of surface model without considering bulk diffusion/reaction results in a contradictory RH dependence of BaP degradation rates at different ozone concentrations. Taking the Zhou scheme for example, using such extrapolation resulted in a contradictory RH dependence of BaP degradation rates at different ozone ranges. The reactions of the Zhou scheme at 50 ppbv ozone were slower in 70% RH than 50% RH (Fig. 1A), contrary to their own conclusion that higher RH enhanced the reactivity of BaP.

text S2. Warm conveyor belts (WCBs) and BaP transport in Gosan winter case.

The frontal activities and WCBs associated with mid-latitude cyclones play a very important role in lifting plumes from the planetary boundary layer (PBL) to the free troposphere (FT), promoting long-range transport of air pollutants (*57*). Thus, such kind of transport processes can influence the chemical distributions of the middle- and upper- troposphere of downwind regions in Northeast Asia, the Pacific Ocean and even North America. In North China, transport processes due to WCBs have been found particularly frequent in summer resulting from the high frequency of mid-latitude cyclones, but they are also important in spring and winter. In order to understand the detailed transport mechanism for the high concentration of BaP in the middle troposphere of the Northern Hemisphere mid-latitudes, we chose a typical event during 25–26 February 2003 as case study.

Figure S5 shows that the Gosan outflow case in winter is a good example of PBL-FT transport. A mid-latitude cyclone (low pressure centered at 118° E, 43° N) was located in the north to North China Plain on early 25 Feb 2003 (fig. S5A). High moisture (represented by specific humidity) demonstrated a strong northeastward belt-shape transport from the boundary layer in the warm air frontal zone to the middle troposphere over the warm front, with clockwise shape belts overrunning the fronts (fig. S5C). Similarly, BaP showed a high concentration belt in front of the cold front (~ 850 hPa) and then got transported over the warm front (~700 hPa), hence, experienced fast eastward transport by westerlies (or jets) in the middle-troposphere (fig. S5B, 5D, 5F). A T-shape plume could be identified from the 700 hPa SH and BaP distributions over the warm front (fig. S5D). It includes a branch transported poleward in addition to the eastward branch. Ding et al. (*58*) reported a similar event in the same region and found that the WCB associated with the cyclone played the key role in lifting air pollutants from the boundary layer to the middle troposphere, and also pointed out that such kind of lifting provides the most important contribution for intercontinental and poleward transports in the Northern Hemisphere. To clearly demonstrate the structure of WCBs and other related flows in the cyclone, a conceptual model is given in fig. S6. Since cyclone is one of the most dominant synoptic features in the mid-latitudes, such kind of WCB-induced lifting could be the main contribution to high and long-range transported pollutants, like BaP.

table S1. Flow tube experiments of multiphase degradation of BaP with ozone. Langmuir-Hinshelwood first-order reaction rate coefficient $k = \frac{k_{max} k_{o3}[O_3]}{1+k_{o3}[O_3]}$. For Kahan scheme, $k = \frac{A*[O_3]}{B+[O_3]}$. $[O_3]$ is in molecules cm^{-3}.

Scheme	Substrate	Coating	O_3 (ppmv)	T (K)	RH (%)	k_{max} (s^{-1})	k_{O3} (10^{-15} cm^3)
Pöschl (*4*)	spark discharge soot	None	0.05–1	296 ±2	0	0.015±0.001	270±40
					25	0.016±0.001	280±20
Kwamena (*22*)	azelaic acid	None	2–45	298±5	0	0.048±0.008	1.2±0.4
					72	0.060±0.018	2.8±1.4
	NaCl				0	0.032	<0.12
Kahan (*5*)	octanol	None	15–950	room	0	A=(5.5±0.2)*$10^{-3}$$s^{-1}$	B=(2.8±0.4)*10^{15} molec cm^{-3}
Zhou (*6*)	ammonium sulfate	None	4–25	296 ± 3	<5%	0.034 ± 0.002	14 ± 4
		bis(2-ethylhexyl)sebacate	6–32			0.051 ± 0.001	4.1 ± 0.1
		phenylsiloxane oil	4–32			0.047 ± 0.004	13 ± 4
		eicosane	6–32			shut off	shut off
Zhou (*11*)	ammonium sulfate	a-pinene SOA 5—10 nm	1.5–16	296 ± 3	<5%	0.042 ± 0.004	5.1 ± 0.9
		a-pinene SOA 20—80 nm	8–24		<5%	0.022 ± 0.003	2.3 ± 0.4
			3–24		50%	0.023 ± 0.004	14 ± 4.4
			3–28		70%	0.039 ± 0.004	6.2 ± 1.1

table S2. Kinetic parameters used in the KM-SUB simulation for the ozonolysis of BaP to reproduce experiment results of the Zhou scheme.

Parameter	Description	Value
α_{s,O_3}	surface accommodation coefficient of O_3	1 *
τ_{d,O_3} (s)	Desorption lifetime of O_3	3.2 x 10^{-9} *
$E_{a,pc}$ (kJ mol^{-1})	Activation energy from physisorbed O_3 to ROI	42 *,†
$E_{a,ox}$ (kJ mol^{-1})	Activation energy from ROI to oxidized BaP	80 *,†
k_{BR} (cm^3 s^{-1})	Second-order bulk reaction rate coefficient between BaP and O_3	5 x 10^{-18} †
$K_{sol,cc}$ (mol cm^{-3} atm^{-1})	Henry's law coefficient of O_3	6 x 10^{-4} †

* ref (*23*); † ref (*11*)

table S3. Parameterization of multiphase degradation rate for the ozonolysis of BaP. First-order reaction rate coefficients k (s^{-1}) are given by the Hill equation $k = \text{base} + \frac{\text{max}-\text{base}}{1+(\frac{\text{xhalf}}{[O_3]})^{\text{rate}}}$ with $[O_3]$ in ppbv. The R^2 of these Hill equation fits are all larger than 0.99. For each grid cell, the parameters are read from the look-up table with temperature and relative humidity (RH) closest to the temperature and humidity of the grid cell. When equally close, the smaller parameter value is adopted.

70% RH				
Temperature (°C)	**base**	**max**	**rate**	**xhalf**
40	1.67e-4	1.29e-2	0.682	1.25e3
35	1.19e-4	1.29e-2	0.682	1.25e3
30	8.52e-5	9.02e-3	0.696	1.23e3
25	5.94e-5	6.33e-3	0.707	1.27e3
23	4.84e-5	5.14e-3	0.700	1.25e3
15	2.55e-5	2.72e-3	0.711	1.29e3
10	1.58e-5	1.68e-3	0.706	1.27e3
5	9.49e-6	1.00e-3	0.698	1.24e3
0	6.85e-6	5.64e-4	0.704	1.11e3
-5	5.31e-6	3.10e-4	0.713	1.01e3
-10	3.83e-6	1.48e-4	0.731	7.33e2
-15	8.93e-7	1.05e-4	0.580	1.88e3
-20	1.16e-6	2.58e-5	0.673	3.35e2

50% RH				
Temperature (°C)	**base**	**max**	**rate**	**xhalf**
40	1.65e-4	1.80e-2	0.672	1.21e3
35	1.16e-4	1.27e-2	0.678	1.24e3
30	8.24e-5	8.68e-3	0.688	1.22e3
25	5.44e-5	5.71e-3	0.688	1.21e3
23	2.64e-5	3.08e-3	0.618	7.97e2
15	2.20e-6	1.10e-3	0.544	5.83e2
10	7.84e-7	2.60e-4	0.559	7.50e1
5	-4.79e-7	7.19e-5	0.564	1.31e1
0	-7.02e-6	2.18e-5	0.464	1.05e0
-5	-4.06e-6	6.54e-6	0.459	1.24e-1
-10	-1.89e-6	2.02e-6	0.429	1.44e-2
-15	2.58e-7	7.22e-7	0.175	1.28e-1
-20	1.79e-7	2.60e-7	0.689	1.11e3

Dry				
Temperature (°C)	**base**	**max**	**rate**	**xhalf**
40	1.61e-4	1.74e-2	0.667	1.19e3
35	1.10e-4	1.19e-2	0.667	1.21e3
30	6.75e-5	7.31e-3	0.653	1.11e3
25	2.3e-5	3.10e-3	0.586	7.02e2
23	-1.90e-5	9.28e-4	0.446	1.59e2
15	-2.65e-5	3.09e-4	0.341	8.38e1
10	-4.28e-5	1.03e-4	0.191	4.41e0
5	-1.12e-5	3.49e-5	0.142	4.33e0

0	3.39e-6	1.03e-5	0.382	8.85e2
-5	1.37e-6	5.67e-6	0.780	2.96e3
-10	4.53e-7	1.57e-6	0.979	1.63e3
-15	1.44e-7	2.10e-6	0.924	1.39e4

table S4. Comparisons of observed and predicted BaP concentrations in the regional WRF-Chem model and the global EMAC model. (**A**) Observed and predicted BaP concentrations (ng m^{-3}) over the period 2007–2009*. (**B**) Mean bias (prediction - observation) (ng m^{-3}) and relative bias ((prediction - observation) / observation) of BaP for various types of sites in Fig. 2A.

(**A**)

	Alert, Canada	Spitsbergen, Norway	Pallas, Finland	All mid-latitude stations
No. months	34†	23†	19†	405†
Mean				
Observation	1.40E-03	4.08E-03	1.01E-02	1.41E-01
Kwamena	8.15E-07	6.92E-06	1.22E-03	5.75E-02
ROI-T	1.64E-05	5.48E-05	4.68E-03	7.98E-02
Kahan	6.25E-03	5.22E-03	5.33E-02	2.72E-01
Pöschl	1.61E-07	1.07E-06	1.25E-04	5.88E-03
Median				
Observation	4.78E-04	8.80E-04	2.84E-03	3.74E-02
Kwamena	7.41E-07	2.73E-06	1.18E-03	1.82E-02
ROI-T	1.35E-05	2.61E-05	3.84E-03	3.24E-02
Kahan	4.45E-04	1.28E-03	4.64E-02	3.34E-01
Pöschl	1.48E-07	6.05E-07	1.16E-04	3.07E-03
Geometric mean ‡				
Observation	6.70E-04	1.38E-03	3.62E-03	4.60E-02
Kwamena	7.79E-07	4.00E-06	1.19E-03	2.57E-02
ROI-T	1.19E-05	2.89E-05	3.98E-03	3.43E-02
Kahan	4.61E-04	1.68E-03	4.21E-02	3.43E-01
Pöschl	1.57E-07	8.13E-07	1.20E-04	2.26E-03
Root mean square error				
Kwamena	6.26E-03	7.78E-03	2.37E-02	2.79E-01
ROI-T	6.25E-03	7.77E-03	2.24E-02	2.72E-01
Kahan	5.98E-03	1.14E-02	6.17E-02	5.71E-01
Pöschl	6.26E-03	7.78E-03	2.41E-02	2.89E-01

*Although improved performances, the ROI-T scheme still tends to underestimate BaP in the Arctic (sites Alert and Spitsbergen), probably because current atmospheric models generally underestimate co-emitted black carbon in the Arctic due to missing sources (*59, 60*). Therefore, the actual inflow of BaP to the Arctic could be even stronger.
†Values below limit of quantitation (LOQ) are treated as 0. Number of data <LOQ is 21 for Alert, 8 for Spitsbergen, 1 for Pallas and 0 for all mid-latitude stations.
‡Geometric mean is used in the study.

(**B**)

	Xianghe	Gosan	Arctic	Mid-latitude
Kwamena	6.76E-1	-7.88E-3	-5.99E-03	-8.40E-02
	(0.87)	(-0.39)	(-3.17)	(-1.83)
ROI-T	-1.44E-2	-1.36E-3	-4.82E-03	-6.16E-02
	(-1.80E-2)	(-6.80E-2)	(-2.55)	(-1.34)
Kahan	1.22	1.38E-1	1.42E-02	3.35E-01
	(1.56)	(6.90)	(7.51)	(7.28)
Pöschl	7.33E-3	-1.80E-2	-6.38E-03	-1.36E-01
	(9.40E-3)	(-0.90)	(-3.38)	(-2.96)

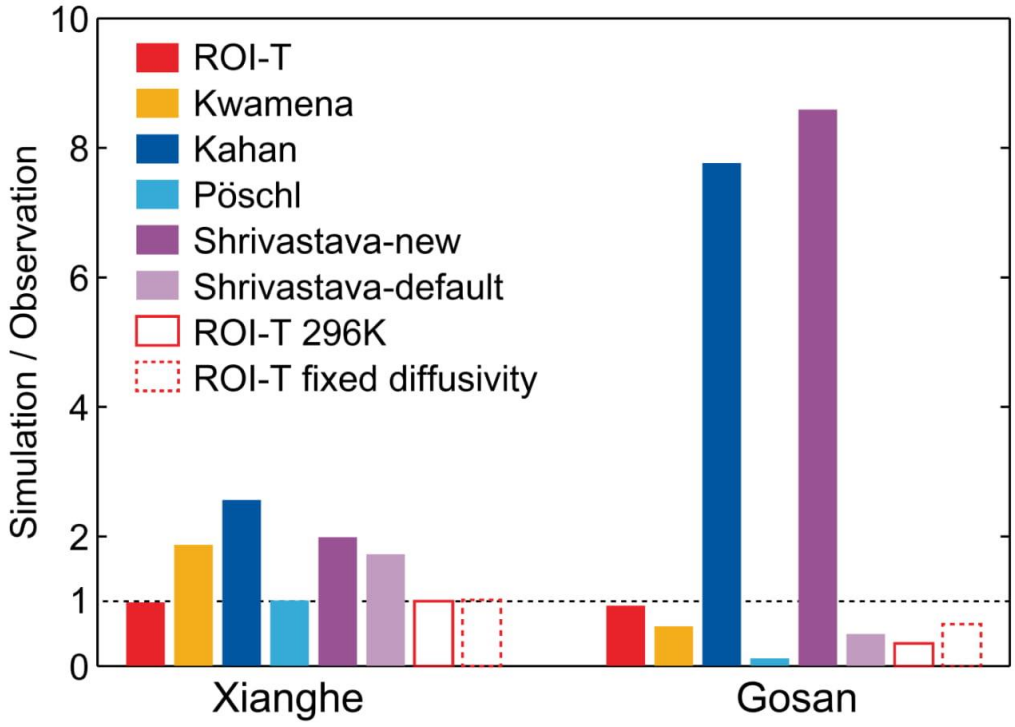

fig. S1. Same as Fig. 2B but with three more sensitivity studies. "Shrivastava-default" uses the default setting (the same as the thin coating case in the Zhou scheme (*11*)) in Shrivastava et al. (*14*) "ROI-T 296 K" fixes both OA diffusion coefficient and chemical reaction rate of BaP with ROI at 296 K level. "ROI-T fixed diffusivity" only fixes OA diffusion coefficient at 296 K level but allows the chemical reaction rate of BaP with ROI to change with temperature.

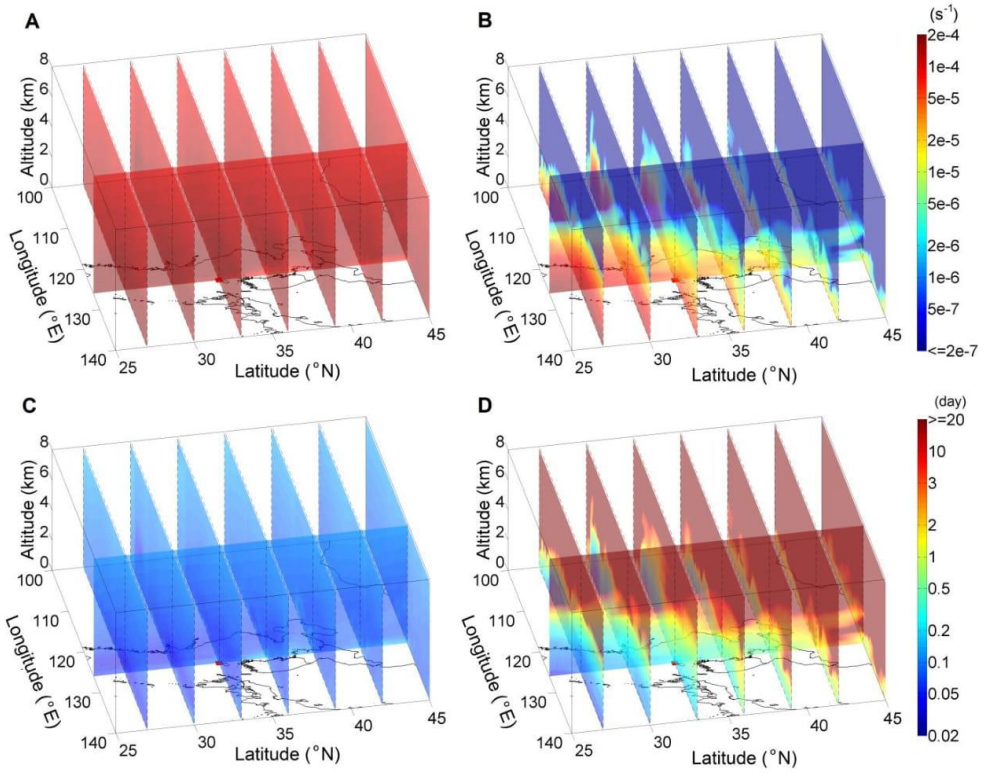

fig. S2. Multiphase degradation rate and chemical lifetime. Multiphase degradation rate k (s^{-1}, (**A**) for the Kwamena scheme, (**B**) for the ROI-T scheme) and chemical life time (day, (**C**) for the Kwamena scheme, (**D**) for the ROI-T scheme) on 24 February 2003 in the East Asia outflow case.

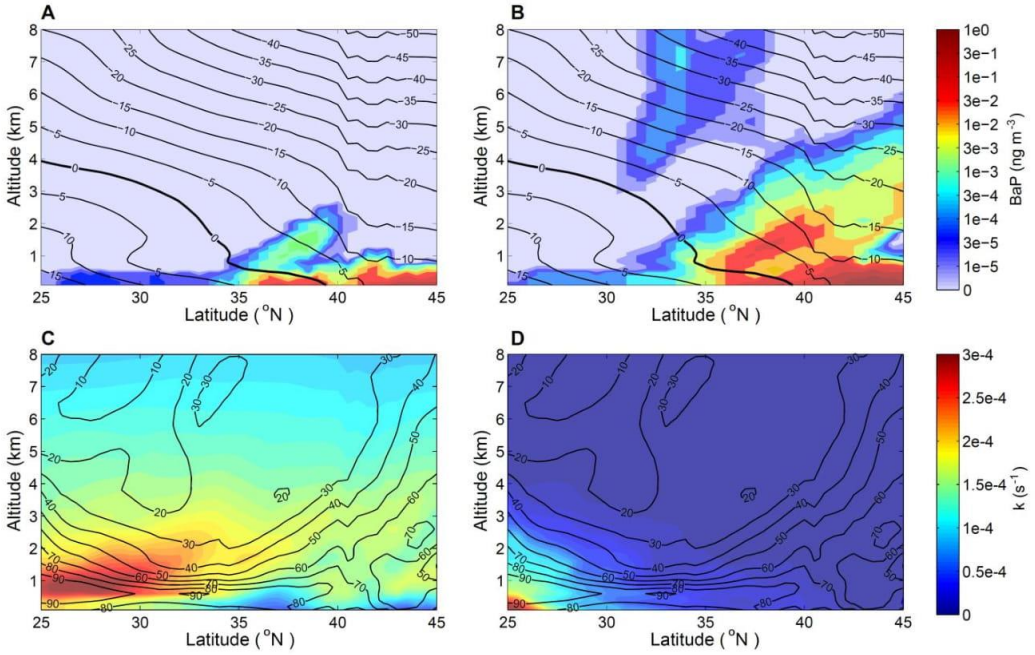

fig. S3. BaP concentrations and multiphase degradation rate. BaP concentrations (ng m^{-3}, (**A**) for the Kwamena scheme, (**B**) for the ROI-T scheme) and multiphase degradation rate k (s^{-1}, (**C**) for the Kwamena scheme, (**D**) for the ROI-T scheme) at a cross section of 126° E on 24 February 2003 in the East Asia outflow case. Temperature (ºC) contours are shown in A and B. RH (%) contours are shown in C and D.

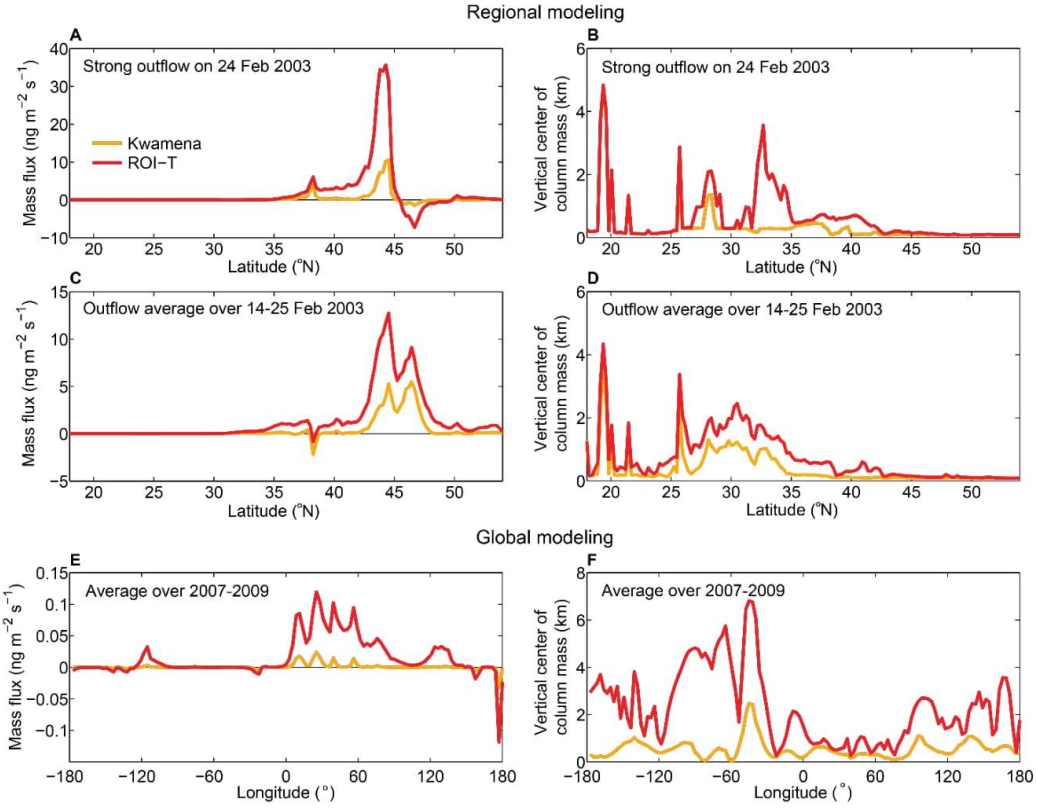

fig. S4. Net meridional mass flux and vertical center of column mass for BaP in different cases. (**A**) BaP mass fluxes and (**B**) vertical center of column mass at 126°E averaged during the East Asia outflow episode 24 February 2003. (**C**) BaP mass fluxes and (**D**) vertical center of column mass at 126°E averaged over simulation period 14–25 February 2003. (**E**) BaP mass fluxes and (**F**) vertical center of column mass across 65°N averaged over the years 2007–2009.

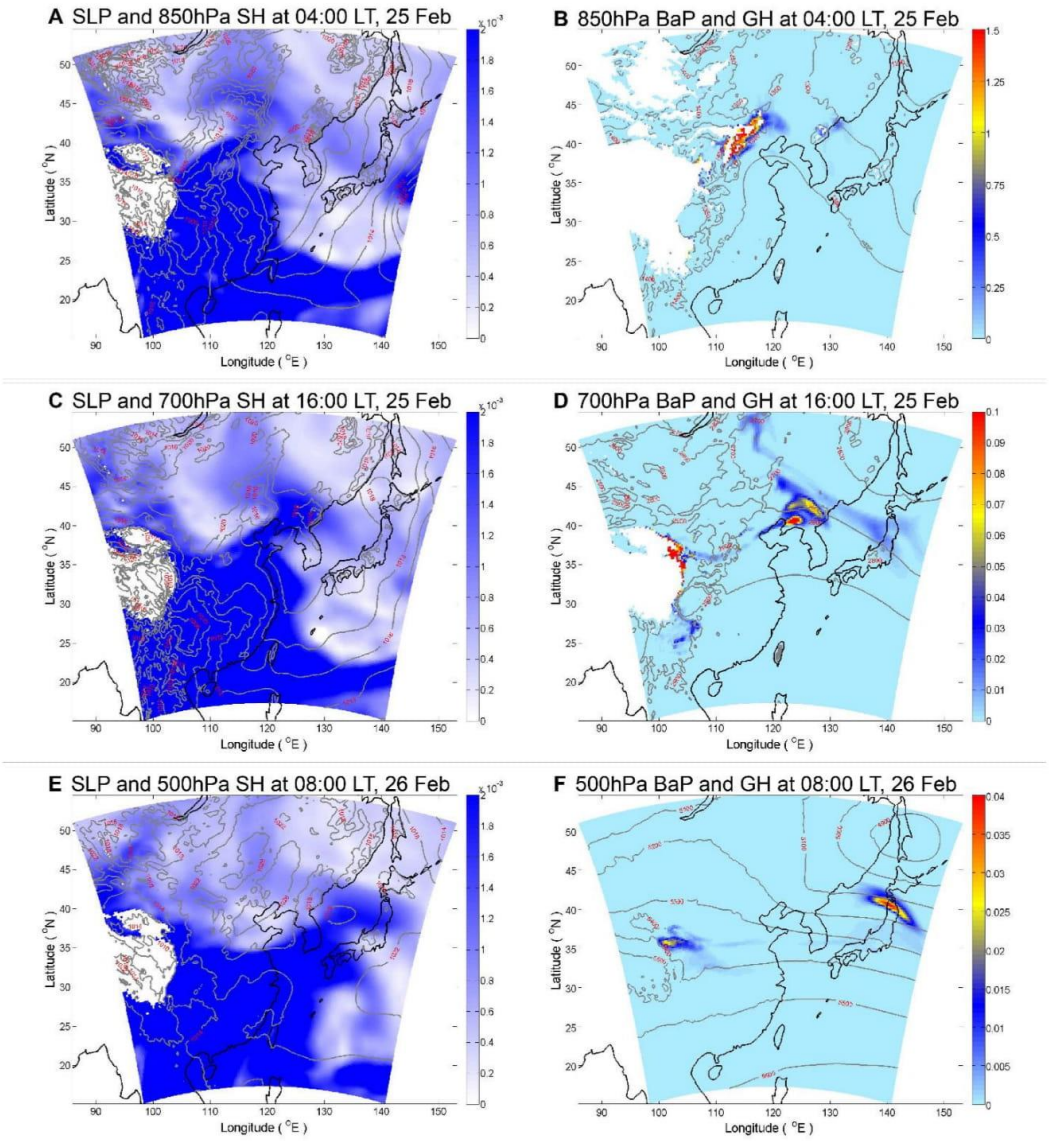

fig. S5. BaP transport due to WCB and frontal activities associated with mid-latitude cyclones for the Gosan winter case. The left column shows specific humidity (SH, g g^{-1}) and sea level pressure (SLP, hPa, contour lines) at different pressure level (**A**) 850 hPa, (**C**) 700 hPa, and (**E**) 500 hPa for a cyclone in East Asia during 25–26 February, 2003. The right column (**B**, **D**, **F**) gives BaP concentrations (BaP, ng m^{-3}) with the ROI-T scheme and geopotential height (GH, m, contour lines) at different pressure level corresponding to figures in the left panel. Note that the brown and rose bold lines show the surface cold fronts and warm fronts, respectively.

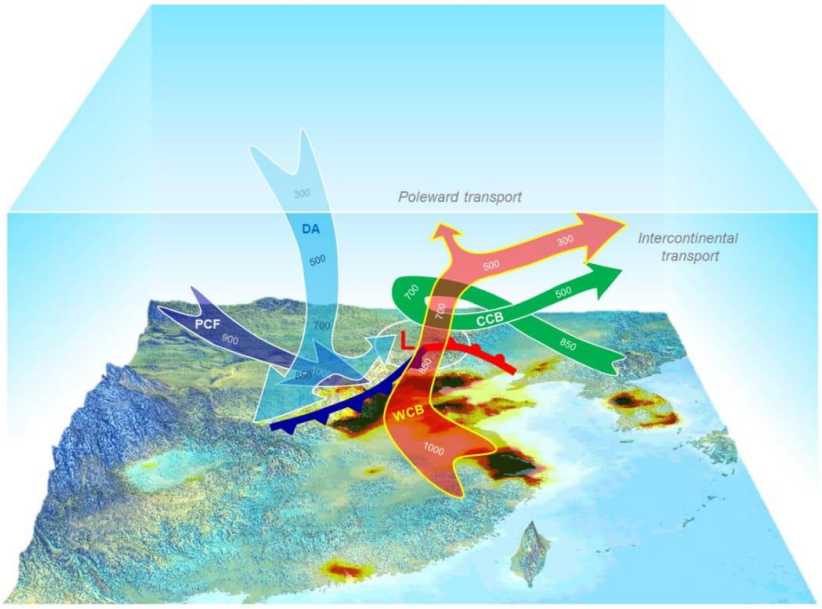

fig. S6. A conceptual scheme for air pollution transport due to middle-latitude cyclone. The warm conveyor belt (WCB) is the most efficient transport process for lifting air mass from boundary layer to middle- even upper- troposphere, which further contributes to intercontinental and poleward transport. Cold conveyor belt (CCB), dry air (DA) stream and post cold front (PCF) airstream contribute to the formation of WCB. The numbers marked on these belts indicate the pressure level (Figure modified with permissions from ref. *57*).

B.3 Lammel et al., Atmos. Chem. Phys., submitted

Re-volatilization of soil accumulated pollutants triggered by the summer monsoon in India

Gerhard Lammel [1,2*], Céline Degrendele [2], Sachin S. Gunthe [3], Qing Mu [1], Akila Muthalagu [3], Ondřej Audy [2], C.V. Biju [4], Petr Kukučka [2], Marie D. Mulder [2], Mega Octaviani [1], Petra Příbylová [2], Pourya Shahpoury [1], Irene Stemmler [5], Aswathy E. Valsan [3]

[1] Max Planck Institute for Chemistry, Multiphase Chemistry Department, Hahn-Meitner-Weg 1, 55128 Mainz, Germany

[2] Masaryk University, Research Centre for Toxic Compounds in the Environment, Kamenice 5, 62500 Brno, Czech Republic

[3] Indian Institute of Technology Madras, Environmental and Water Resources Engineering Division, Chennai 600036, India

[4] College of Engineering Munnar, Department of Civil Engineering, P. B. No. 45, County Hills, Munnar 685612, India

[5] Max Planck Institute for Meteorology, Ocean in the Earth System Department, Bundesstr. 53, 20146 Hamburg, Germany

Author contributions

G.L. conceived the study. C.V.B., S.S.G., G.L., A.M., P.S., and A.E.V. prepared and conducted the air and soil sampling and field measurements. O.A., P.K. and P.P. did the chemical analysis of samples. G.L. and S.S.G. did the field data analysis. C.D. and M.D.M. provided meteorological analyses. C.D., Q.M., M.O. and I.S. prepared model input. C.D. and G.L. designed the 1D model. C.D. and Q.M. incorporated model parameterizations, and performed and analyzed the 1D and 3D model runs, respectively. C.D., S.S.G., G.L., Q. M. and I.S. discussed the results. G.L. wrote the manuscript with input from all coauthors.

Re-volatilisation of soil accumulated pollutants triggered by the summer monsoon in India

Gerhard Lammel [1,2*], Céline Degrendele [2], Sachin S. Gunthe [3], Qing Mu [1], Akila Muthalagu [3], Ondřej Audy [2], C.V. Biju [4], Petr Kukučka [2], Marie D. Mulder [2], Mega Octaviani [1], Petra Příbylová [2], Pourya Shahpoury [1], Irene Stemmler [5], Aswathy E. Valsan [3]

[1] Max Planck Institute for Chemistry, Multiphase Chemistry Department, Hahn-Meitner-Weg 1, 55128 Mainz, Germany

[2] Masaryk University, Research Centre for Toxic Compounds in the Environment, Kamenice 5, 62500 Brno, Czech Republic

[3] Indian Institute of Technology Madras, Environmental and Water Resources Engineering Division, Chennai 600036, India

[4] College of Engineering Munnar, Department of Civil Engineering, P. B. No. 45, County Hills, Munnar 685612, India

[5] Max Planck Institute for Meteorology, Ocean in the Earth System Department, Bundesstr. 53, 20146 Hamburg, Germany

Abstract

Persistent organic pollutants that have accumulated in soils can be re-mobilised by volatilisation in response to chemical equilibrium with the atmosphere. Clean air masses from the Indian Ocean, advected with the onset of the summer monsoon, are found to trigger or enhance re-volatilisation of the nowadays banned chemicals hexachlorocyclohexane (HCH) and polychlorinated biphenyls (PCBs) from background soils in southern India. The air is polluted during transport by the southwesterly monsoon winds across the subcontinent. For HCH and dichlorodiphenyltrichloroethane (DDT), air-surface exchange has declined since the ban of these substances from agriculture, but re-mobilisation of higher chlorinated PCBs may have reached a historical high, 40 years after peak emission.

1. Introduction

Persistent organic pollutants pose a hazard to humans and wildlife as they may reach harmful concentrations in biota upon accumulation along food chains. Semivolatile substances (i.e., vapour pressure at 293 K in the range 10^{-6} – 10^{-2} Pa) tend to re-volatilise from land and sea surfaces to which they had previously been deposited, once a level of contamination in chemical equilibrium with air pollution is reached (Bidelman, 1999; Cousins et al., 1999; Meijer et al., 2003; Kurt-Karakus et al., 2006; Růzičková et al., 2008; Wong et al., 2007; Degrendele et al., 2016). The potential to re-volatilise is relevant to assess risks from chemicals as it enhances the long-range transport potential, hence, facilitates transport to and accumulation in remote areas, which are pristine with regard to primary (direct)

contamination (Wania and Mackay, 2008; Semeena and Lammel, 2005; Wania and Westgate, 2008; Lammel and Stemmler, 2012). In the terrestrial environment, soils represent the main reservoir of the more lipophilic substances (log $K_{oa} \gtrsim 6$), while smaller mass fractions are stored in the atmosphere, vegetation and freshwater as suggested by field studies (Meijer et al., 2003) and modelling (Wania, 2006; Lammel et al., 2007; Lammel and Stemmler, 2012). Thus, understanding the dynamics of soil contamination and exchange with the overlying air is important for assessing spatio-temporal scales of the distribution and impact of local pollution. Air-soil dynamics occurs on various time scales, from multi-year long-term trends (Lammel and Stemmler, 2012) to seasonal cycling and short-term fluctuations (Bidleman, 1999). One key region, where persistent organic pollutants have been heavily used, is South Asia. In India, high levels of organochlorine pesticides (OCPs) were found in both abiotic (Ramesh et al., 1989, 1991; Shunthirasingham et al., 2010; Rajendran et al., 1999; Kumari et al., 1996; UNEP, 2002; Pozo et al., 2011; Chakraborty and Zhang, 2012; Bajwa et al., 2016) and biotic (Ramesh et al., 1990, 1992; Senthilkumar et al., 2001; UNEP, 2002) environmental samples. The country is considered as a hot spot for DDT and hexachlorocyclohexane (HCH) with no evidence of decline (Sharma et al., 2014). Besides OCPs, also polychlorinated biphenyls (PCBs) and polybrominated diphenylethers (PBDEs) are of relevance in South Asia, where they were used as flame-retardants. High levels of PBDEs were reported in India (Zhang et al., 2008) and waste might be a significant on-going source of penta- and hexachlorobenzene (PeCB, HCB), PCBs (Senthilkumar et al., 2001; Wong et al., 2010; Zhang et al., 2011; Sharma et al., 2014) and PBDEs (Breivik et al., 2012; Sharma et al., 2014). Thus far, studies on environmental exposure of the Indian subcontinent have been mostly limited to urban areas (Chakraborty and Zhang, 2012; Sharma et al., 2014; Chakraborty et al., 2015), while the continental background was scarcely addressed. The air-soil dynamics of OCPs or other semivolatile substances related to monsoon has not been studied yet. In India, air pollution levels are expected to drop with the onset of the summer monsoon. Triggered by the seasonal shift of the intertropical convergence zone, the large-scale advection pattern switches from regional (South Asia and adjacent seas) to intercontinental (from the Indian Ocean with influence from the relatively clean southern hemisphere (IMD, 2014).

Here we study air and soil pollution in India, first time with focus on the impact of the summer monsoon on air-surface exchange. The hypothesis is tested, whether drop of concentrations in air at the onset of the summer monsoon mobilizes pollutants stored in soils. To this end, (1) field observations in background soils in the Western Ghats, the first highlands that the southwest monsoon winds encounter, were performed before and during the onset of the monsoon (May-June 2014). These were complemented by (2) regional scale chemistry-transport modelling of the monsoon onset on the Indian subcontinent using a 3D air pollution model, WRF-Chem, coupled to a soil compartment. Finally, (3) the long-term chemodynamics is assessed by multi-media mass balance modelling, forced by climate and 3D modelling data.

2. Methods

2.1 Sites and sampling

Air samples were collected from 5 May – 10 June, 2014, 90 km inland from the Arabian Sea coast, on a slope oriented southwest in the northern outskirts of the town Munnar (10.093°N/77.068°E, Fig. 4) at 1600 m a.s.l., with the mountain ridge's elevation in the area ranging from 1950 – 2450 m a.s.l.. The site is reached freely, i.e. without topographic obstacles, by air masses that are advected through the sector 180-360°N. It is directly

adjacent to tea plantations (south to west) and deciduous forest (northwest to northeast). Additional land cover includes shrubs (south, east) and, to a lesser extent, agricultural fields and residential areas (south to southeast). 24 air samples were collected. The 2014 monsoon season in the area was characterized by scattered rainfall at the monsoon onset, after which rainfall became persistent from the last week of June (Valsan et al., 2016).

For air sampling a high volume sampler (Digitel DH-77) equipped with a quartz fibre filter and 2 polyurethane foam (PUF) plugs (Gumotex Břeclav, density 0.030 g cm^{-3}, 100 mm diameter, total depth 12 cm, cleaned by extraction in acetone and dichloromethane) was used. Soil samples were taken from each one plot in the tea plantation, in shrubs and in forest, at distances within 1 km from each other. The uppermost 5 cm soil was collected (using spade, Edelman auger and sieve). Each soil sample is a composite (pooled sample), produced from equal amounts of soil collected from 6 individual spots at distances of 1 m from each other. Three replicates of each composite sample were analysed. At all plots the samples were nitisol (GOI, 1985; FAO, 2014), horizon A, which was brownish, loose, single grain structure, with fine roots in the shrubs and forest. Soil samples were homogenized by sieving and mixing. PUF samples were spiked to control analyte losses during handling, shipping and storage.

2.2 Chemical and data analysis

For organic analysis all samples were extracted with dichloromethane in an automatic extractor (Büchi B-811). Surrogate extraction standards (PCB30, PCB185,^{13}C BDEs 28, 47, 99, 100, 153, 154, 183, 209) were spiked on each sample prior to extraction. The volume was reduced after extraction under a gentle nitrogen stream at ambient temperature, and clean-up was achieved on a Florisil column. Samples were analysed using a GC-MS/MS (gas chromatograph coupled with a tandem mass spectrometer) Agilent 7890 coupled to Agilent 7000B with a SGE HT-8 column (60 m x 0.25 mm x 0.25 μm) for *α*-, *β*-HCH, *γ*-, and *δ*-HCH (i.e., 4 HCH isomers), *o,p'*- and *p,p'*-DDE, -DDD and –DDT (6 DDX compounds), penta- and hexachlorobenzene (PeCB, HCB), PCB28, -52, -101, -118, -153, -138 and -180 (i.e., 7 indicator PCBs), aldrin, dieldrin, endrin, *α*- and *γ*-chlordan, *α*- and *β*-endosulfan, endosulfan sulphate, and mirex. More details are given in the Supplementary Information, S1.1.

The mean of 3 field blank values was subtracted from the air sample values. Values below the mean + 3 standard deviations of the field blank values were considered to be <LOQ. Field blank values of a number of analytes in air samples were below the instrument limit of quantification (ILOQ), which corresponded to 0.006-0.012 pg m^{-3} for PCB/OCPs, and 0.50-5.2 pg m^{-3} for PBDEs (Table S1). LOQs ranged 0.006-0.06 pg m^{-3} for PCBs, 0.006-0.12 pg m^{-3} for OCPs (with few exceptions higher) and 0.001-0.01 pg m^{-3} for PBDEs (SI S1.1, Table S1).

Organic and elemental carbon in filter samples, as well as total organic carbon in soil was determined by a thermal-optical method (Sunset Lab., USA; EUSAAR protocol).

The pollutant fugacities (Harner et al., 2001) have been derived from concentrations in soil and air (details in Supporting Information S1.2). The onset of the monsoon on site was dated with high temporal resolution based on air parcel history (back trajectory analysis, Supporting Information S1.3).

2.3 Modelling atmospheric transport, chemistry and air-soil exchange

The response of air-soil exchange to the drop in air concentration, subsequent to the monsoon onset, was studied by the regional scale simulation of meteorology and chemistry using the WRF-Chem-PAH/POP model. The WRF-Chem-PAH/POP has been recently extended from the regional model WRF-Chem version 3.6.1 (Grell et al., 2005; Mu et al., 2017), to also represent the chemistry, in- and below-cloud scavenging, gas-particle partitioning and surface gas exchange of semivolatile organics (described in Supporting Information S1.4.1, input data in S1.4.3). The simulation of the period 1-30 June 2014, with a spatial resolution of 27×27 km²; and a time step of 150 s of the South Asian domain (5-32°N/69-89°E), was driven by NCEP re-analyses (6-hourly, 1° × 1° resolution). Physical and chemical spin-up time was 4 days. Primary emissions were considered for DDT and PCBs (SI S1.4.1), while the secondary emissions were modelled based on initializing the soils of India uniformly by the observed levels in background soils (shrub, forest, section 2.1). Non-zero air concentrations, observed before and during monsoon at the site (see above), were advected continuously at all boundaries of the domain (SI S1.4.1). In the model experiment pre-monsoon levels were continuously replaced by monsoon levels according to the northward propagation of the monsoon, while in the control run pre-monsoon levels were kept constant at the boundaries.

2.3 Multi-decadal simulation of pollution of air and soil in India

The air–soil mass exchange flux of the semivolatile organic compounds studied were simulated by a non-steady state one-dimensional (series of 7 two-boxes) model of inter-compartmental mass exchange (multi-media mass balance model (Lammel, 2004; SI Fig. S1). The boxes represent 7 zones in the north-south direction in India, 7.4-33.4°N, each 3.75° wide. For each box the mass balances for the two compartments planetary boundary layer and top soil were solved. The processes considered in air are wet and dry (particle) deposition, chemical removal from air by reaction with the hydroxyl radical, air-surface mass exchange flux (dry gaseous deposition and volatilisation), and loss by transport to the free troposphere, while in the soil atmospheric deposition fluxes, air-surface mass exchange flux, and degradation (as first order process) were considered (Supporting Information S1.4.2, input data in S1.4.3). In addition to a 50-year model run, the sensitivity of soil pollution to a number of input parameters as well as under a hypothetic no-monsoon scenario was studied.

3. Results

3.1 Field observations

Relatively low pollution levels in soils (0.07-0.11 ng g^{-1} for Σ_4HCH, 0.18-0.43 ng g^{-1} for Σ_6DDX, and 0.25-0.28 ng g^{-1} for Σ_7PCB) confirm the classification as "background" site (Table 1). Actually, these HCH and DDX levels are lower than ever reported from soils in India, which previously ranged 1.6-835 and 14-934 ng g^{-1} for HCH (excluding hot spots) and DDX, respectively (Sharma et al., 2014). The soil sample from a tea plantation showed elevated levels of DDT and its metabolites (27.9 ng g^{-1} Σ_6DDX), pointing to previous application (Table S2).

Indeed, measured air concentrations of carbonaceous aerosol and organic pollutants reach a distinctly lower level during the monsoon, dropping by a factor of 2-10, except for PBDEs, which apparently increased (Fig. 1, Table S3). These concentration changes from before to after (Fig. 1) were all significant on the $p < 0.05$ level, most on the $p < 0.01$ level, except for PBDEs which was insignificant, even on the $p < 0.1$ level (unpaired Student t-test). Precipitation increased by a factor of ≈2 upon the monsoon onset (from 3.8 to 8.0 mm day^{-1}),

Table 1. Observed concentrations in soil, c_s (ng g^{-1}; together with standard deviation based on 3 replicates) of (a) pesticides, (b) PCBs, and (c) PBDEs quantified species only. TOC = total organic carbon content (% of dry mass).

a.

Land use	Tea plantation	Shrubs	Forest
TOC	4.4	10.75	4.0
PeCB	0.018±0.001	0.017±0.002	0.010±0.000
HCB	0.021±0.001	0.023±0.005	0.019±0.000
α-HCH	0.036±0.005	0.020±0.001	0.010±0.000
β-HCH	0.016±0.000	0.019±0.000	<0.010
γ-HCH	0.054±0.011	0.055±0.001[a]	0.055±0.003
δ-HCH	< 0.010	< 0.010	< 0.010
ε-HCH	< 0.010	< 0.010	< 0.010
o,p'-DDE	1.83±0.12	0.012±0.001	0.006±0.000
p,p'-DDE	12.13±0.50	0.22±0.05	0.077±0.004
o,p'-DDD	0.49±0.03	0.007±0.001	<0.010
p,p'-DDD	0.17±0.01	0.025±0.002[a]	0.14±0.00
o,p'-DDT	11.34±0.71	0.044±0.001[a]	0.025±0.003
p,p'-DDT	1.90±0.14	0.12±0.00[a]	0.060±0.026

b.

	Tea plantation	Shrubs	Forest
PCB28	0.054±0.008	0.055±0.000[a]	0.060±0.002
PCB52	0.048±0.022	0.050±0.005[a]	0.053±0.007
PCB101	0.043±0.009	0.050±0.007[a]	0.051±0.004
PCB118	0.021±0.005	0.025±0.002	0.026±0.003
PCB153	0.034±0.008	0.040±0.007	0.038±0.008
PCB138	0.031±0.008	0.037±0.005	0.038±0.005
PCB180	0.015±0.004	0.014±0.001	0.013±0.008

c.

	Tea plantation	Shrubs	Forest
BDE28	<0.35	0.77±0.22	0.54±0.38
BDE47	5.09±0.53	7.83±0.01 [a]	7.69±0.38
BDE66	0.96±0.14	0.55±0.52	<0.70
BDE100	0.32±0.04	<0.81	0.71±0.18
BDE99	1.77±0.05	1.99±0.08 [a]	1.81±0.34
BDE85	<0.27	<1.50	<0.32
BDE154	<0.31	<0.25	<0.25
BDE153	<0.68	<0.40	<0.43
BDE183	<0.48	1.58±0.09	<0.88

[a] based on 2 replicates

associated with convective activity (Valsan et al., 2016). With 2.3-17.7 pg m^{-3} Σ_4HCH and 0.36-10.4 pg m^{-3} Σ_6DDX (Table S3) the measurements at Munnar range at the lower end of the range reported from rural sites in India in years after ban in agriculture (listed in Table S6c). 1.3-8.5 pg m^{-3} endosulfan (including endosulfan sulfate) measured in Munnar in 2014, shortly after the ban of the pesticide is 3 orders of magnitude below what was reported 2006-07 (i.e., 1000-9200 pg m^{-3} at rural locations of South India; Pozo et al., 2011).

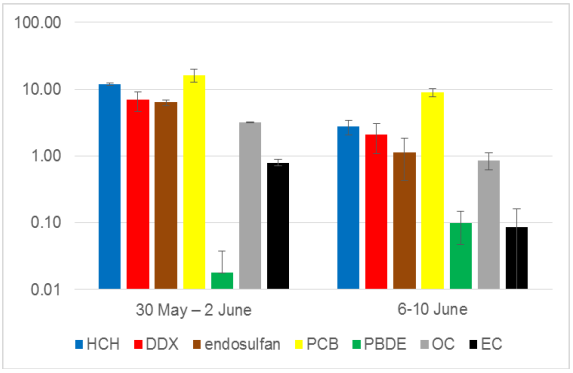

Fig. 1. Observed concentrations in air, c_a, of pesticides (Σ_4HCH, Σ_6DDX, Σ_3Endosulfan), Σ_7PCB, Σ_9PBDEs (pg m^{-3}), OC and EC (µg m^{-3}) before and after onset of southwest monsoon in Munnar, India, 2014. Error bars reflect standard deviations. All concentration changes are significant ($p < 0.05$ level, t-test), except for PBDEs.

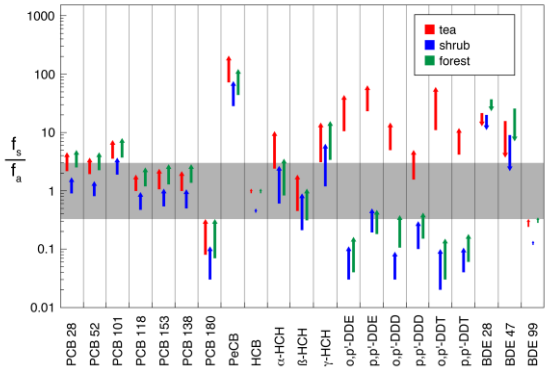

Fig. 2: Change of air-soil chemical equilibrium with the monsoon onset. Arrows denote direction and amount of change of fugacity ratio, f_s/f_a, over various soils from prior to posterior onset. $f_s / f_a < 1$ denotes downward (net-deposition), while $f_s / f_a > 1$ denotes upward (net-volatilisation) flux. The shaded zone ($0.33 < f_s/f_a < 3$) indicates insignificance of deviation from 1 due to input data uncertainties.

Similarly, the range of 2.8-70 pg m^{-3} Σ_7PCBs measured in 2014 at Munnar lies distinctly below 32-440 pg m^{-3} reported for the same substances at rural coastal sites in 2006 (Zhang et al., 2008).

The fugacity ratio f_s/f_a is used to characterize air-soil exchange (Supplementary, Text S1.2). Calculations indicate both downward (PCB180, DDT and metabolites over forest and shrub soils, BDE99) and upward (PCB101, PeCB,

DDT and metabolites over tea garden soils, BDE28, BDE47; Fig. 2) diffusive air-soil exchange fluxes prior to the monsoon. With the monsoon onset f_s/f_a generally increases (except for PBDEs, of which concentrations in monsoon air were somewhat elevated compared to pre-monsoon air; Table S3). This can trigger a change of flux direction for the tri- to hexachlorinated PCBs (i.e., all targeted except PCB180) and α- and β-HCH (Fig. 2). For example α- and γ-HCH were close to phase equilibrium before onset, but net-volatilisation occurred during monsoon, while β-HCH changed from net-depositional to near phase equilibrium.

3.2 Response of air-soil gas exchange of pollutants to monsoon onset

Findings from the field campaign were used to constrain the regional WRF-Chem model simulations for the Indian subcontinent. In the model experiment the pre-contaminated soil (as observed at the background site, mean of soil samples, except for DDX, i.e., forest soil) is exposed to a drop of atmospheric concentrations, forced from the domain boundaries along with the monsoon onset and its northward propagation. In a control experiment pre-monsoon air concentrations are prescribed at the boundaries throughout the simulation (detailed in Methods and Supporting Information, S1.4.1).

Within a few days after monsoon onset in southern India, the advection of air from the Indian Ocean has reduced HCH and PCBs' atmospheric levels over southern India and the Bay of Bengal, and to a lesser extent over central India (Fig. 3, centre panels). Three weeks after onset in southern India, the northern monsoon boundary has passed over India except the northwestern states Gujarat and Rajastan (i.e., north of ≈22°N and west of ≈77°E; Valsan et al., 2016), but the distributions of HCH and PCB in air maintain significant gradients with high, i.e. only moderately

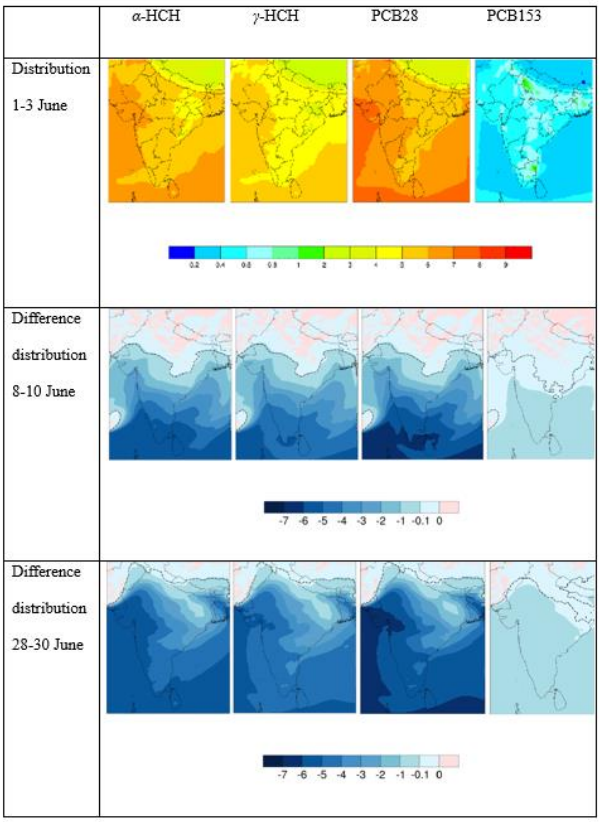

Fig. 3: Air pollutant distributions. α-HCH, γ-HCH, PCB28, and PCB153 (pg m^{-3}) predicted concentrations in near-ground air prior to monsoon onset (1-3 June, top panels) and difference distribution due to monsoon advection (experiment – control; centre panels: 8-10 June, bottom panels: 28-30 June 2014). The difference is significant ($P < 0.05$, t-test) south of the dotted line.

reduced (by < 1 pg m^{-3}) levels in the north and east, and low levels after a decline of > 3 pg m^{-3} of HCH isomers and > 5 pg m^{-3} of PCB28, respectively, in the south and southwest. The response of the air-soil system subject to the monsoon leads to a spatially inhomogeneous distribution of pollutants across India. It is dominated by clean air advection in the south and southwest, but only moderately decreased air pollution in northern and eastern parts of the sub-continent, as the air has received secondary emissions from the soils. The latter increases with distance from the coasts after monsoon onset. The differences in concentrations before and during monsoon are significant ($P < 0.05$, t-test) in south, central and parts of northern India (Fig. 3b,c). The model results show that HCH isomers and PCB28 concentrations drop by

≈80%, ≈20% and ≈4% at 9, 22 and 29°N, respectively, PCB153 by ≈40% and ≈10% at 9° and 22°N, respectively, while they increase by ≈1% at 29°N (Table S5a). The model realistically reproduces the decline of atmospheric concentration at the field site (Southern India, 9°N; Table S6a, b). In the model, the HCH and PCB volatilisation fluxes are enhanced in the south (by 0.02-0.78 pg m^{-2} h^{-1} i.e., 3-11%; Table S5b) by the drop in air pollution, and to a lesser degree in central India (0.002-0.19 pg m^{-2} h^{-1}), and even less or negligible at a northern India site (<0.0001-0.007 pg m^{-2} h^{-1}).

The southwesterly summer monsoon is associated with strong convection that effectively lifts air pollution to high altitudes in the troposphere. The monsoon outflow from India is predominantly directed towards western Asia, Africa and the Mediterranean, while a smaller fraction is transported towards east Asia (Lawrence and Lelieveld, 2010).

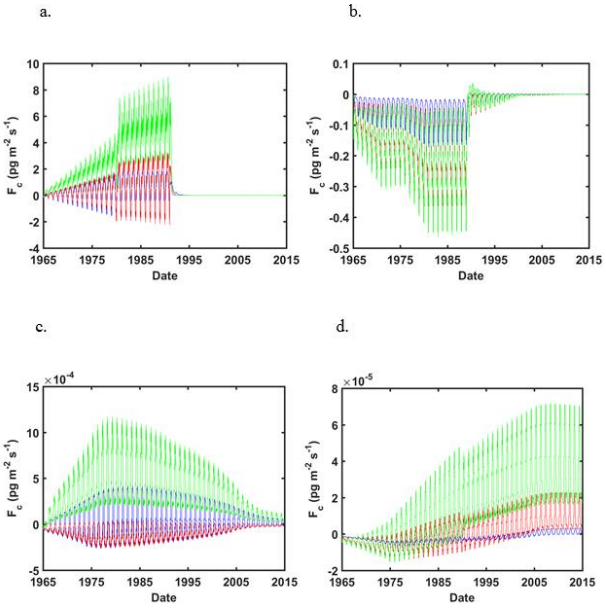

Fig. 4. Predicted multidecadal diffusive air-surface exchange fluxes. 1D model. F_c (positive = upward, negative = downward; lower) of (a) *α*-HCH, (b) *p,p'*-DDT, (c) PCB28, (d) PCB153 in the northern (29.7-33.4°N, blue), central (18.5-22.3°N, red) and southern (7.4-11.2°N, green) zones of India during 1965 – 2014. Predicted concentrations in air and soil are shown in SI, Fig. S4.

3.3 Multidecadal air-surface cycling of POPs and historic trends

To put the above described seasonal feature into historical context, with long-term trends of air/soil contamination, a multi-media mass balance box model was developed and applied for several measured contaminants.

As a result of historical applications in agriculture and industry, POPs have been accumulating in soils in India over decades (Fig. S3), partly continuing beyond peak emission. The atmospheric concentrations of PCBs have decreased since ≈1974, and *α*-HCH and DDT since ≈1989, but soil concentrations only decreased for *p,p'*-DDT, while they have levelled off for *α*-HCH, or are even still on the rise (PCB153, Fig. S4). Apart from changes over time, in general related to substance usage, the spatial variation of the pollutants' concentrations in mostly agricultural soil in India (Ramesh et al., 1991; Kumari et al., 1996; Sharma et al., 2014) is very large i.e., ≥ 2 orders of magnitude. No data from background sites are available (Table S6c). The simulated pesticide values, 0.5-20 ng g^{-1} *α*-HCH and 50-5000 and 1-200 ng g^{-1} DDT in the 1990s and 2000s, respectively (Fig. S2), fall into the ranges spanned by the observations (Table S6c). For PCBs, no soil data were reported (UNEP, 2002).

A north-south gradient is predicted for the pollutants (Fig. S3), which is certainly influenced by the emission distribution (maximum in North India, in the Indo-Gangetic Plain) as well as to the direction of advection in air (prevailing westerly, with northerly component). For α-HCH, such a gradient was also reflected in soil distributions in India which were based on a gridded mass balance model (Xu et al., 2013). While PCB28 have turned net-

volatilisational after a few years upon release into the environment, this was much later for the highly lipophilic PCB153, ≈1 decade in southern India, ≈2 decades in central and even later in northern India (Fig. 4d). Nowadays, the diffusive air-surface exchange flux of the pesticides α-HCH and DDT is expected in the 0.1-1 fg m^{-2} h^{-1} range, several orders of magnitude lower than before or shortly after the ban (Fig. 4a-b). In contrast and related to on-going emissions from old industrial facilities, the strong decrease in PCB usage did not strongly impact air-surface cycling. The magnitude of fluxes remained within the same order of magnitude, 0.1-1 fg m^{-2} h^{-1}, being even on the rise in the case of PCB153 (Fig. 4c-d). The air-ground flux fluctuations are expectedly mediated by storage of part of the pollutant burden in vegetation, not resolved in the model.

The results of simulation of a fictive no-monsoon scenario suggest that the effects of monsoon have been limiting pollution of soils by HCH and PCB28 somewhat (<20% in 2014), while they have been contributing to DDT and PCB153 in soils by ≈50% and ≈10%, respectively (SI S2.2.3, Table S8). This suggests that monsoon's effect on re-volatilisation of soil burdens in response to drop in air concentrations at the onset of the monsoon is a secondary effect for DDT and PCB153, while monsoon's enhancement of air-to-soil transfer by wet deposition is the primary effect. This trend could be explained by the higher significance of wet deposition for DDT and PCB153, which are more partitioning to the particulate phase than HCH and PCB28, whereas the efficiency of gas scavenging is generally low for POPs (Atlas and Giam, 1988; Bidleman, 1988; Shahpoury et al., 2015).

4. Discussion

Both, field measurements and modelling results reveal a thus far overlooked mechanism of pollutant cycling over the Indian subcontinent, i.e. monsoon-driven mobilisation from

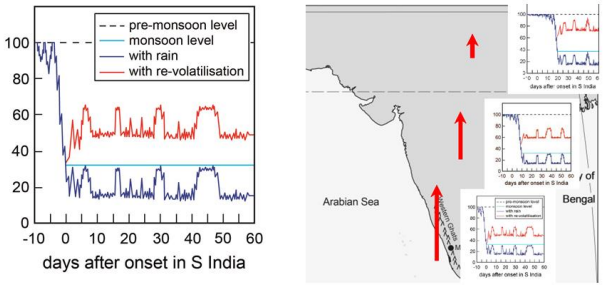

Fig. 5. Illustration of temporal (left) and spatial (right) variation of semivolatile and persistent substances' advection over southern, central and northern India in response to the monsoon onset and its northward propagation. Field site Munnar.

previously contaminated soils. The decline of POP levels in the southwesterly flow upon monsoon onset is partly related to the advection of clean air from the Indian Ocean (seasonal shift of the ITCZ), and partly by the washout of particulate pollutants (Fig. 5), as well as deepening of the planetary boundary layer. In contrast, washout of gaseous organic pollutants is very limited, because of low water solubility (Atlas and Giam, 1988; He and Balasubramanian, 2010; Shahpoury et al., 2015). Because of the convective vertical transport during the monsoon, pollutants can be released at the cloud top and subsequently undergo long-range transport in the upper troposphere over and beyond South Asia. During transport over the Indian subcontinent near the surface, air masses collect pollution emitted from primary and secondary sources at the ground in urban and rural areas. We have shown here that secondary sources are partly triggered by the low concentrations in relatively pristine air, most pronounced in areas that receive marine background air, i.e. in southwestern India. This corresponds to a seasonal decrease of the soil burden by a few percent relative to the annual mean. This secondary source (re-volatilisation) weakens as a function of distance from the coast, as the monsoon advection propagates across the subcontinent (Table S4b, Fig. 5). The 2014 southwesterly monsoon was relatively weak (South Asian summer monsoon index; Li and Zeng, 2002) compared to the long-term mean.

For strong monsoon events a stronger re-volatilisation is expected, but also a more efficient air-to-soil transfer of pollutants by wet deposition. The simulation under a no-monsoon scenario suggests that the latter process dominates for the least water soluble and least volatile (high partitioning to the particulate phase) pollutants. Scavenging and air-to-soil transfer of POPs under monsoon rains had hardly been studied in the field and should be addressed.

Secondary emissions, originating from past deposition to soils, also contribute to the long-range transport of atmospheric POPs to remote areas in central Asia (Sheng et al., 2013; Gong et al., 2015). A similar trend of pollutant release from soils can be expected for other semivolatile organic substances such as polycyclic aromatic hydrocarbons (actually indicated by observations on site, not reported here) and brominated chemicals.

Associated content:

Supporting Information Fugacity calculations, air mass history analysis and model descriptions and input data. Field data, model results and sensitivities.

Author information:

Corresponding Author phone: +49 6131 305 7601, e-mail: g.lammel@mpic.de

Corresponding author address: Multiphase Chemistry Department, Max Planck Institute for Chemistry, Hahn-Meitner-Weg 1, 55128 Mainz, Germany.

Notes The authors declare no competing financial interest.

Acknowledgements We thank Tabish Umar Ansari (IIT) and Roman Prokeš (MU) for on-site and logistic support, Milán Šáňka (MU) for assistance with soil sampling and data, and Jos Lelieveld (MPIC), Andreas Fink (Karlsruhe Institute of Technology), and Fei Ge (MPIM), for discussion. This research was supported by the Max Planck Society and the Czech Ministry of Education, Youth and Sports (LO1214 and LM2015051). S.S.G. acknowledges the financial support from DST-Max Planck Partner Group on Bioaerosol Research at IIT.

References

Atlas, E., and Giam, C. S.: Ambient concentration and precipitation scavenging of atmospheric organic pollutants, Water Air Soil Pollut., 38, 19–36, 1988.

Bajwa, A., Ali, U., Mahmood, A., Chaudhry, M.J.I., Jabir, H.S., Li, J., Zhang, G., Jones, K.C., and Malik, R.N.: Organochlorine pesticides (OCPs) in the Indus River catchment area, Pakistan: Status, soil-air exchange and black carbon mediate distribution. Chemosphere, 152, 292-300, 2016.

Bidleman, T.F.: Atmospheric processes wet and dry deposition of organic compounds are controlled by their vapor-particle partitioning. Environ. Sci. Technol., 22, 361-367, 1988.

Bidleman, T.F.: Atmospheric transport and air-surface exchange of pesticides, Water Air Soil Pollut., 115, 115-166, 1999.

Breivik, K., Gioia, R., Chakraborty, P., Zhang, G., and Jones, K.C.: Are reductions in industrial organic contaminants emissions in rich countries achieved partly by Export of toxic wastes? Environ. Sci. Technol., 45, 9154-9160, 2012.

Chakraborty, P., and Zhang, G.: Organochlorine pesticides, polychlorinated biphenyls, and polybrominated diphenylethers in the Indian atmosphere, in: Global contamination trends of persistent organic chemicals (Loganathan, B.G., Lam, P.K.S., eds.), CRC Press, Boca Raton, USA, 2012, pp. 179-202

Chakraborty, P., Zhang, G., Li, J., Sivakumar, A., and Jones, K.C.: Occurrence and sources of selected organochlorine pesticides in the soil of seven major Indian cities: assessment of air-soil exchange. Environ. Poll., 204, 74-80, 2015.

Cousins, I.T., Beck, A.J., and Jones, K.C.: A review of the processes involved in the exchange of semivolatile organic compounds (SVOC) across the air-soil interface, Sci. Total Environ., 228, 5-24, 1999.

Degrendele, C., Audy, O., Hofman, J., Kučerik, J., Kukučka, P., Mulder, M.D., Přibylová, P., Prokeš, R., Sáňka, M., Schaumann, G.E., and Lammel, G.: Diurnal variations of air-soil exchange of semi-volatile organic compounds (PAHs, PCBs, OCPs and PBDEs) in a central European receptor area. Environ. Sci. Technol., 50, 4278–4288, 2016.

FAO: World reference base for soil resources 2014, United Nations Food and Agricultural Organisation World Soil Resources Reports Vol. 106, FAO, Rome, 2014, 191 pp.

Grell, G. A., Peckham, S. E., Schmitz, R., McKeen, S. A., Frost, G., Skamarock, W. C., and Eder, B.: Fully coupled "online" chemistry within the WRF model, Atmos. Environ., 39, 6957-6975, 2005.

GOI: India soil map, Government of India, National Bureau of Soil Survey and Land Use Planning, Nagpur, India, 1985

Gong, P., Wang, X.P., Xue, Y.G., Sheng, J.J., Gao, S.P., Tian, L.D., and Yao, T.D.: Influence of atmospheric

circulation on the long-range transport of organochlorine pesticides to the western Tibetan Plateau, Atmos. Res., 166, 157-164, 2015.

Harner, T., Bidleman, T.F., Jantunen, L.M.M., and Mackay, D.: Soil-air exchange model of persistent pesticides in the U.S. Cotton Belt. Environ. Toxicol. Chem., 20, 1612–1621, 2001.

He, J., and Balasubramanian, R.: The exchange of SVOCs across the air-sea interface in Singapore's coastal environment. Atmos. Chem. Phys., 10, 1837-1852, 2010.

IMD: Climate diagnostic bulletin of India – Monsoon season (June – September) 2014, National Climate Centre, Indian Meteorological Department, Pune, India, 2014, 23 pp.

Kumari, B., Singh, R., Madan, V.K., Kumar, R., and Kathpal, T.S.: DDT and HCH compounds in soils, ponds and drinking water of Haryana, India. Bull. Environ. Contam. Toxicol., 57, 787–793, 1996.

Kurt-Karakus, P.B., Bidleman, T.F., Staebler, R.M., and Jones, K.C.: Measurement of DDT fluxes from a historically treated agricultural soil in Canada, Environ. Sci. Technol., 40, 4578-4585, 2006.

Lammel, G.: Effects of time-averaging climate parameters on predicted multicompartmental fate of pesticides and POPs. Environ. Pollut., 128, 291-302, 2004.

Lammel, G., and Stemmler, I.: Fractionation and current time trends of PCB congeners: Evolvement of distributions 1950-2010 studied using a global atmosphere-ocean general circulation model, Atmos. Chem. Phys., 12, 7199-7213, 2012.

Lammel, G., Klöpffer, W., Semeena, V.S., Schmidt, E., and Leip, A.: Multicompartmental fate of persistent substances: Comparison of predictions from multi-media box models and a multicompartment chemistry-atmospheric transport model, Environ. Sci. Pollut. Res., 14, 153-165, 2007.

Lawrence, M.G., and Lelieveld, J.: Atmospheric pollutant outflow from southern Asia: a review. Atmos. Chem. Phys., 10, 11017-11096, 2010.

Li, J.P., and Zeng, Q.P.: A unified monsoon index. Geophys. Res. Lett., 29, 1274, 2002.

Meijer, S.N., Shoeib, M., Jantunen, L.M.M., Jones, K.C., and Harner, T.: Air-soil exchange of organochlorine pesticides in agricultural soils – 1. Field measurements using a novel in situ sampling device, Environ. Sci. Technol., 37, 1292-1299, 2003.

Mu, Q., Lammel, G., Gencarelli, C.N., Hedgecock, I.M., Chen, Y., Přibylová, P., Teich, M., Zhang, Y.X., Zheng, G.J., van Pinxteren, D., Zhang, Q., Herrmann, H., Shiraiwa, M., Spichtinger, P., Su, H., Pöschl, U. and Cheng, Y.F.: Regional modelling of polycyclic aromatic hydrocarbon: WRF/Chem-PAH model development and East Asia case study. Atmos. Chem. Phys., 17, 12253-12267, 2017.

Pozo, K., Harner, T., Lee, S.C., Sinha, R.K., Sengupta, B., Loewen, M., Geethalakshmi, V., Kannan, K., and Volpi, V.: Assessing seasonal and spatial trends of persistent organic pollutants (POPs) in Indian agricultural regions using PUF disk passive air samplers. Environ. Pollut., 159, 646-653, 2011.

Rajendran, R.B., Venugopalan, V.K., and Ramesh, R.: Pesticide residues in air from coastal environment, South India. Chemosphere, 39, 1699-1706, 1999.

Ramesh, A., Tanabe, S., Tatsukawa, R., and Subramanian, A.N.: Seasonal variations of organochlorine insecticides residues in air from Porto Novo, South India. Environ. Pollut., 62, 213-222, 1989.

Ramesh, A., Tanabe, S., Subramanian, A., Mohan, D., Venugoplan, V.K., and Tatsukawa, R.: Persistent organochlorine residues in green mussels from coastal waters of South India. Mar. Pollut. Bull., 21, 587-590, 1990.

Ramesh, A., Tanabe, S., Murase, H., Subramanian, A., and Tatsukawa, R.: Distribution and behaviour of persistent organochlorine insecticides in paddy soil and sediments in the tropical environment: a case study in South India. Environ. Pollut., 74, 293-307, 1991.

Ramesh, A., Tanabe, S., Kannan, K., Subramanian, A., Kumaran, P.L., and Tatsukawa, R.: Characteristic trend of persistent organochlorine contamination in wildlife from a tropical agricultural watershed, South India. Arch. Environ. Contam. Toxicol., 23, 26-36, 1992.

Růžičková, P., Klánová, J., Čupr, P., Lammel, G., and Holoubek, I.: An assessment of air-soil exchange of polychlorinated biphenyls and organochlorine pesticides across central and southern Europe, Environ. Sci. Technol., 42, 179-185, 2008.

Semeena, V.S., and Lammel, G.: The significance of the grasshopper effect on the atmospheric distribution of persistent organic substances, Geophys. Res. Lett., 32, L07804, 2005.

Senthilkumar, K., Kannan, K., Subramanian, A., and Tanabe, S.: Accumulation of organochlorine pesticides and polychlorinated biphenyls in sediments, aquatic organisms, birds, bird eggs and bat collected from southern India, Environ. Sci. Pollut. Res., 8, 35-47, 2001.

Shahpoury, P., Lammel, G., Holubová Šmejkalová, A., Klánová, J., Přibylová, P., and Váňa, M.: Polycyclic aromatic hydrocarbons, polychlorinated biphenyls, and chlorinated pesticides in background air in central Europe - investigating parameters affecting wet scavenging of polycyclic aromatic hydrocarbons. Atmos. Chem. Phys., 15, 1795-1805, 2015.

Sharma, B.M., Bharat, G.K., Tayal, S., Nizzetto, L., Čupr, P., and Larssen, T.: Environment and human exposure to persistent organic pollutants (POPs) in India: A systematic review of recent and historical data. Environ. Int., 66, 48-64, 2014.

Sheng, J.J., Wang, X.P., Gong, P., Joswiak, D.R., Tian, L.D., Yao, T.D., and Jones, K.C.: Monsoon-driven transport of organochlorine pesticides and polychlorinated biphenyls to the Tibetan Plateau: Three years atmospheric monitoring study. Environ. Sci. Technol., 47, 3199-3208, 2013.

Shunthirasingham, C., Oyiliagu, C.E., Cao, X.S., Gouin, T., Wania, F., Lee, S.C., Pozo, K., Harner, T., and Muir, D.C.G..: Spatial and temporal pattern of pesticides in the global atmosphere. J. Environ. Mon., 12, 1650-1657, 2010.

UNEP: Regionally based assessment of persistent toxic substances – Indian Ocean regional report, United Nations Environment Programme, Châtelaine, Switzerland, 2002, 104 pp.

Valsan, A.W., Ravikrishna, R., Biju, C.V., Pöhlker, C., Després, V.R., Huffman, J.A., Pöschl, U., and Gunthe, S.S.: Fluorescent biological aerosol particle measurements at a tropical high altitude site in southern India during southwest monsoon season. Atmos. Chem. Phys., 16, 9805-9830, 2016.

Wania, F.: Potential of degradable organic chemicals for absolute and relative enrichment in the Arctic, Environ. Sci. Technol., 40, 569-577, 2006.

Wania, F., and Mackay, D.: Global fractionation and cold condensation of low volatile organic chlorine compounds in polar regions, Ambio, 22, 10-18, 1993.

Wania, F., and Westgate, J.N.: On the mechanism of mountain cold-trappoing of organic chemicals, Environ. Sci. Technol., 42, 9092-9098, 2008.

Wong, M.H., Wu, S.C., Deng, W.J., Yu X.Z., Luo, Q., Leung, A.O.W., Wong, C.S.C., Luksemburg, W.J., and Wong, A.S.: Export of toxic chemicals – a review of the case of uncontrolled electronic waste recycling. Environ. Pollut., 149, 131-140, 2007.

Wong, F., Alegria, H. A., and Bidleman, T. F.: Organochlorine pesticides in soils of Mexico and the potential for air-soil exchange, Environ. Pollut., 158, 749-755, 2010.

Xiao, H., Li, N., and Wania, F.: Compilation, evaluation, and selection of physical-chemical property data for α-, β- and γ-hexachlorocyclohexane, J. Chem. Eng. Data, 49, 173–185, 2004.

Zhang, G., Chakraborty, P., Li, J., Balasubramanian, T., Kathiresan, K., Takahashi, S., Subramanan, A., Tanabe, S., and Jones, K.C.: Passive sampling of organochlorine pesticides, polychlorinated biphenyls, and polybrominated diphenyl ethers in urba, rural and wetland sites along the coastal length of India. Environ. Sci. Technol., 42, 8218-8223, 2008.

Zhang, T.T., Fiedler, H., Yu, G., Solorzano Ochoa, G., Carroll, W.F., Gullett, B.K., Marklund, S., and Touati, A.: Emissions of unintentional persistent organic pollutants from open burning of municipal solid waste from developing countries. Chemosphere, 84, 994-1001, 2011.

Supplementary Information

Re-volatilisation of soil accumulated pollutants triggered by the summer monsoon in India

Gerhard Lammel [1,2], Céline Degrendele [2], Sachin S. Gunthe [3], Qing Mu [1], Akila Muthalagu [3], Ondřej Audy [2], C.V. Biju [4], Petr Kukučka [2], Marie D. Mulder [2], Mega Octaviani [1], Petra Příbylová [2], Pourya Shahpoury [1], Irene Stemmler [5], Aswathy E. Valsan [3]

[1] Max Planck Institute for Chemistry, Multiphase Chemistry Department, Hahn-Meitner-Weg 1, 55128 Mainz, Germany
[2] Masaryk University, Research Centre for Toxic Compounds in the Environment, Kamenice 5, 62500 Brno, Czech Republic
[3] Indian Institute of Technology Madras, Environmental and Water Resources Engineering Division, Chennai 600036, India
[4] College of Engineering Munnar, Department of Civil Engineering, P. B. No. 45, County Hills, Munnar 685612, India
[5] Max Planck Institute for Meteorology, Ocean in the Earth System Department, Bundesstr. 53, 20146 Hamburg, Germany

Contents

S1. Methodology

S1.1 Chemical analysis

The GC temperature programme for PCBs, HCHs, DDTs, PeCB and HCB was 80°C (1 min hold), then 40°C min-1 to 200°C, and finally 5°C min^{-1} to 305°C. Injection was splitless at 280°C, the injection volume was 3 µL, He was used as carrier gas at constant flow 1.5 mL min^{-1}.

The injection volume was 3 µL. PBDEs were analysed using GC-HRMS (gas chromatography with high resolution mass spectrometry) on a Restek RTX-1614 column (15 m × 0.25 mm × 0.1 µm). The resolution was set to > 10000 for BDE 28–183, and > 5000 for BDE 209. ^{13}C BDEs 77 and 138 were used as injection standards. The MS was operated in EI+ mode at the resolution of >10000. The temperature programme was 80°C (1 min hold), then 20°C min^{-1} to 250°C, followed by 1.5°C min^{-1} to 260°C and 25°C min^{-1} to 320°C (4.5 min hold). The injection volume was 3 µL in splitless mode at 280°C, with He used as a carrier gas at constant flow of 1 mL min^{-1}.

Recovery of native analytes ranged 88-103% for PCBs, 75-98% for OCPs, 70-95% for drin pesticides and 55-75% for PBDEs. The results for OCPs and PCBs were not recovery corrected. For PBDEs, isotope dilution method was used, the average recoveries ranged 78-128%. No replicates of sample extracts were run.

Table S1: QA parameters of chemical analysis. Instrument limits of quantification (LOQ), given as masses and concentrations, the latter for a typical sample volume (1600 m³), range of the limits of quantification (LOQs, defined as the maximum of the ILOQ and the average of field blank values plus three times their standard deviation) for soil (pg g^{-1} or ng g^{-1}), gaseous (PUF) and filter (QFF) (pg m^{-3}) of (a) OCPs, (b) PCBs and (c) PBDEs. n.t. = not targeted.

a.

	ILOQ (pg)	LOQ		
		Soil (ng g^{-1})	PUF (pg m^{-3})	QFF (pg m^{-3})
HCB	0.0062	0.01-0.03	0.38	0.0062
PeCB	0.0062	0.02-0.05	0.10	0.0062
α-HCH	0.0125	0.02-0.04	0.075	0.0125
β-HCH	0.0125	0.04-0.08	0.0125	0.0125
γ-HCH	0.0125	0.03-0.07	0.11	0.029
δ-HCH	0.0125	0.01	0.010	0.012
o,p'-DDE	0.0125	0.02-0.05	0.0125	0.0125
p,p'-DDE	0.0062	0.02-0.05	0.29	0.0062
o,p'-DDD	0.0062	0.03-0.06	0.0062	0.0062
p,p'-DDD	0.0062	0.02-0.05	0.0062	0.0062
o,p'-DDT	0.0125	0.03-0.05	0.037	0.0125
p,p'-DDT	0.0062	0.02-0.04	0.046	0.0062
Heptachlor	0.5	n.t.	0.027	0.5
Aldrin	0.5	n.t.	0.054	0.5
Dieldrin	0.5	n.t.	0.13	0.5
Endrin	0.5	n.t.	0.43	0.5
α-chlordane	0.5	n.t.	0.026	0.5
γ-chlordane	0.5	n.t.	0.024	0.5

α-endosulfan	0.5	n.t.	0.077	0.5
β-endosulfan	0.5	n.t.	0.13	0.5
Endosulfan sulfate	0.5	n.t.	0.31	0.5
Mirex	0.5	n.t.	0.012	0.5

b.

	ILOQ (pg)	LOQ		
		Soil (ng g^{-1})	PUF (pg m^{-3})	QFF (pg m^{-3})
PCB28	0.0062	0.01-0.03	0.39	0.0062
PCB52	0.0062	0.02-0.03	0.058	0.0062
PCB101	0.0062	0.04-0.08	0.036	0.0062
PCB118	0.0062	0.02-0.03	0.0062	0.0062
PCB153	0.0062	0.03-0.05	0.051	0.0062
PCB138	0.0125	0.03-0.05	0.034	0.0125
PCB180	0.0062	0.02-0.05	0.024	0.0062

c.

	ILOQ (pg)	LOQ		
		Soil (pg g^{-1})	PUF (pg m^{-3})	QFF (pg m^{-3})
BDE28	1.45	0.29-0.35	0.0016	0.0018
BDE47	0.27	0.054	0.0043	0.0013
BDE100	0.48	0.096-0.81	0.00051	0.00065
BDE99	0.81	0.162	0.00081	0.0011
BDE154	2.80	0.25-0.31	0.0029	0.0036
BDE153	5.19	0.40-0.68	0.0054	0.0052
BDE183	2.55	0.48-0.88	0.0028	0.0026

S1.2 Fugacity calculations

Fugacities of OCPs in soil (f_s) and air (f_a) were calculated as (Harner et al., 2001):

(S1) $f_s = c_s\, H(T) / (0.411\ \phi_{OM}\, K_{OW})$

(S2) $f_a = c_a\, R_g\, T$

with c_s, c_a being the concentrations in the media (mol m^{-3}), H(T) is the temperature dependent Henry's law constant (Pa m^3 mol^{-1}), ϕ_{OM} is the mass fraction of organic matter in soil, K_{OW} is the octanol–water partitioning coefficient, R_g is the universal gas constant (8.314 J mol^{-1} K^{-1}), and T is temperature (K). The factor 0.411 improves the correlation between the soil-air partitioning coefficient and K_{OW} (Hippelein and McLachlan, 1998; Meijer et al., 2003a). H(T) was obtained using the van't Hoff equation:

(S3) $\ln(H_1/H_2) = -\Delta H_{vap}(1/T_1 - 1/T_2)/R_g$

with temperatures T_1 and T_2 (K), H_1 and H_2 being the Henry's law constants at these temperatures, and enthalpy of vaporisation ΔH_{vap} (J mol^{-1}).

Physico-chemical data were taken from literature (Li et al., 2003; Xiao et al., 2004; Shen and Wania, 2005). 48h-means of the soil temperature are input into equ. (S1), assumed to be given by the 48h-mean near-ground air temperature. Soil density, ρ_s, needed to calculate c_s (mol m^{-3}) from measured values (in ng g^{-1}), is unknown and assumed to be equal to the mean value for this region, 1.04 g cm^{-3} (taken from the global model, MCTM, see S1.4.2). It is assumed that particulate organic matter (OM) mass equals 1.67 times the total organic carbon mass, TOC.

Contributions to the uncertainty of the fugacity ratio, f_s / f_a, are the uncertainties of measured concentrations c_s (±20%), c_a (±20%), Henry coefficient and OM/TOC. Values $0.3 < f_s/f_a < 3.0$ are conservatively considered to not safely differ from phase equilibrium (as commonly accepted e.g., Bruhn et al., 2003; Castro-Jiménez et al., 2012; Zhong et al., 2012; Mulder et al., 2014).

S1.3 Air mass history analysis

The discrepancies of dating of the onset of monsoon, based on hydrological, convection or circulation indices (Wang and Fan, 1999; Wang et al., 2001; Fasullo and Webster, 2003), or on local weather monitoring (IMD, 2014) are about ±1 day. In 2014, monsoon arrival in Kerala was dated to 6 June (IMD, 2014; Devi and Yadav, 2015). As the origin of air masses arriving in southern India switch from northern hemispheric to southern hemispheric with the onset of southwest monsoon, the tracking of air mass histories allows for higher temporal resolution. We analysed air masses histories, 3-hourly, using the HYSPLIT model (Draxler and Rolph, 2003) and the FLEXPART Lagrangian dispersion model (Stohl et al., 1998, 2005) at various arrival heights, 0-6000 m a.s.l.. The meteorological data (0.5° × 0.5° resolution, 3-hourly) were taken from ECMWF for FLEXPART runs and from NCEP for HYSPLIT runs. For FLEXPART runs, Lagrangian particles were released continuously.

S1.4 Modelling

S1.4.1 Regional-scale 3D air pollution model

Model: WRF-Chem integrates meteorological, gas-phase chemistry, and aerosol components. The planetary boundary layer parameterisation uses the Mellor–Yamada–Janjic scheme (Janjic, 1994) and Smagorinsky first-order closure for vertical and horizontal sub-grid-scale fluxes, respectively. Surface layer and soil-atmosphere interaction parameterisations follow (Janjic, 1994, and Chen and Dudhia, 2001), respectively. Cumulus is parameterised using the Grell-3D Ensemble scheme (Grell and Devenyi, 2002). Hydrometeors (cloud water and ice, rain, snow and graupel) microphysics follows the Purdue–Lin scheme (Lin et al., 1983). Short- and longwave radiation are calculated following the Goddard scheme (Chou and Suarez, 1994) and Mlawer et al., 1997, respectively. Photolysis rates are derived on an hourly basis using the Fast-J scheme (Wild et al., 2000). A modal aerosol is described based on the Modal Aerosol Dynamics Model for Europe (MADE; Ackermann et al., 1998). Secondary organic aerosol is diagnosed using the Secondary Organic Aerosol Model (SORGAM; Schell et al., 2001). Modes considered by MADE/SORGAM are the nucleation, accumulation and coarse modes. The model has recently been extended by parameterisations for air-soil exchange and gas-particle partitioning (Mu et al., 2017) such as to

describe the cycling of semivolatile organics of organic substances. Gas-particle partitioning is described using a single-parameter linear free-energy relationship, an absorption model (K_{oa} model; Finizio et al., 1997).

The air-soil gas exchange flux is described by a parameterisation of the Jury model (e.g. Hansen et al., 2004; Jury et al., 2003).

(S4) $$F_c = -\nu_s [(1-\theta)\, c_a - c_s/K_{sa}]$$

where v_s is the exchange velocity between the air and the soil (m s^{-1}), θ is the particulate mass fraction, c_a and c_s are the air and soil concentrations (kg m^{-3}), respectively and K_{sa} is the soil-air exchange partitioning coefficient (dimensionless). Therefore, a positive F_c indicates volatilisation while a negative value characterizes deposition. The exchange velocity between the air and the soil, v_s, is defined as (Strand and Hov, 1996; Hansen et al., 2004):

(S5) $$\nu_s = [D_G^{air}\, f_a^{10/3} + D_L^{water}\, l^{10/3}\, K_{aw}(T)^{-1}]\, (1 - f_l - f_a)^{-2} / (h_s/2)$$

where D_G^{air} and D_L^{water} are the diffusion coefficient in air and water (m^2 s^{-1}), respectively, f_a and f_l represent the air and liquid fraction in soil (dimensionless) and K_{aw} is the air-water partitioning coefficient (dimensionless). The influence of temperature on K_{aw} was taken into account using van't Hoff equations. K_{sa} used in this study were defined as (Karickhoff, 1981):

(S6) $$K_{sa} = 0.411\, f_{OC}\, \rho_s\, K_{OA}(T)$$

where f_{OC} is the fraction of organic carbon in soil (0.010 g_{OC} g_{soil}^{-1}; upper value in the range of values spanned across the climate zones of India, see below S1.4.2), ρ_s is the soil density (1.35 kg L^{-1}; estimate, Jury et al., 2003), K_{OA} is the temperature dependent octanol-air partitioning coefficient and 0.411 is a constant with units of L kg^{-1}. In agreement with the experimental soil sampling, the model soil is a 0.05 m thick layer which was assumed to contain 50% of soil, 30% of water and 20% of air (Jury et al; 2003).

Substances:

For modelling each 2 PCBs and HCH isomers are selected. These 4 POPs span a wide range of physico-chemical properties i.e., from low to moderate volatile and from lipophilic to moderately water soluble (Table S4). DDT could not be included as its emissions are insufficiently known for

an episode simulation: The emission time (often twice i.e., once during summer and once during monsoon; NVBDCP, 2009) and emission factor (to account for release of indoor sprayed DDT to the ambient air) are basically unknown. Similarly, PeCB, HCB and PBDEs could not be covered by modelling, because of lack of emission estimates.

Emissions: Primary emissions are considered for PCBs (gridded data, upper emission estimate for the year 2014; Breivik et al., 2007) and distributed across grid cells for India. During the episode PCB emissions are temperature driven, scaled according to vapour pressure. Herewith, it is accounted for the fact that the prevailing sources i.e., buildings and open installations, are following ambient temperature variation (as found elsewhere in post-ban times; Gasic et al., 2010). Suspected on-going emissions of α- and γ-HCH, partly legal, but not reported (Sharma et al., 2014), are neglected.

Boundary conditions: In the model experiment, air concentrations representing pre-monsoon or monsoon background conditions are input continuously at all boundaries of the domain. For monsoon conditions, the background air concentrations, advected to the continent from the model domain boundaries are appropriately represented by the concentrations measured on site after onset of the monsoon (mean of the period 6-10 June 2014), while for pre-monsoon conditions they are represented by the concentrations measured on site before mixing with monsoon air (we adopt the mean of the period 30 May – 2 June 2014). PCB and HCH air concentrations measured on site are appropriate, as these are representing background conditions. Adopting these measured values, we implicitly assume that concentration changes along transport from the domain boundaries over sea to land will be negligible, and trust that propagation of southwest monsoon northward is well captured by model (nudged) meteorology. Hereby, in order to mimick the northward propagation of monsoon in the model experiment, the boundary conditions are switched from pre-monsoon to monsoon conditions progressively from south to north by 0.75°N/day, passing 10°N (latitude of Munnar) on 6 June. The vertical profiles and the tendencies of the atmospheric concentrations of the pollutant species at the boundaries are scaled (or adopted) according to the vertical profile and the concentration at the site, respectively, of a long-lived tracer, namely CO of the global chemistry model output used for boundary conditions in WRF/Chem i.e., MOZART (Emmons et al., 2010). In the control experiment, a second run, the pre-monsoon background conditions are input throughout the whole run.

S1.4.2 1D multi-media mass balance box model

Compartments simulated

Although small mass fractions of lipophilic substances (log $K_{oa} \gtrsim 6$) cycling in continents are stored in above- and below-ground parts of vegetation (Calamari et al., 1991; Meijer et al., 2003b; Lammel et al., 2007) and in freshwater and ice, we refrain from including vegetation, freshwater or cryosphere compartments, apart from air and soil (Fig. 1). Freshwater/wetlands and glaciers are neglected, because of the small area they cover on the Indian subcontinent, and largely peripheral locations. As to vegetation, bioaccumulation of lipophilic substances in leaves and needles follows equilibrium with air and soil typically within 2 months for the most hydrophobic chemicals, shorter for less hydrophobic (Paterson and Mackay, 1991; Paterson et al., 1994). Dry particle and wet deposition fluxes, F_{dpdep} and F_{wetdep}, are parameterized such as to include various relevant canopies and account for enhanced air-surface transfer by high canopies (McLachlan and Horstmann 1998). Pollutants' clearance rates of the studied substances from vegetation are not available, therefore, in lack of better knowledge degradation within vegetation is commonly assumed to follow the same kinetics as in the soil, k_{degr}. Hence, while vegetation cycling of pollutants mediates air-surface exchange on seasonal and shorter time scales (e.g., Bao et al., 2016), it is considered to not significantly bias the chemodynamics on the multi-year time scale (Scheringer and Wania, 2003). Moreover, in tropical climate, air-surface exchange is not expected to be influenced by seasonally changing vegetation compartment volume, unlike in temperate climate (Wania and McLachlan 2001). In summary, short-term fluctuations of model predicted air-surface exchange flux, F_c, may be biased by the neglect of explicit air-vegetation and soil-vegetation gas exchanges and are not studied here.

Fig. S1. Schematic representation of 1D multi-media mass balance box model: Processes in the atmospheric boundary layer and topsoil including air-surface exchange (F_c), emission (F_{em}), advection (F_{adv}), dry particle deposition (F_{dpdep}), wet deposition (F_{wetdep}), removal from the residual layer ($F_{vertdil}$), and degradation (k_{degr}). Series of 7 two-boxes with heights h_a and h_s, connected by F_{adv}, spanning in total 7.4-33.4°N.

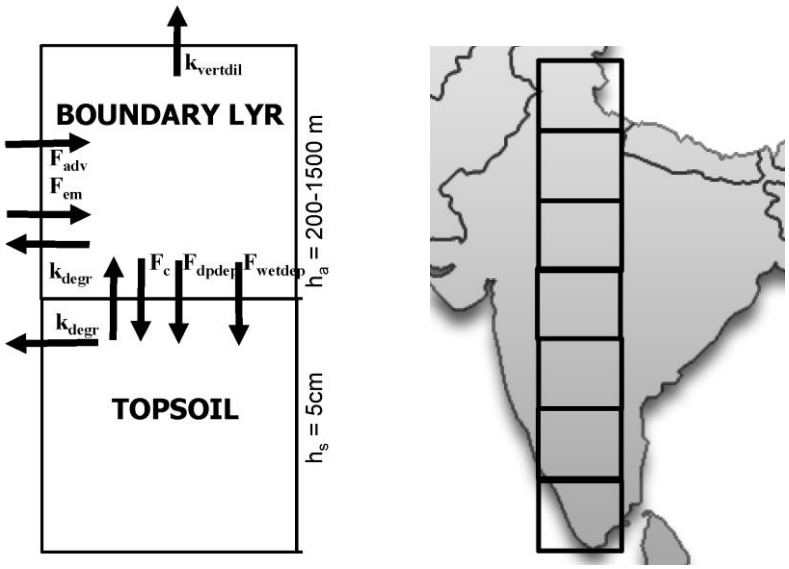

Mass balance equations:

(S7) $$\frac{dba}{dt} = -\left[(1-\theta)\, k_{OH}^{(2)}\, c_{OH} + v_{dep\,p}\,\theta / h_{mix} + W_t\right] \times b_a + F_c + F_{em}$$

(S8) $$\frac{dbs}{dt} = +\left(v_{pdep}\,\theta / h_{mix} + W_t\right) \times b_a - F_c - k_s^{(1)}\, b_s$$

where b_a and b_s are the air and soil burden (kg m^{-2}), respectively, θ is the particulate fraction (dimensionless), $k_{OH}^{(2)}$ is the 2nd order degradation rate coefficient of the reaction with OH radicals (cm^3 $molec^{-1}$ s^{-1}), c_{OH} is the OH concentration in the air (molec cm^{-3}), v_{pdep} is the dry particulate deposition velocity (m s^{-1}), h_{mix} is the boundary layer (BL) depth (m), W_t is the scavenging coefficient (s^{-1}), F_c is the air-surface exchange flux (kg m^{-2} s^{-1}), F_{em} is the emission flux (kg m^{-2} s^{-1}), $k_s^{(1)}(T)$ is the 1st order degradation rate in the soil (s^{-1}; default temperature dependence assuming doubling per 10 K increase). The particle deposition velocity $v_{dep\,p}$ was derived using an empiric relationship for particle size dependent lifetime (Jaenicke, 1988):

(S9) $$v_{dep\,p}(D) = h_{mix} / \tau_{dry}(D) = h_{mix} \times \left[(D/0.6)^2 + (D/0.6)^{-2}\right] / b$$

where b is a constant and D is the mean particle size (μm). We adopted b = 10^6 s, as this leads to $v_{dep\ p} > 0.01$ cm s^{-1} for h_{mix} = 200-8000 m as suggested by field studies covering a wide range of canopies (Ruijgrok et al., 1995; Pryor et al., 2008) and D = 0.2 μm for all SOCs investigated in agreement with previous field studies (Landlová et al., 2014; Degrendele et al; 2016; Zhu et al., 2017). The wet scavenging coefficient, W_t, is derived as the ratio of the wet deposition flux, F_{wet}, and the air burden, b_a, both adopted from global multicompartment chemistry-transport model (MCTM) output for the study area (Semeena et al., 2006; Lammel and Stemmler, 2012). In the MCTM, the air burden, b_a, is fed from advection and primary and secondary emissions, the latter include also vegetation surfaces, apart from soils and other ground surfaces. Therefore, W_t, is implicitly accounting for vegetation canopies.

The air-surface gaseous exchange flux, F_c, is defined as above (see S1.4.1). Again, K_{sa} is calculated using fraction of organic carbon in soil, f_{OC}, and soil density, ρ_s (Karickhoff, 1981; see above S1.4.1). f_{OC}, and ρ_s in the 7 zones are adopted from MCTM input i.e., globally mapped soil data (Batjes, 1996; Dunne and Willmott, 1996; Semeena et al., 2006), and range 0.0033-0.0104 g_{OC} g_{soil}^{-1} and 1.04-1.45 kg L^{-1}, respectively.

Air and soil concentrations were calculated from the air and soil burden as $c_a = b_a/h_{mix}$ and $c_s = b_s/h_s$ with h_s the soil depth (m). In agreement with the experimental soil sampling, the model soil depth is 0.05 m. Monthly mean concentrations of the hydroxyl radical, c_{OH}, are extrapolated from a climatology (Spivakovsky et al., 2000; 3-monthly data) and range (0.38-2.09) $\times 10^6$ molec cm^{-3} across the 7 zones and all months. Neighboring cells are connected by southward advection, replacing c_a exactly once per time step (F_{adv}, Δt = 7 h). Substance specific input parameters, including their temperature dependencies, are listed in Table S2. The dry particulate deposition flux was defined as:

(S10) $F_{drydep} = v_{dep}\, \theta\, c_a$

θ is calculated using gas-particle partitioning models, namely an absorption model (K_{oa}; Finizio et al., 1997) for chlorinated substances. Total particulate matter and OM concentrations in near-ground air are taken from a global chemistry-climate model (ECHAM/MESSy Atmospheric Chemistry) with a modal aerosol sub-model (HAM; Pringle et al., 2010).

Advection and boundary layer depth: India is represented as 7 zones in N-S direction, each 3.75°N wide (7.4-33.4°N; Fig. S1). The prevailing wind direction throughout most of the year and across most of the zones is westerly, with a northerly component, actually not linked to a particular monsoon phase. The annual mean northerly component at 850 hPa (≈1400 m a.s.l.) across the 7 zones amounts to 1.63 m s^{-1} (in the longitude band 76.85-80.65°E), which corresponds to a characteristic advection time of 7 h between neighbouring latitudinal zones. 850 hPa is chosen to represent the altitude of prevailing transport within the BL. BL depth, h_{mix}, varies in the range 550-1300 m during monsoon and somewhat higher, 750-1900 m in the pre-monsoon season (1965-2001 monthly means for the 7 zones in 7.4-33.4°N/76.85-80.65°E taken from ERA-40 re-analysis data; ECMWF, see also Patil et al., 2013). The terrain height varies across the 7 zones between ≈100 m in the coastal plain of Tamil Nadu and the Indo-Gangetic Plain, and > 1000 m in the central highland and Himalayan foothills. The diurnal variation of the boundary layer depth (at 12:00 and 18:00h UTC, ERA-40 data, ECMWF) is considered to derive a pollutant loss term from the BL into the free troposphere: before sunrise, 10% of the pollutant burden which resides in the residual layer (e.g., Stull, 1988) is removed, such that only 90% is preserved for being included into the BL following the morning increase of BL depth (corresponding to a vertical dilution with a varying rate coefficient $k_{vertdil}$).

Substances: For modelling, 2 PCBs, one HCH isomer (α-HCH) and DDT were selected. These 4 POPs span a wide range of physic-chemical properties i.e., from very low to moderate volatile and from lipophilic to moderately water soluble (Table S4). On the multidecadal time scale, DDT is covered too, despite the limitations related to emissions since the ban in agriculture, 1989 (see S1.4.1, above).

Emissions: Historical, gridded primary emission data were adopted for the 7 latitudinal zones. Such gridded data were available for α-HCH (annual data; Li et al., 2000), DDT (extrapolated from every tenth year; Semeena and Lammel, 2003), and PCBs (annual data; Breivik et al., 2007; upper estimates used). For post-ban remaining emissions 10^{-5} of the last pre-ban emissions are assumed for α-HCH. For DDT applied indoors in governmental health programs of India (since 1990), total amounts emitted were available (extrapolated from every tenth year; Pacyna et al., 2010). It is assumed that the DDT emissions of 1980 had continued until the ban, 1989. DDT usage in India after 1989 is inconsistently reported (e.g., 1126 or 3347 t in 2010; Pacyna et al., 2010;

UNEP, 2016). The lower values were adopted. For PCBs and pesticides used in agriculture (α-HCH, DDT) annual sums were homogeneously entried throughout the year. However, post-ban PCB emissions are mostly from buildings and open installations and, therefore, are simulated to be driven by vapour pressure (scaled to mean hourly ambient temperature variation at a central India site, 22°N). Furthermore, as DDT application since the year 1990 have been mostly twice per year, before and during SW monsoon, with some local flexibility (NVBDCP, 2009), temporally homogeneous application to all land is assumed in the model throughout January to August, while zero emissions are assumed throughout September to December.

Initialisation of simulation: The initial soil concentrations of all compounds investigated were set to zero at t_0 (1965). Initial air concentration is considered for the northernmost cell, while the other cells receive advection from the northern neighbor cell. Advection into the BL box of the northernmost zone is from the northern hemispheric background during non-monsoon months and zero during monsoon months. For non-monsoon months, annual mean levels observed at the Himalayas foothills (site Surkanda Devi, 2200 m a.s.l., 2006-07; Pozo et al., 2011) are considered for PCBs, for other years scaled with the emissions.

Time dependent input parameters: emission flux (annual), (monthly and day/night), mixing height (monthly, daily 10% loss into residual layer), air temperature (monthly, for gas-particle partitioning), soil temperature (monthly, for air-surface exchange flux), wet deposition flux (monthly).

Model evaluation and sensitivity study:

Regarding the input data uncertainties, concentrations in air and soil are predicted well, except for DDT which concentrations in air, c_a, are largely overestimated (Table 6b). This results probably from the very uncertain emission estimates for recent years (above, S1.4.1). Furthermore, as part of the substance is sorbed to aerosol particles (particulate mass fraction $\theta > 0$; Landlová et al., 2014, the mean value observed at the site was $\theta = 0.04$), lifetime in air is strongly influenced by wash-out of particles and might be affected by discrepancies between predicted and observed precipitation. DDT concentration in soil, c_s, is overestimated, too, and very sensitive to k_{soil}, which is an estimate only (no experimental data available). For PCB28 the soil concentration is underpredicted by one order of magnitude.

The direction of diffusive air-surface exchange flux, F_c, in southern India is well predicted for all substances. The effect of onset of SW monsoon on the magnitude of the air-surface exchange flux is well predicted for the pesticides studied, but out of phase for the PCBs. The observed seasonality of F_c (Fig. S4) results from the combination of emission and deposition patterns. In the model, PCB sources, both primary and secondary emissions are following ambient temperature (primary emissions i.e., evaporation from buildings, facilities, scaled with vapour pressure). Maximum seasonal concentrations of DDT compounds in the outflows from the Indo-Gangetic Plain into the Himalayas had been observed during June-July, which was explained by flooding-related application (Sheng et al., 2013).

In general, long-term budgeting of POPs cycling is limited by data availability, with degradation rates in soil being estimated from a wide range of observed disappearance rates. Declining DDT and HCH levels in soil, modelled in this study, were based on upper estimates of degradation rates (Mackay et al., 2006), and may be uncertain by one order of magnitude on this spatial scale. Apart from DDT and HCH, also the concentration and, hence, air-surface exchange flux of PCB28 is sensitive to k_{soil}. The sensitivities of 1D multi-media mass balance box model output parameters to input data variation is listed in Table S7.

S1.4.3 Model input data

Table S2. Physico-chemical properties and kinetic data of studied substances

Property	**PCB28**	**PCB153**	***α*-HCH**	***γ* HCH**	***p,p'*-DDT**
Saturation vapour pressure (p_{sat}) (mPa)	13.06[b,d]	0.101[b,d]	3.3 [m]	76[m]	0.025[a,c]
Henry's Law coefficient (Pa m³ mol^{-1})	30.4[d]	19.4[d]	0.73[m]	0.30[m]	1.1[h]
Water solubility at 298 K (mg L^{-1})	0.23[d]	1.11×10^{-3}[d]	2.0 [m]	7.3 [m]	0.149[d]
Enthalpy of vapourisation (ΔH_{vap}) (kJ mol^{-1})	89.3[g]	103.5[f]	67.0[m]	74.8[m]	118[e]
Enthalpy of solution (ΔH_{sol}) (kJ mol^{-1})	27[e]	27[e]	7.63[m]	15.1[m]	27[e]
Octanol-air partitioning coefficient (log K_{oa}) at 298 K	8.06[i]	9.44[i]	7.47[m]	7.75[m]	9.73[h]
OH gas-phase rate coefficient ($k_{OH\text{-}g}$) at 298 K (10^{-12} cm³ $moles^{-1}$ s^{-1})	1.06[j]	0.164[j]	0.15[n]	0.19[n]	0.5[e]
$\Delta E/R$ of OH reaction (K^{-1})	0[e]	0[e]	−1300[n]	−1710[n]	0[e]
Degradation rate coefficient in soil (k_{soil}) (10^{-9} s^{-1})	19.3[k,l]	0.35[k,l]	110[o,l]	20 [c,l]	4.05[o,l]

[a] at 293K
[b] at 298K
[c] Hornsby et al., 1996
[d] Li et al., 2003
[e] estimated
[f] Puri et al., 2001
[g] Puri et al., 2002
[h] Shen and Wania, 2005
[i] $K_{oa} = K_{ow}/K_{aw}$; K_{ow} from Li et al., 2003, K_{aw} based on water solubility and vapour pressure
[j] Anderson and Hites, 1996
[k] Wania and Daly, 2002
[l] assumed to double per 10 K temperature increase (EU, 1006)
[m] Xiao et al., 2004
[n] Brubaker and Hites, 1998
[o] Beyer et al., 2000

S2 Results

S2.1 Field observations

Table S3. Observed concentrations in air, c_a (sum of gaseous and particulate phases) of (a) pesticides, (b) PCBs, (c) PBDEs (pg m^{-3}) and (d) organic and elemental carbon (μg m^{-3}) during the entire campaign (5 May - 10 June) and 96 h periods shortly before (30 May-2 June) and after (6-10 June) onset of southwest monsoon.

a.

	Mean (entire campaign 5 May - 10 June 2014)	Pre-monsoon period 30 May – 2 June 2014	Monsoon period 6-10 June 2014
HCB	8.01	11.2	8.25
PeCB	0.72	1.16	0.13
α-HCH	4.70	6.37	1.34
β-HCH	0.66	0.72	0.19
γ-HCH	4.15	4.14	0.88
δ-HCH	0.77	0.60	0.33
ε-HCH	0.11	0.10	0.01
o,p'-DDE	0.53	0.58	0.17
p,p'-DDE	2.23	1.87	0.35
o,p'-DDD	0.23	0.35	0.11
p,p'-DDD	0.30	0.39	0.06
o,p'-DDT	1.84	2.36	0.62
p,p'-DDT	1.33	1.38	0.43
Heptachlor	0.004	<0.058	<0.026
Aldrin	0.016	<0.12	<0.052
Dieldrin	0.11	0.032	0.049
Endrin	0.39	<0.92	<0.41
α-chlordan	0.035	0.041	0.009
γ-chlordan	0.055	0.050	<0.024
α-endosulfan	2.72	3.53	0.80
β-endosulfan	0.26	0.20	<0.13
endosulfan sulfate	1.76	2.61	0.41
Mirex	0.021	0.012	0.013

b.

	Mean	Pre-monsoon period 30 May – 2 June 2014	Monsoon period 6-10 June 2014
PCB28	10.8	10.1	5.51
PCB52	4.54	4.41	2.36
PCB101	0.78	0.64	0.34
PCB118	0.46	0.32	0.18
PCB153	0.58	0.40	0.21
PCB138	0.43	0.28	0.14
PCB180	0.38	0.13	0.13

c.

	Mean	Pre-monsoon period 30 May – 2 June 2014	Monsoon period 6-10 June 2014
BDE28	0.013	0.002	0.025
BDE47	0.031	0.008	0.025
BDE100	0.005	<0.002	0.007
BDE99	0.018	0.003	0.022
BDE154	0.006	<0.009	0.002
BDE153	0.008	<0.017	<0.003
BDE183	0.028	0.004	<0.003

d.

	Mean	Pre-monsoon period 30 May – 2 June 2014	Monsoon period 6-10 June 2014
Organic carbon	4.28	3.19	0.86
Elemental carbon	1.09	0.80	0.08

S2.2 Modelling

S2.2.1 Regional-scale 3D air pollution model

Table S4. 3D model predicted response of the air-soil sub-system to advection of monsoon air at selected sites in southern, central and northern India, (a) concentrations in air under monsoon, c_{pred} (pg m^{-3}) and change upon onset, $\Delta c_{pred}/c_{pred}$ (%) [a] in brackets and (b) change of diffusive air-soil gas exchange flux upon onset of monsoon, ΔF_c (pg m^{-2} h^{-1}, positive upward) and $\Delta F_{pred}/F_{pred}$ (%) [b] in brackets. Monsoon/pre-monsoon periods are 8-10 June/1-3 June, 20-22 June/8-10 June, and 28-30 June/20-22 June at 9, 22 and 29°N, respectively.

a.

C	S India (Munnar, 9°N)	C India (22°N)	N India (29°N)
α-HCH	1.1 (-79%)	2.2 (-17%)	4.7 (-4%)
γ-HCH	0.73 (-83%)	1.7(-19%)	3.9 (-4%)
PCB28	1.2 (-79%)	2.4 (-17%)	5.2 (-4%)
PCB153	0.37 (-40%)	0.34 (-11%)	0.46 (+1%)

b.

F	S India (Munnar, 9°N)	C India (22°N)	N India (29°N)
α-HCH	0.29 (+ 5%)	0.09 (+ 1%)	0.004 (±0%)
γ-HCH	0.78 (+ 3%)	0.19 (± 0%)	0.007 (±0%)
PCB28	0.11 (+ 4%)	0.04 (+ 8%)	0.002 (±0%)
PCB153	0.02 (+11%)	0.002 (+97%)	<0.0001 (+1%)

[a] defined as $(\Delta c_{exp} - \Delta c_{ctrl})/c_{premonsoon}$, with: $\Delta c = c_{monsoon} - c_{premonsoon}$

[b] defined as $(\Delta F_{exp} - \Delta F_{ctrl})/F_{premonsoon}$, with: $\Delta F = F_{monsoon} - F_{premonsoon}$

Table S5. Comparison of model-predicted (3D model) and observed air concentration change with observations, concentrations under monsoon, c_{obs}, c_{pred} (pg m^{-3}) and change $\Delta c/c(\%)$ [a] upon onset, $\Delta c = c_{monsoon} - c_{premonsoon}$ (3D model, for Munnar, 9°N)

	c_{obs} ($\Delta c_{obs}/c_{obs}$)	c_{pred} ($\Delta c_{pred}/c_{pred}$)
α-HCH	1.3 (-83%)	1.1 (-79%)
γ-HCH	0.88 (-87%)	0.73 (-83%)
PCB28	5.5 (-55%)	1.2 (-79%)
PCB153	0.21 (-55%)	0.37 (-40%)

S2.2.2 1D multi-media mass balance box model

Table S6. Comparison of model-predicted and observed (a) air concentration change with observations, concentrations under monsoon, c_{obs}, c_{pred} (pg m^{-3}) and change $\Delta c/c$ (%) [a] upon onset, $\Delta c = c_{monsoon} - c_{premonsoon}$ (3D model, for Munnar, 9°N), (b) in air (pg m^{-3}) and soil (pg g^{-1}) (1D model for southern zone; pre-monsoon = May average, monsoon = June average), and (c) historically. N = North India, S = South India

a.

	c_{obs} ($\Delta c_{obs}/c_{obs}$)	c_{pred} ($\Delta c_{pred}/c_{pred}$)
α-HCH	1.3 (-83%)	1.1 (-79%)
γ-HCH	0.88 (-87%)	0.73 (-83%)
PCB28	5.5 (-55%)	1.2 (-79%)
PCB153	0.21 (-55%)	0.37 (-40%)

b.

	Air				Soil	
	Pre-monsoon		Monsoon		Pre-monsoon	
	Observed	Modelled	Observed	Modelled	Observed[b]	Modelled
α-HCH	7.73	11	1.13	1.4	0.010-0.036	0.0011
p,p'-DDT	1.54	70	0.33	75	0.060	0.061
PCB28	10.54	3.3	4.89	0.74	0.054-0.060	0.0013
PCB153	0.47	0.43	0.18	0.38	0.034-0.040	0.023

c.

		Air		Soil	
		Predicted	Observed	Predicted	Observed
α-HCH	1965-74	N 10^3-10^5 S 2×10^3-2×10^5		1-20	
	1975-84	N 10^4-2×10^5 S 2×10^4-2×10^5		2-40	
	1985-94	N 0.1-2×10^5 S 0.03-3×10^5	S 1.5-35.5[ce]	N 0.02-40 S 0.001-40	N 17-46[h] S 70-90 (<5-≈400)[j]
	1995-2004	N 6-20 S 3-20		N 0.02-0.04 S 0.001-0.003	N 1.6-835[ci]
	2005-14	N 6-20 S 3-20	NS 50-670[cg] S 100-360[cf]	N 0.02-0.04 S 0.001-0.003	
DDT	1965-74	N 10^3- 2×10^4 S 4×10^2- 2×10^4		N 0.6-5 S 1-20	
	1975-84	N 2×10^3- 5×10^4 S 8×10^3- 5×10^4	S 0.16-5.93[de]	N 5-20 S 20-30	
	1985-94	N 150- 5×10^4 S 8×10^3- 5×10^4		N 2-20 S 2-30	N <1-45[h] ≈0.6 (<0.1-≈2)[j]
	1995-2004	N 20-2000 S 2-7000	NS 20-1010[dg] S 120-140[df]	N 0.3-6 S 0.2-6	N 14-934[dh]
	2005-14	N 10-200 S 0.8-400		N 0.02-1 S 0.02-0.4	

[a] for predicted defined as $(\Delta c_{exp} - \Delta c_{ctrl})/c_{premonsoon}$, with: $\Delta c = c_{monsoon} - c_{premonsoon}$

[b] range of 3 soil samples, except for DDT (forest soil sample only)

[c] $\sum_4$HCH

[d] DDX

[e] coastal town (Rajendran et al., 1999)
[f] rural (Pozo et al., 2011)
[g] rural coastal (Zhang et al., 2008)
[h] agricultural soils (Kumari et al., 1996)
[i] agricultural or urban soils (Sharma et al., 2014)
[j] agricultural soils (Ramesh et al., 1991)

Fig. S2. Multidecadal 1D model predicted concentrations, c_a (pg m^{-3}), in the atmospheric boundary layer and diffusive air-surface exchange fluxes, F_c (pg m^{-2} s^{-1}), of (a) α-HCH, (b) *p,p'*-DDT, (c) PCB28, (d) PCB153 concentrations in the atmospheric boundary layer, c_a, (upper) and diffusive air-surface exchange fluxes, F_c (positive = upward, negative = downward; lower) in the southernmost zone of India (7.4-11.2°N) 1965-2014.

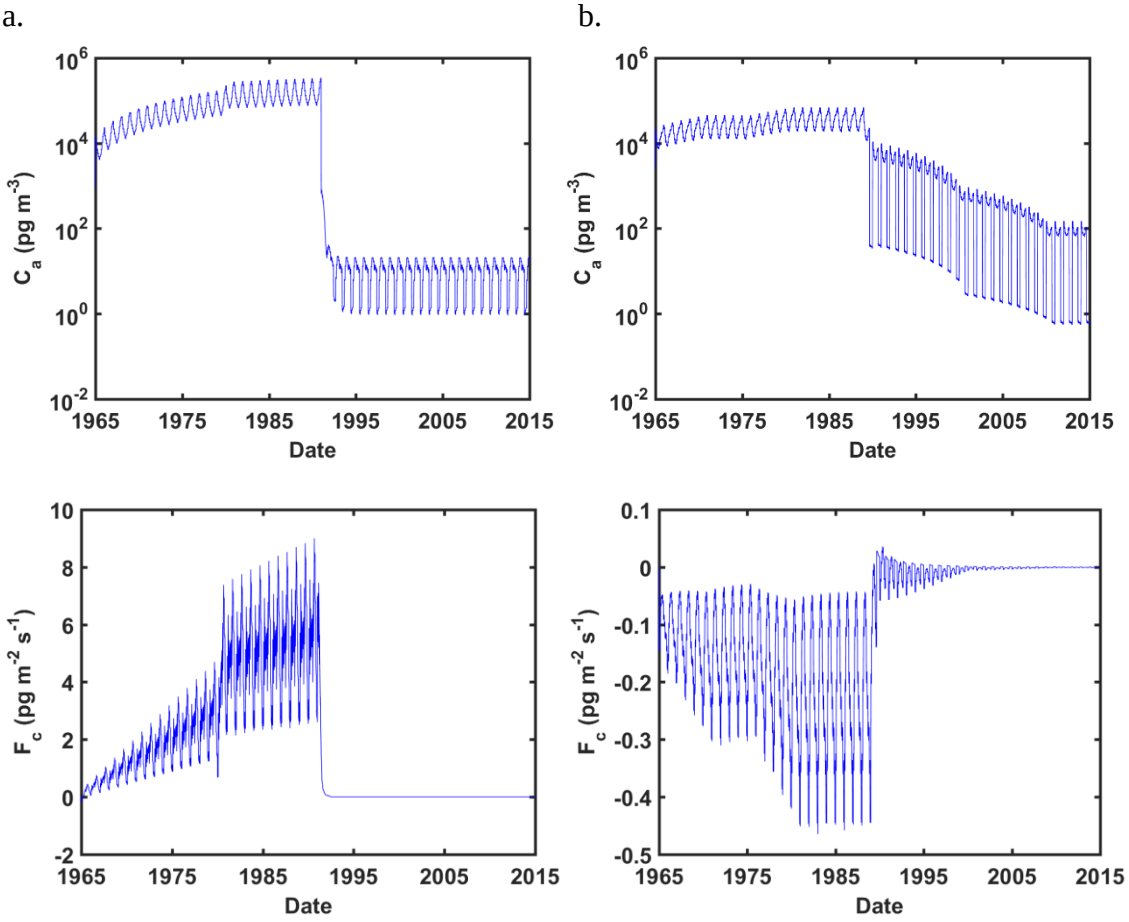

c.

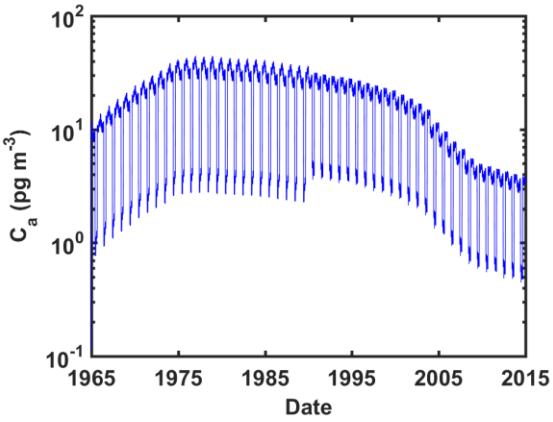
10^2
10^1
10^0
10^{-1}
C_a (pg m^{-3})
1965
1975
1985
1995
2005
2015
Date

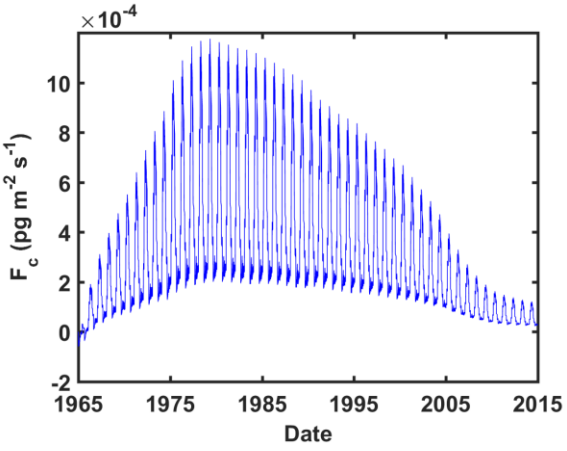
$\times 10^{-4}$
10
8
6
4
2
0
-2
F_c (pg m^{-2} s^{-1})
1965
1975
1985
1995
2005
2015
Date

d.

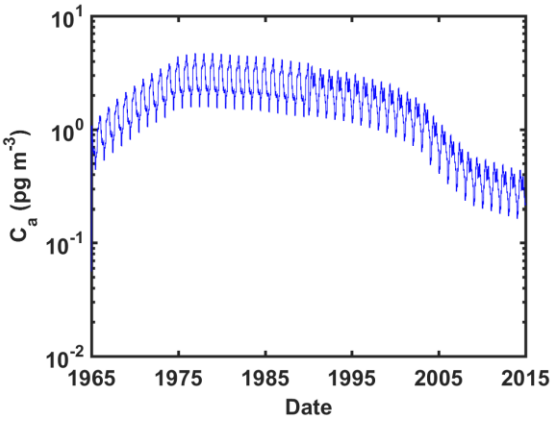
10^1
10^0
10^{-1}
10^{-2}
C_a (pg m^{-3})
1965
1975
1985
1995
2005
2015
Date

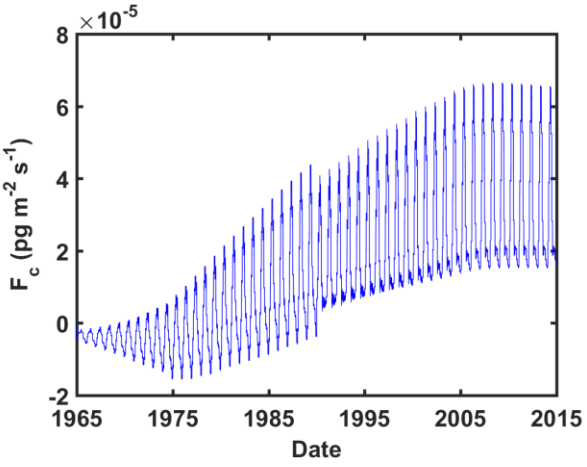
$\times 10^{-5}$
8
6
4
2
0
-2
F_c (pg m^{-2} s^{-1})
1965
1975
1985
1995
2005
2015
Date

Fig. S3. Multidecadal 1D model predicted concentrations in the atmospheric boundary layer, c_a, (upper), and topsoil (lower) of (a) α-HCH, (b) *p,p'*-DDT, (c) PCB28, (d) PCB153 in a northern (29.7-33.4°N, blue), central (18.5-22.3°N, red), and southern (7.4-11.2°N, green) zone of India 1965-2014.

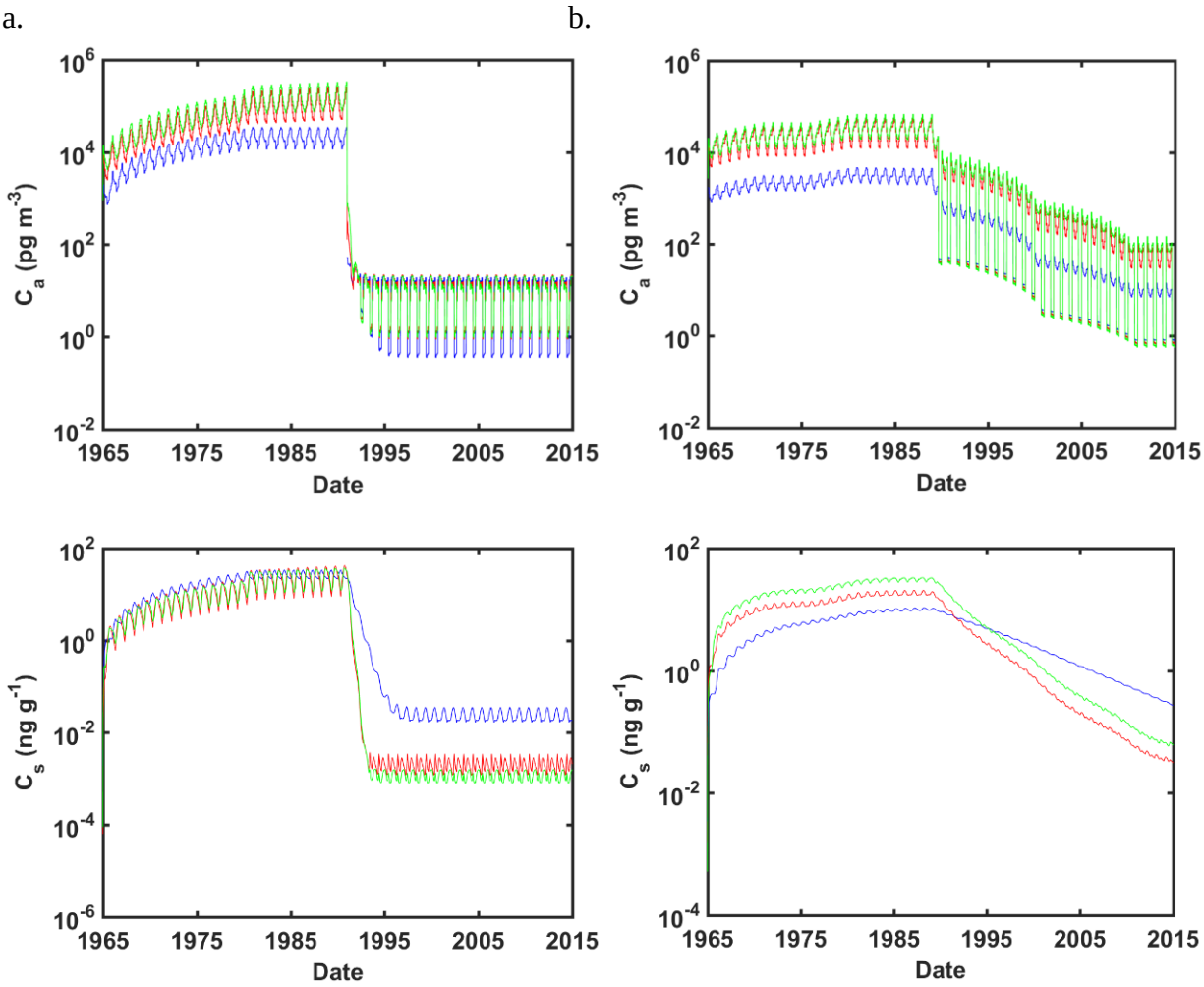

c.

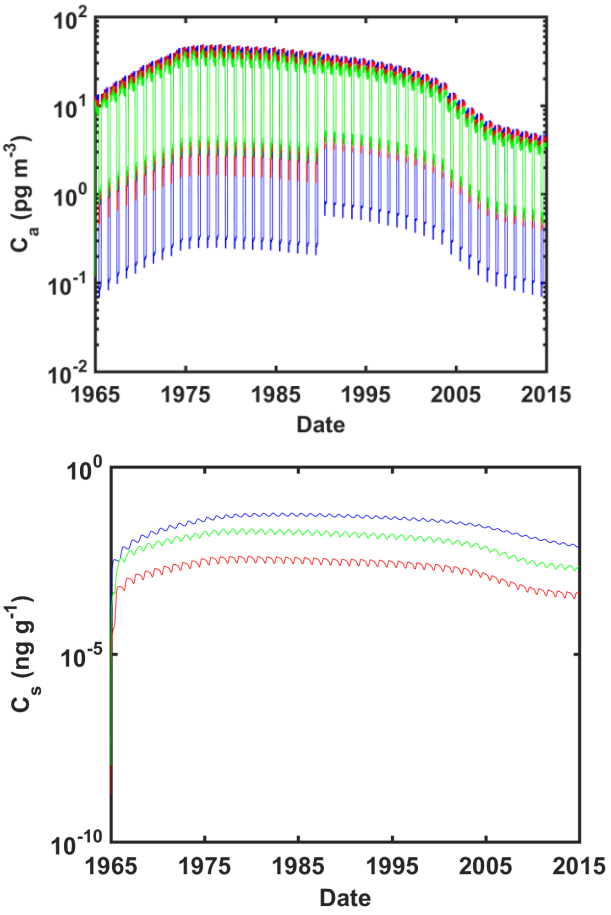
10^{2}
10^{1}
10^{0}
10^{-1}
10^{-2}
C_a (pg m^{-3})
1965
1975
1985
1995
2005
2015
Date
10^{0}
10^{-5}
10^{-10}
C_s (ng g^{-1})
1965
1975
1985
1995
2005
2015
Date

d.

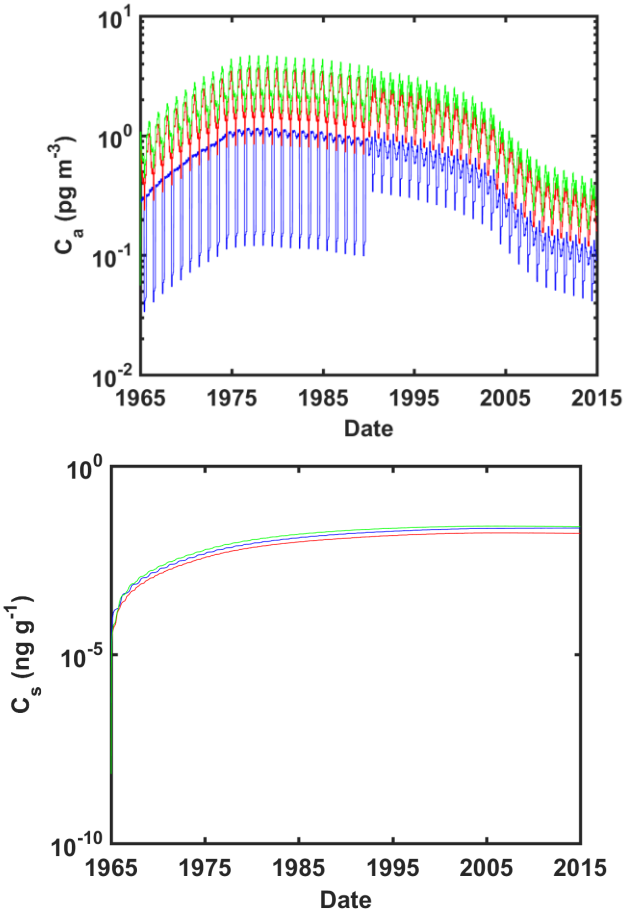
10^{1}
10^{0}
10^{-1}
10^{-2}
C_a (pg m^{-3})
1965
1975
1985
1995
2005
2015
Date
10^{0}
10^{-5}
10^{-10}
C_s (ng g^{-1})
1965
1975
1985
1995
2005
2015
Date

S2.2.3 Model sensitivities

Sensitivities of the 1D multi-media mass balance box model output parameters are listed in Table S7. The effect of monsoon on multicompartmental cycling is studied using a fictive no-monsoon scenario, which assumes no air concentration drop at the onset of the monsoon season into the BL box of the northern most zone (but preserves mean of non-monsoon months during the monsoon months), and no seasonal change of the wet deposition flux and the mxing height (but replace the scavenging coefficient W_t, and BL depth, h_{mix}, by the respective mean of non-monsoon months during the monsoon months) (Table S8).

Table S7. Sensitivities of 1D multi-media mass balance box model output parameters to input data variation

Input parameter studied	Variation (lower / upper) against default (S1.4.2)	Sensitivity	
		Low	Linear or high
k_{OH}	×0.33 / ×3	c_a of all	with background advection c_a of HCH and PCB28
k_{soil}	×0.33 / ×3	c_s and F_c of PCB153	c_s and F_c of HCH, DDT (most), PCB28
$F_{emission}$	×0.33 / ×3	c_a of HCH, PCB28	c_a almost linear for DDT, PCB153
h_{mix}	×0.33 / ×3	c_a of HCH, PCB28	c_a almost linear for DDT, PCB153
Daily removal from residual layer (vertical dilution)	Set to 0 / ×0.33 / ×3	c_a of all	
$c_{a\ bckgrd}$	Set to 0	c_a of DDT, PCB153	c_a of HCH, PCB28

Table S8. Comparison of 1D model predicted concentrations in air (pg m^{-3}) and soil (pg g^{-1}) under historic emissions and climate (S1.4.2) vs. under historic emissions but a fictive no-monsoon scenario (see S2.2.3, above) in the southern zone (7.4-11.2°N) 2014. Pre-monsoon = May average, monsoon = June average.

	Air				Soil	
	Pre-monsoon		Monsoon		Monsoon	
	Historic	No-monsoon	Historic	No-monsoon	Historic	No-monsoon
α-HCH	11	11	1.4	13	1.1	1.3
p,p'-DDT	70	70	75	104	59	28
PCB28	3.3	3.3	0.74	3.6	1.18	1.21
PCB153	0.43	0.43	0.38	0.61	23	20

References

Ackermann, I.J., Hass, H., Memmesheimer, M., Ebel, A., Binkowski, F.S., Shankar, U., 1998. Modal aerosol dynamics model for Europe: Development and first applications. Atmos. Environ. 32, 2981-2999.

Anderson, P.N.; Hites, R.A., 1996. OH radical reactions: The major removal pathway for polychlorinated biphenyls from the atmosphere. Environ. Sci. Technol. 30, 1756-1763.

Bao, Z., Haberer, C.M., Maier, U., Beckingham, B., Amos, R.T., Grathwohl, P., 2016. Modeling short-term concentration fluctuations of semi-volatile pollutants in the soil–plant–atmosphere system. Sci. Total Environ. 569-570, 159-167.

Batjes, N.H, 1996. Total carbon and nitrogen in the soils of the world. Europ. J. Soil Sci. 47, 151-163.

Beyer, A., Mackay, D., Matthies, M., Wania, F., Webster, E., 2000. Assessing long-range transport potential of persistent organic pollutants. Environ. Sci. Technol. 34, 699-703.

Breivik, K., Sweetman, A., Pacyna, J.M., Jones, K.C, 2007. Towards a global historical emission inventory for selected PCB congeners – a mass balance approach. 3. An update. Sci. Total Environ. 377, 296-307.

Brubaker, W., Hites, R.A., 1998. OH reaction kinetics of gas-phase α– and γ–hexachlorocyclohexane and hexachlorobenzene. Environ. Sci. Technol. 32, 766-769.

Bruhn, R., Lakaschus, S., McLachlan, M.S., 2003. Air/sea gas exchange of PCBs in the southern Baltic sea, Atmos. Environ. 37, 3445–3454.

Calamari, D., Bacci, E., Focardi, S., Gaggi, C., Morosini, M., Vighi, M., 1991. Role of plant biomass in the global environmental partitioning of chlorinated hydrocarbons. Environ. Sci. Technol. 25, 1489-1495.

Castro-Jiménez, J., Berrojalbiz, N., Wollgast, J., Dachs, J., 2012. Polycyclic aromatic hydrocarbons (PAHs) in the Mediterranean Sea: Atmospheric occurrence, deposition and decoupling with settling fluxes in the water column, Environ. Pollut. 166, 40–47.

Chen, F., Dudhia, J., 2001. Coupling an advanced land surface-hydrology model with the Penn State-NCAR MM5 modeling system. Part I: Model implementation and sensitivity. Mon. Weather. Rev. 129, 569-585.

Chou, M., Suarez, M., 1994. An efficient thermal infrared radiation parameterization for use in general circulation models, NASA Technical Memorandum No. 104606, Vol. 3, NASA Goddard Space Flight Centre, Greenbelt, USA.

Degrendele, C., Okonski, K., Melymuk, L., Audy, O., Kohoutek, J., Čupr, P., 2016. Pesticides in the atmosphere: a comparison of gas-particle partitioning and particle size distribution of legacy and current-use pesticides. Atmos. Chem. Phys. 16, 1531–1544.

Devi, S., Yadav, B.P., 2015. Regional characteristics of the 2014 southwest monsoon. In: Monsoon 2014 – a report (Pai, D.S., Bhan, S.C., eds.), India Meteorological Department, Pune, pp. 1-17

Draxler, R.R., Rolph, G.D., 2003. HYSPLIT (HYbrid Single-Particle Lagrangian Integrated Trajectory), NOAA Air Resources Laboratory, Silver Springs, USA. Available from: http://www.arl.noaa.gov/ready/hysplit4.html.

Dunne, K.A., Willmott, C.J, 1996. Global distribution of plant-extractable water capacity of soil. Int. J. Climatol. 16, 841-859.

Emmons, L.K., Walters, S., Hess, P. G., Lamarque, J.F., Pfister, G.G., Fillmore, D., Granier, C., Guenther, A., Kinnison, D., Laepple, T., Orlando, J., Tie, X., Tyndall, G., Wiedinmyer, C., Baughcum, S.L., Kloster, S, 2010. Description and evaluation of the Model for Ozone and Related chemical Tracers, version 4 (MOZART-4), Geosci. Model Dev. 3, 43-67.

EU, 1996. Technical guidance document in support of the commissions directive 5 93/67/EEC on risk assessment for the notified substances and the commission regulation (EC) 1488/94 on risk assessment for existing substances. European Commission, Brussels.

Fasullo, J., Webster, P.J., 2003. A hydrological definition of Indian monsoon onset and withdrawal. Journal of Climate 16, 3200-3211.

Finizio, A., Mackay, D., Bidleman, T., Harner, T, 1997. Octanol-air partition coefficient as a predictor of partitioning of semi-volatile organic chemicals to aerosols. Atmos. Environ. 31, 2289-2296.

Gasic, B., MacLeod, M., Klánová, J., Scheringer, M., Ilić, P., Lammel, G., Pajović, A., Breivik, K., Holoubek, I., Hungerbühler, K., 2010. Quantification of sources of PCBs to the atmosphere in urban areas: A comparison of cities in North America, Western Europe and former Yugoslavia. Environ. Pollut. 158, 3230-3235.

Grell, G.A., Devenyi, D., 2002. A generalized approach to parameterizing convection combining ensemble and data assimilation techniques. Geophys. Res. Lett, 29, 1693.

Hansen, K.M., Christensen, J.H., Brandt, J., Frohn, L.M., Geels, C, 2004. Modelling atmospheric transport of α-hexachlorocyclohexane in the Northern Hemisphere with a 3-D dynamical model: DEHM-POP. Atmos. Chem. Phys. 4, 1125-1137.

Harner, T., Bidleman, T.F., Jantunen, L.M.M., Mackay, D., 2001. Soil-air exchange model of persistent pesticides in the U.S. Cotton Belt. Environ. Toxicol. Chem. 20, 1612–1621.

Hippelein, M., McLachlan, M. S., 1998. Soil/air partitioning of semivolatile organic compounds. 1. Method development and influence of physical-chemical properties. Environ. Sci. Technol. 32, 310–316.

Hornsby, A.G., Wauchope, R.D., Herner, A., 1996. Pesticide properties in the environment. Springer, New York, 227 pp.

IMD, 2014. Monsoon season (June – September) 2014, Climate Diagnostic Bulletin of India, National Climate Centre, Indian Meteorological Department, Pune, India, 23 pp.

Jaenicke, R., 1988. Aerosol physics and chemistry. Landolt-Börnstein Neue Ser. 4b, 391–457.

Janjic, Z.I., 1994. The Step-Mountain Eta Coordinate Model - Further developments of the convection, viscous sublayer, and turbulence closure schemes. Mon. Weather. Rev. 122, 927-945.

Jury, W.A., Spencer, W.F., Farmer, W.J., 1983. Behaviour assessment model for trace organics in soil: I. Model description. J. Env. Qual. 12, 558–564.

Karickhoff, S.W., 1981. Semi-empirical estimation of sorption of hydrophobic pollutants on natural sediments and soils. Chemosphere 10, 833−846.

Kumari, B., Singh, R., Madan, V.K., Kumar, R., Kathpal, T.S., 1996. DDT and HCH compounds in soils, ponds and drinking water of Haryana, India. Bull. Environ. Contam. Toxicol. 57, 787–793.

Lammel, G., Stemmler, I., 2012. Fractionation and current time trends of PCB congeners: Evolvement of distributions 1950-2010 studied using a global atmosphere-ocean general circulation model. Atmos. Chem. Phys. 12, 7199-7213.

Lammel, G., Klöpffer, W., Semeena, V.S., Schmidt, E., Leip, A., 2007. Multicompartmental fate of persistent substances: Comparison of predictions from multi-media box models and a multicompartment chemistry-atmospheric transport model, Environ. Sci. Pollut. Res. 14, 153-165.

Landlová, L., Čupr, P., Franců, J., Klánová, J., Lammel, G., 2014. Composition and effects of inhalable size fractions of atmospheric aerosols in the polluted atmosphere. Part I. PAHs, PCBs and OCPs and the matrix chemical composition. Environ. Sci. Pollut. Res. 21, 6188-6204.

Li, Y.F., Scholtz, M.T., van Heyst, B.J., 2000. Global gridded emission inventories of α-hexachlorocyclohexane. J. Geophys. Res. 102, 6621–6632.

Li, N., Wania, F., Lei, Y.D., Daly, G.L., 2003. A comprehensive and critical compilation, evaluation, and selection of physical–chemical property data for selected polychlorinated biphenyls. J. Phys. Chem. Ref. Data 32, 1545.

Lin, Y.L., Farley, R.D., Orville, H.D., 1983. Bulk parameterization of the snow field in a cloud model. J. Clim. Appl. Meteor. 22, 1065-1092.

Mackay, D., Shiu, W.Y., Ma, K.C., Lee, S.C., 2006. Physical-Chemical Properties and Environmental Fate for Organic Chemicals, Vol. 4, CRC Press, Boca Raton, USA, 970 pp

McLachlan M.S., Horstmann M., 1998. Forests as filters of airborne organic pollutants: A model, Environ. Sci. Technol. 32, 413–420.

Meijer, S.N., Shoeib, M., Jones, K.C., Harner, T., 2003a. Air-soil exchange of organochlorine pesticides in agricultural soils. 2. Laboratory measurements of the soil-air partition coefficient. Environ. Sci. Technol. 37, 1300–1305.

Meijer, S.N., Shoeib, M., Jantunen, L.M.M., Jones, K.C., Harner, T., 2003b. Air-soil exchange of organochlorine pesticides in agricultural soils – 1. Field measurements using a novel in situ sampling device, Environ. Sci. Technol. 2003, 37, 1292-1299

Mlawer, E.J., Taubman, S.J., Brown, P.D., Iacono, M.J., Clough, S.A., 1997. Radiative transfer for inhomogeneous atmospheres: RRTM, a validated correlated-k model for the longwave. J. Geophys. Res., 102, 16663-16682.

Mu, Q., Lammel, G., Gencarelli, C.N., Hedgecock, I.M., Chen, Y., Přibylová, P., Teich, M., Zhang, Y.X., Zheng, G.J., van Pinxteren, D., Zhang, Q., Herrmann, H., Shiraiwa, M., Spichtinger, P., Su, H., Pöschl, U., Cheng, Y.F, 2017. Regional modelling of polycyclic aromatic hydrocarbon: WRF/Chem-PAH model development and East Asia case studies. Atmos. Chem. Phys. 17, 12253-12267.

Mulder, M.D., Heil, A., Kukučka, P., Klánová, J., Kuta, J., Prokeš, R., Sprovieri, F., Lammel, G., 2014. Air-sea exchange and gas-particle partitioning of polycyclic aromatic hydrocarbons in the Mediterranean. Atmos. Chem. Phys. 14, 8905-8915.

NVBDCP, 2009. Operational manual for implementation of malaria programme 2009, Government of India, Directorate of National Vector Borne Disease Control Programme, Directorate General of Health Services Ministry of Health and Family Welfare, New Delhi, 275 pp.

Octaviani, M., Stemmler, I., Lammel, G., Graf, H.F., 2015. Atmospheric transport of persistent organic pollutants to and from the Arctic under present-day and future climate. Environ. Sci. Technol. 49, 3593-3602.

Pacyna, J.M., Sundseth, K., Cousins, I., 2010. Database of physic-chemical properties and historic/future emission estimates for selected chemicals; D11, ArcRisk project, unpublished, Norwegian Institute for Air Research, Kjeller, Norway.

Paterson S., Mackay D., 1991. Correlation of the equilibrium and kinetics of leaf-air exchange of hydrophobic organic chemicals. Environ. Sci. Technol. 25, 866-871.

Paterson S., Mackay D., McFarlane C., 1991. A model of organic chemical uptake by plants from soil and the atmosphere. Environ. Sci. Technol. 28, 2259-2266.

Patil, M.N., Patil, S.D., Waghmare, R.T., Dharmaraj, T, 2013. Planetary Boundary Layer height over the Indian subcontinent during extreme monsoon years. J. Atmos. Solar-Terr. Phys. 92, 94-99.

Pozo, K., Harner, T., Lee, S.C., Sinha, R.K., Sengupta, B., Loewen, M., Geethalakshmi, V., Kannan, K., Volpi, V, 2011. Assessing seasonal and spatial trends of persistent organic pollutants (POPs) in Indian agricultural regions using PUF disk passive air samplers. Environ. Pollut. 159, 646-653.

Pringle, K.J.; Tost, H.; Message, S.; Steil, B.; Giannadaki, D.; Nenes, A.; Fountoukis, C.; Stier, P.; Vignati, E.; Lelieveld, J., 2010. Description and evaluation of GMXe: a new aerosol submodel for global simulations (v1). Geosci. Model Dev. 3, 391-412.

Pryor, S., Gallagher, M., Sievering, H., Larsen, S. E., Barthelmie, R.J., Birsan, F., Nemitz, E., Rinne, J., Kulmala, M., Grönholm, T., Taipale, R., Vesala, T, 2008. A review of measurement and modelling results of particle atmosphere-surface exchange. Tellus B 60, 42–75.

Puri, S.; Chickos, J.S.; Welsh, W.J., 2001. Determination of vaporization enthalpies of polychlorinated biphenyls by correlation gas chromatography. Anal. Chem. 73, 1480-1484.

Puri, S.; Chickos, J.S.; Welsh, W.J., 2002. Three-dimensional quantitative structure-property relationship (3D-QSPR) models for prediction of thermodynamic properties of polychlorinated biphenyls (PCBs): enthalpies of fusion and their application to estimates of enthalpies of sublimation and aqueous solubilities. J. Chem. Inf. Comput. Sci. 43, 55-62.

Rajendran, R.B.; Venugopalan, V.K.; Ramesh, R., 1999. Pesticide residues in air from coastal environment, South India. Chemosphere 39, 1699-1706.

Ramesh, A., Tanabe, S., Murase, H., Subramanian, A., Tatsukawa, R., 1991. Distribution and behavior of persistent organochlorine insecticides in paddy soil and sediments in the tropical environment: a case study in South India. Environ. Pollut. 74, 293-307.

Ruijgrok, W., Davidson, C.I., Nicholson, K.W, 1995. Dry deposition of particles – implications and recommendations for mapping deposition over Europe. Tellus B 47, 587-601.

Schell, B., Ackermann, I.J., Hass, H., Binkowski, F.S., Ebel, A., 2001. Modeling the formation of secondary organic aerosol within a comprehensive air quality model system. J. Geophys. Res., 106, 28275-28293.

Scheringer, M., Wania, F., 2003. Multimedia models of global transport and fate of persistent organic pollutants. In: Handbook of Environmental Chemistry (Fiedler, H., ed.), Vol. 3O, pp. 237-269.

Semeena, S.; Lammel, G., 2003. Effects of various scenarios upon entry of DDT and γ-HCH into the global environment on their fate as predicted by a multicompartment chemistry transport model. Fresenius. Environ. Bull. 12, 925-939.

Semeena, V.S., Feichter, J., Lammel, G., 2006. Significance of regional climate and substance properties on the fate and atmospheric long-range transport of persistent organic pollutants – examples of DDT and *γ*-HCH, Atmos. Chem. Phys. 6, 1231-1248.

Shahpoury, P., Lammel, G., Albinet, A., Sofuoğlu, A., Domanoğlu, Y., Sofuoğlu, C.S., Wagner, Z., Ždimal, V., 2016. Model evaluation for gas-particle partitioning of polycyclic aromatic hydrocarbons in urban and non-urban sites in Europe – comparison between single- and poly-parameter linear free energy relationships. Environ. Sci. Technol. 50, 12312-12319.

Sharma, B.M., Bharat, G.K., Tayal, S., Nizzetto, L., Čupr, P., Larssen, T., 2014. Environment and human exposure to persistent organic pollutants (POPs) in India: A systematic review of recent and historical data. Environ. Int. 66, 48-64.

Shen, L.; Wania, F., 2005. Compilation, evaluation, and selection of physical−chemical property data for organochlorine pesticides. J. Chem. Eng. Data 50, 742-768.

Sheng, J.J., Wang, X.P., Gong, P., Joswiak, D.R., Tian, L.D., Yao, T.D., Jones, K.C., 2013. Monsoon-driven transport of organochlorine pesticides and polychlorinated biphenyls to the Tibetan Plateau: Three year atmospheric monitoring study. Environ. Sci. Technol. 47, 3199-3208.

Spivakovsky, C.M., Logan, J.A., Montzka, S.A., Balkanski, Y.J., Foreman-Fowler, M., Jones, D.B.A., Horowitz, L.W., Fusco, A.C., Brenninkmeijer, C.A.M., Prather, M.J., Wofsy, S.C., McElroy, M.B., 2000. Three-dimensional climatological distribution of tropospheric OH: update and evaluation. J. Geophys. Res. 105, 8931–8980.

Stockwell, W.R., Kirchner, F., Kuhn, M., Seefeld, S., 1997. A new mechanism for regional atmospheric chemistry modeling. J. Geophys. Res., 102, 25847-25879.

Stohl, A., Hitzenberger, M., Wotawa, G., 1998. Validation of the Lagrangian particle dispersion model FLEXPART against large scale tracer experiments. Atmos. Environ. 32, 4245-4264.
Stohl, A., Forster, C., Frank, A., Seibert, P., Wotawa, G., 2005. Technical Note: The Lagrangian particle dispersion model FLEXPART version 6.2. Atmos. Chem. Phys. 5, 2461-2474.
Strand, A., Hov, Ø., 1996. A model strategy for the simulation of chlorinated hydrocarbon distributions in the global environment. Water Air Soil Poll., 86, 283–316.
Stull, R.B., 1988. An introduction to boundary layer meteorology, Kluwer, Dordrecht, the Netherlands, 670 pp.
UNEP, 2016. Report of the effectiveness evaluation on DDT pursuant to the Article 16 of the Stockholm Convention. Report UNEP/POPS/DDT-EG.6/INF/2, United Nations Environment Programme, Geneva, 11 pp.
Wang, B., Fan, Z., 1999. Choice of South Asian summer monsoon indices. Bull. Amer. Meteor. Soc. 80, 629-638.
Wang, B., Wu, R., Lau, K.M., 2001. Interannual variability of Asian summer monsoon: Contrast between the Indian and western North Pacific-East Asian monsoons. J. Clim. 14, 4073-4090.
Wania, F.; Daly, G.L., 2002. Estimating the contribution of degradation in air and deposition to the deep sea to the global loss of PCBs. Atmos. Environ. 36, 5581-5593.
Wania, F., McLachlan, M.S., 2001. Estimating the influence of forests on the overall fate of semivolatile organic compounds using a multimedia fate model. Environ. Sci. Technol. 35, 582-590
Wild, O., Zhu, X., Prather, M.J., 2000. Fast-j: Accurate simulation of in- and below-cloud photolysis in tropospheric chemical models. J. Atmos. Chem. 37, 245-282.
Xiao, H., Li, N.Q., Wania, F, 2004. Compilation, evaluation and selection of physic-chemical property data for α-, β- and γ-HCH. J. Chem. Eng. Data 49:173–185.
Zhang, G.; Chakraborty, P.; Li, J.; Balasubramanian, T.; Kathiresan, K.; Takahashi, S.; Subramanian, A.; Tanabe, S.; Jones, K.C., 2008. Passive sampling of organochlorine pesticides, polychlorinated biphenyls, and polybrominated diphenyl ethers in urban, rural and wetland sites along the coastal length of India. Environ. Sci. Technol. 42, 8218-8223.
Zhong, G., Xie, Z., Möller, A., Halsall, C., Caba, A., Sturm, R., Tang, J., Zhang, G., Ebinghaus, R., 2012. Currently used pesticides, hexachlorobenzene and hexachlorocyclohexanes in the air and seawater of the German Bight (North Sea), Environ. Chem. 9, 405–414.
Zhu, Q.Q., Zheng, M.H., Liu, G.N., Zhang, X., Dong, S.J., Gao, L.R., Liang Y., 2017. Particle size distribution and gas–particle partitioning of polychlorinated biphenyls in the atmosphere in Beijing, China. Environ. Sci. Pollut. Res. 24, 1389-1396.